

# Accuracy analysis of multi-axis machines by 3D length measurements

**Citation for published version (APA):**

Florussen, G. H. J. (2002). *Accuracy analysis of multi-axis machines by 3D length measurements*. [Phd Thesis 1 (Research TU/e / Graduation TU/e), Mechanical Engineering]. Technische Universiteit Eindhoven.  
<https://doi.org/10.6100/IR555456>

**DOI:**

[10.6100/IR555456](https://doi.org/10.6100/IR555456)

**Document status and date:**

Published: 01/01/2002

**Document Version:**

Publisher's PDF, also known as Version of Record (includes final page, issue and volume numbers)

**Please check the document version of this publication:**

- A submitted manuscript is the version of the article upon submission and before peer-review. There can be important differences between the submitted version and the official published version of record. People interested in the research are advised to contact the author for the final version of the publication, or visit the DOI to the publisher's website.
- The final author version and the galley proof are versions of the publication after peer review.
- The final published version features the final layout of the paper including the volume, issue and page numbers.

[Link to publication](#)

**General rights**

Copyright and moral rights for the publications made accessible in the public portal are retained by the authors and/or other copyright owners and it is a condition of accessing publications that users recognise and abide by the legal requirements associated with these rights.

- Users may download and print one copy of any publication from the public portal for the purpose of private study or research.
- You may not further distribute the material or use it for any profit-making activity or commercial gain
- You may freely distribute the URL identifying the publication in the public portal.

If the publication is distributed under the terms of Article 25fa of the Dutch Copyright Act, indicated by the "Taverne" license above, please follow below link for the End User Agreement:

[www.tue.nl/taverne](http://www.tue.nl/taverne)

**Take down policy**

If you believe that this document breaches copyright please contact us at:

[openaccess@tue.nl](mailto:openaccess@tue.nl)

providing details and we will investigate your claim.

Accuracy Analysis of Multi-axis Machines  
by 3D Length Measurements

CIP-DATA LIBRARY TECHNISCHE UNIVERSITEIT EINDHOVEN

Florussen, Guidorus H.J.

Accuracy Analysis of Multi-axis Machine by 3D Length Measurements/  
by Guidorus H.J. Florussen. - Eindhoven : Technische Universiteit  
Eindhoven, 2002.

Proefschrift. - ISBN 90-386-2943-5

NUGI 841

Subject headings: multi-axis machines / accuracy analysis / length measure-  
ment / Double Ball Bar / thermally induced errors / geometrical errors / fast  
error assessment / error compensation / error component determination

This thesis was prepared with the L<sup>A</sup>T<sub>E</sub>X 2<sub>ε</sub> documentation system

Printed by Ponsen & Looijen bv., Wageningen

Copyright ©2002 by G.H.J. Florussen, Eindhoven, the Netherlands

This research was supported by Stimulus (EC), Project 1013 and the Tech-  
nology Foundation STW, applied science division of NWO and the technology  
programme of the Ministry of Economic Affairs, Project EWO.5423.

# Accuracy Analysis of Multi-axis Machines by 3D Length Measurements

PROEFSCHRIFT

ter verkrijging van de graad van doctor  
aan de Technische Universiteit Eindhoven  
op gezag van de Rector Magnificus, prof.dr. R.A. van Santen,  
voor een commissie aangewezen door het College voor Promoties  
in het openbaar te verdedigen op  
dinsdag 4 juni 2002 om 16.00 uur

door

Guidorus Hermanus Johan Florussen

geboren te Afferden

Dit proefschrift is goedgekeurd door de promotoren:

prof.dr.ir. P.H.J. Schellekens

en

prof.dr.ir. M. Steinbuch

Copromotor:

dr.ir. F.L.M. Delbressine

Aan Nelly



# Summary

In this thesis a research project is presented that analyses to what extent 3D length measurements can be used for accuracy analysis of multi-axis machines. The scope of this research project is focussed on geometrical and thermally induced positioning errors of multi-axis machines, with a serial kinematic structure.

The choice for using length measurements over other measuring devices is motivated by the related costs of measurement. These costs are determined by the measurement equipment, manpower required and, especially, by the required measurement (setup) time. Since the length measurements proposed can be executed in a short period of time with relatively little effort and specialistic knowledge, a large reduction of the related costs has been realised.

Since the major part of the measured positioning errors of a multi-axis machine reveals systematic behaviour, machine error models can be constructed to describe the error measured coherently with respect to the responsible error sources. Applying such machine error models results in a significantly improved positioning behaviour of the respective machine, when performing error compensation.

For this purpose, a geometrical and a thermal error model have been derived and proposed in this thesis. The geometrical error model contain some unknown parameters, which are estimated from length measurement data using least squares regression techniques. In order to be able to determine all the parameters of the geometrical error model, the measurement setup must satisfy certain conditions, as explained in this thesis. Therefore a measurement strategy is proposed, prescribing the spatial distribution of the length measurements to be performed in the machine's working volume. These measurements can be executed in three hours only, which is much less than for conventional measurement techniques (typically two days).

For the validation of the geometrical and thermo-mechanical error models, a Maho 700S milling machine is used. The geometrical errors of this machine vary between  $-20\ \mu\text{m}$  and  $+35\ \mu\text{m}$  throughout its working volume and these errors can be reduced to  $\pm 4\ \mu\text{m}$  by using the geometrical error model. In general, the degree of improvement of the machine's positioning behaviour depends on the ratio of the random and systematic part of the geometrical errors measured, which is machine specific. For modern machines a factor 5-7 of improvement concerning its positioning behaviour may be possible. The thermally induced



positioning errors of a machine tool constitute the major part of the positioning errors of the machine considered. For the machine used, its thermal errors exceed  $100\ \mu\text{m}$  and this kind of errors can be predicted for about 60%, using a rather simple error model. To enhance the performance of the thermal error model, further research is required. For the measurement of the thermally induced positioning errors of a machine tool, which vary in time, application of length measurements is introduced in this thesis as a new, pioneering measurement technique.

Besides error compensation, the geometrical error model with its estimated parameters as obtained by using length measurements can also be used for diagnostic purposes, (i.e. error tracing). This means that with the method proposed statements can be made about the origin of certain geometrical errors measured. In addition, the method proposed is also suitable for acceptance testing and periodic inspection of machines. Possibilities to analyse the effect of thermally induced errors for specific operation tasks are available as well e.g. for reducing tolerance levels of workpieces by adjusting machining operations.

# Samenvatting

Dit proefschrift beschrijft een studie naar de mogelijkheden om lengtemetingen in het arbeidsvolume van een machine te gebruiken voor het analyseren van de positioneringsnauwkeurigheid van meer-assige machines. Dit onderzoek richt zich enkel op geometrische en thermische afwijkingen; het effect van andere afwijkingensbronnen op het positioneringsgedrag van machines is buiten beschouwing gebleven. De assen van een dergelijke machine moeten serieel met elkaar in verbinding staan.

Door de keuze voor lengtemetingen wordt een aanzienlijke verlaging van de gerelateerde meetkosten beoogd. Deze kosten worden, behalve door het meetinstrument en de benodigde kennis, voornamelijk bepaald door de meettijd. Aangezien lengtemetingen relatief eenvoudig en snel kunnen worden uitgevoerd zonder specialistische kennis, is een aanzienlijke kostenreductie gerealiseerd met de voorgestelde meettechniek.

Het merendeel van gemeten machine-afwijkingen blijkt in de praktijk systematisch gedrag te vertonen. Door nu modellen op te stellen die deze machine-afwijkingen beschrijven, in relatie tot de bijbehorende foutenbron, kan het positioneringsgedrag van dergelijke machine's aanzienlijk worden verbeterd wanneer deze modellen daadwerkelijk gebruikt worden voor correctiedoeleinden.

Ten behoeve van het corrigeren van een machine voor geometrische en thermische machine-afwijkingen wordt er in dit proefschrift een geometrisch en thermisch fouten-model gepresenteerd. Het geometrische fouten-model bevat parameters welke uit lengtemeetdata worden afgeschat met behulp van lineaire regressie. Hiervoor moet de ruimtelijke verdeling van de lengtemetingen in het arbeidsvolume van de machine wel aan bepaalde voorwaarden voldoen, welke in dit proefschrift zijn geformuleerd. De voorgeschreven lengtemetingen kunnen in slechts drie uur tijd worden uitgevoerd. Conventionele meettechnieken vergen een typische meettijd van zo'n twee dagen.

Metingen ter validatie van de voorgestelde fouten-modellen zijn uitgevoerd op een Maho 700S freesmachine. De geometrische afwijkingen van deze machine variëren van  $-20\ \mu\text{m}$  tot  $+35\ \mu\text{m}$  in zijn arbeidsvolume en deze afwijkingen worden gereduceerd tot slechts  $\pm 4\ \mu\text{m}$  bij toepassing van het geometrische fouten-model. De mate van reductie van machine-afwijkingen hangt af van de verhouding tussen de toevallige en systematische afwijkingen, welke machine specifiek zijn. In het algemeen is verbetering van het positioneringsgedrag van moderne machines met een factor 5-7 mogelijk. Het grootste gedeelte van de gemeten

positioneringsafwijkingen van de beschouwde freesmachine wordt veroorzaakt door zijn thermische gedrag: deze afwijkingen kunnen zelfs groter zijn dan  $\pm 100 \mu\text{m}$ . Met een betrekkelijk eenvoudig thermisch fouten-model kan zo'n 60% van de gemeten lengteveranderingen worden verklaard. Voor een verdere verbetering is aanvullend onderzoek vereist. Het toepassen van lengtemetingen voor het bepalen van thermische machine-afwijkingen kan als innovatief worden beschouwd.

Naast het compenseren voor afwijkingen kan het voorgestelde geometrische fouten-model ook worden gebruikt voor het opsporen en kwantificeren van foutenbronnen. Tevens is de beschreven meetmethode uitermate geschikt voor machine-afname en het uitvoeren van periodieke machine inspecties, bijvoorbeeld ten behoeve van het waarborgen van de kwaliteit van een machinepark. Bovendien kan het model worden toegepast om het effect van thermo-mechanische machine afwijkingen voor specifieke bewerkingen van een werkstuk te analyseren en/of te verbeteren .

# Contents

<b>Summary</b>	<b>i</b>
<b>Samenvatting</b>	<b>iii</b>
<b>1 Introduction</b>	<b>1</b>
1.1 Multi-axis machines . . . . .	1
1.2 Error sources of multi-axis machines . . . . .	3
1.3 Measuring instruments and methods . . . . .	6
1.4 Research objectives and content thesis . . . . .	12
<b>2 Kinematic modelling of multi-axis machines</b>	<b>15</b>
2.1 Link modelling . . . . .	15
2.2 Modelling of joints . . . . .	17
2.2.1 Revolute joints . . . . .	17
2.2.2 Prismatic joints . . . . .	18
2.3 Machine configurations . . . . .	19
2.4 Nominal machine model . . . . .	20
<b>3 Modelling and measurement of geometrical errors</b>	<b>27</b>
3.1 Geometric error modelling . . . . .	27
3.1.1 Axis errors . . . . .	28
3.1.2 Error component functions . . . . .	32
3.1.3 Error propagation . . . . .	33
3.2 Measurement of geometric errors . . . . .	39
3.2.1 Measurement conditions . . . . .	39
3.2.2 Length measurements with a Double Ball Bar . . . . .	41
3.2.3 Design of measurement setup . . . . .	49
3.2.4 Reversal Double Ball Bar measurements . . . . .	56
3.3 Resume . . . . .	58
<b>4 Parameter identification and validation geometrical error model</b>	<b>61</b>
4.1 Estimating geometrical error parameters . . . . .	62
4.1.1 Least squares regression . . . . .	62
4.1.2 Geometrical error model optimisation . . . . .	67
4.2 Validation of the geometrical error model . . . . .	73

---

4.2.1	Validation based on DBB length measurements . . . . .	73
4.2.2	Validation of the error components . . . . .	74
<b>5</b>	<b>Thermally induced errors</b>	<b>79</b>
5.1	Problem description . . . . .	80
5.2	Literature overview . . . . .	81
5.2.1	Research objective . . . . .	84
5.3	Thermo-mechanical modelling of a machine tool . . . . .	85
5.4	Thermal deformation of machine parts . . . . .	86
5.5	Describing the temperature distribution of machine parts . . . . .	88
5.5.1	Approximation methods . . . . .	91
5.5.2	Extended Lumped Capacitance Method . . . . .	92
5.6	Thermal drift of the end-effector . . . . .	99
5.7	Measurement of thermally induced positioning errors . . . . .	100
5.8	Validation of the thermo-mechanical error model . . . . .	104
5.8.1	Validation of the lumped capacitance model . . . . .	107
5.9	Resume . . . . .	108
<b>6</b>	<b>Conclusions and recommendations</b>	<b>111</b>
6.1	Conclusions . . . . .	111
6.1.1	Geometrical errors . . . . .	111
6.1.2	Thermally induced errors . . . . .	113
6.2	Recommendations . . . . .	115
	<b>Bibliography</b>	<b>117</b>
	<b>A Nomenclature, acronyms and symbols</b>	<b>125</b>
	<b>B Double Ball Bar calibration</b>	<b>129</b>
	<b>C Alternative error component functions</b>	<b>137</b>
	<b>D Geometrical error model in matrix notation</b>	<b>141</b>
	<b>E Executing Double Ball Bar measurements</b>	<b>145</b>
	<b>F The singular value decomposition</b>	<b>149</b>
	<b>G Design Double Ball Bar adapter</b>	<b>151</b>
	<b>Curriculum vitae</b>	<b>155</b>
	<b>Acknowledgements</b>	<b>157</b>

# Chapter 1

## Introduction

This thesis deals with the accuracy analysis of multi-axis machines based on 3D length measurements. The general goal is to develop a method for describing the machine's positioning behaviour throughout its working volume resulting from its geometrical and thermo-mechanical error structure. In this chapter the major error sources affecting the machine's accuracy are presented based on a literature overview. Since a large variety of multi-axis machines exists, a selection has to be made for which class the method developed can be applied. The same applies for the type of machine errors to be described.

In this thesis 3D length measurements are used to measure the machine's positioning errors. Our goal is to develop an accurate and reliable measurement method and strategy that can be performed fast with relatively little effort and with minimal costs in order to make it suitable for practical applications in industry. Examples of such applications are machine acceptance tests, machine calibrations, quality control of machines and/or error compensation to improve the machine's positioning performance. Since the measurement related costs are mainly determined by the time required, considerable attention is paid to minimize this time.

### 1.1 Multi-axis machines

Multi-axis machines are used extensively in modern manufacturing, due to their flexibility to perform a large variety of (complex) tasks. Such a task involves the generation of a specified spatial trajectory or a certain position/orientation of an end-effector (like a tool, probe, gripper etc.) with respect to a certain reference, usually a workpiece. These tasks have a relative character and can be divided into three classes [Soo 93]:

1. Measurement;
2. Machining;
3. Manipulating/Handling.

ad 1) Typical multi-axis machines used for measurement tasks are Coordinate Measuring Machines (CMMs). In this case the machine is equipped with a probe able to detect a surface while moving towards the workpiece (disregarding CMMs used in 'scanning mode' where the probe moves continuously in contact with the surface). Two kinds of probing systems can be distinguished: conventional touch-trigger probes and so-called measuring probes. If such a probing-point is detected the machine's axis positions are stored and later the workpiece dimensions and geometry can be estimated by using these stored coordinates. Due to its application only the point accuracy is important for the proper functioning of the machine; the relative probe position in between measuring points is irrelevant.

ad 2) For machining operations the machine's end-effector is used to transform, add or remove material from a workpiece by means of a tool. Obviously the accuracy of the tool trajectory with respect to the workpiece is important here since the tool is in contact with the workpiece while moving. Typical machining operations are milling, turning, grinding, deburring, welding, laser cutting (considering the laser beam as a 'tool') and electrical discharge machining (EDM).

ad 3) In this case the multi-axis machine is used for moving/manipulating a workpiece or object according to a specified trajectory relative to other workpieces or machines. Typical examples of manipulating, handling operations are assembly and (un-) loading of machines. In this case the machine's end-effector contains a certain gripper, possibly extended with additional functions. Examples of such end-effector integrated functions are force controlling units (i.e. for mounting a part with pre-load) and heating units (i.e. for melting a manipulated object) etc. Typical machines belonging to this class are Surface Mounting Devices (SMD) machines, assembly robots, wafer steppers etc.

The classes distinguished here should be considered as a coarse classification due to the versatile nature of existing multi-axis machines. These kind of machines often can perform multiple tasks: a milling machine can be equipped with a probe system and specific software, transforming the machine into a kind of CMM for example. Also application of robot arms used for coordinate metrology and CMMs employed for light machining operations have been reported [Dea 92] [Kef 90].

The accuracy of a task performed by a multi-axis machine is obviously determined by the capabilities of the machine to control the relative end-effector position, orientation and trajectory with respect to the workpiece. For proper functioning of the machine, the tolerance on the relative end-effector position, orientation and trajectory must be below a certain level. In this thesis considerable attention is paid to the errors in this relative trajectory.

In general multi-axis machines contain an end-effector that can be positioned with respect to a workpiece. In between, the machine's axes are present to generate the relative end-effector trajectory, which are parts of the machine's structural loop. The structural loop of a multi-axis machine comprises the mechanical components that realize the relative position and orientation between the end-effector's functional point and the workpiece (including the end-effector

itself). The machine's axes present in this structural loop can be connected in three different ways:

- Serial;
- Parallel;
- Hybrid configuration.

The most common way to connect the machine's axes is by means of a serial kinematic structure. In this case a change in axis position is reflected directly in the relative end-effector position. Most conventional machines and robots belong to this class of machines which is subject of this thesis.

Gough [Gou 62] used multi-axis machines equipped with a parallel kinematic structure in 1949 for testing tyres. In this case the machine's axes are connected in a parallel way. Complex geometrical relations exist between the relative end-effector position and the axis positions due to the spatial axis configuration. This idea is later employed by Stewart [Ste 65] in the base of a flight simulator for generating movements in six degrees of freedom, as reported in 1965. This class of machines are referred to as Stewart platforms or so-called hexapods and this idea is used for general-purpose multi-axis machines later, mainly high speed machining. Although this class of machines is gaining considerable attention in recent research (last decade) [Soo 97] [Tlu 99] [Wec 02] [Hoc 02] their presence in workshops is still rare. This thesis does not deal with this class of multi-axis machines.

Besides pure serial or parallel kinematic structures also combinations of these structures exist [Tön 01].

Disregarding the kinematic structure of a multi-axis machine, the end-effector position and orientation relative to the workpiece is measured preferably directly when considering its accuracy. This means that the machine is equipped with certain measuring systems able to determine directly the relative end-effector position and orientation without the need to consider a part of the machine's structural loop. A typical example is a wafer-stepper, meeting extreme accuracy levels. The presence of such direct measuring systems in a machine can, however, seriously limit the machine's capabilities to perform tasks in its working volume (i.e. collisions, dirt, the working volume itself). Therefore the relative end-effector position and orientation is often measured indirectly. The latter means that the relative end-effector position and orientation is computed using the machine's axis positions and their configuration. This implies that the structural loop of the machine has to be considered. This thesis does not deal with machines equipped with direct measuring systems.

## 1.2 Error sources of multi-axis machines

The accuracy of a multi-axis machine is affected by many errors sources. These errors sources may cause a change in the geometry of the machine's components present in the machine's structural loop. Due to the change in geometry



of these components, the actual end-effector position and orientation relative to the workpiece differs from its nominal position and orientation. The resulting relative orientation and positioning error are drawn in Figure 1.1. The

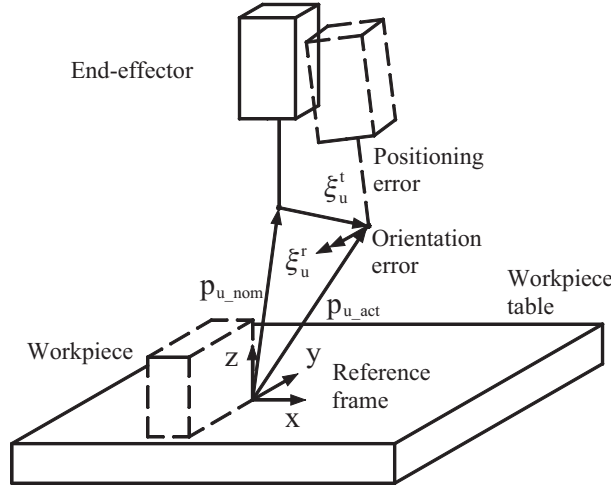


Figure 1.1: The positioning error vector  $\xi_u^t$  and the orientation error vector  $\xi_u^r$  of the end-effector relative to a reference frame.

positioning error of a multi-axis machine on one hand is defined as the actual end-effector position minus the nominal position and is denoted as a vector  $\xi_u^t$ . The orientation error on the other hand is defined by the difference between the actual and nominal orientation of the machine's end-effector with respect to the workpiece table and is denoted by a vector  $\xi_u^r$ . In this way, the relative error of the end-effector with respect to the workpiece is denoted as a six dimensional error vector  $\xi_u$ :

$$\xi_u = \begin{bmatrix} \xi_u^t \\ \xi_u^r \end{bmatrix}. \quad (1.1)$$

In this thesis the term 'positioning behaviour' refers to this six dimensional error vector (including the orientation error) while the term 'positioning error' is used for the relative error of the end-effector position (excluding the orientation error) as denoted by error vector  $\xi_u^t$ .

The error vector  $\xi_u$  is not constant but depends on the current state of the machine. This state contains those variables and entities that describe the current condition of the machine and is denoted by  $u$ . Examples of such variables are the machine's axis positions, the end-effector length, component temperatures and strains, etc. As a result, the error vector  $\xi_u$  varies (smoothly) throughout the machine's workspace (and in time). To indicate this dependency,

a subscript  $u$  is added to the vectors to specify a certain state of the machine. Therefore, the actual relative end-effector position equals:

$$\mathbf{p}_{u-act} = \mathbf{p}_{u-nom} + \boldsymbol{\xi}_u^t. \quad (1.2)$$

The relative orientation error of the end-effector just equals  $\boldsymbol{\xi}_u^r$  since the nominal relative end-effector orientation error is zero.

The magnitude of this error vector  $\boldsymbol{\xi}_u$  depends on the sensitivity of the machine's structural loop for various error sources. In literature the following major error sources are reported that affect the accuracy of the relative end-effector position and orientation [Soo 93] [Spa 95] [Wee 95] [Deh 98] [Hoc 80] [Kna 83] [Sch 93]:

1. Geometrical errors;
2. Finite stiffness of the structural loop under different, quasi-static load;
3. Thermo-mechanical errors;
4. Dynamical errors.

ad 1) Geometrical errors are errors due to imperfect geometry and dimensions of machine components present in the machine's structural loop, axis misalignment (i.e. squareness errors) and errors of the machine's measuring systems. Over short-term time intervals these kind of errors are considered to be constant although these errors can be subject to change due to wear and a limited long-term stability of machine components.

ad 2) In some cases the weight and position of a workpiece can have a significant influence on the machine's accuracy due to the finite stiffness of the structural loop. A Maho 700S milling machine for instance can be loaded with workpieces up to 500 kg resulting in a non-negligible deflection of the machine's structural loop up to 100  $\mu$ rad [Soo 93] [Spa 95]. Besides this effect, the machine's accuracy is also affected by gravity forces on the machine (components) itself. The latter machine deformations are always present and are therefore considered to be part of the machine's geometrical errors. Since the weight of a workpiece is not necessarily constant (due to material removal) the term 'quasi-static' is used.

ad 3) Due to the presence of internal and external heat sources in multi-axis machines, the temperature distribution of the machine's structural loop differs from 20 °C: the reference temperature defined in standard [ISO 1]. Typical examples of such heat sources are heat generated by friction in spindle bearings, gear boxes, joints, drives, the machining process, electronic and hydraulic systems, the operator, and environment temperature. Since most materials used in multi-axis machines expand significantly with temperature, the relative end-effector position and orientation changes. The resulting thermal (instationary) distortion of the machine's structural loop often dominate the accuracy of an executed task [Spa 95] [Ber 01].

ad 4) The trajectory realized is also affected by the dynamical behaviour of the machine's structural loop due to its finite stiffness. In this case (rapidly)

varying forces are considered instead of quasi-static ones (see item 2). These varying forces are due to dynamic spindle error motions, imperfections of the controller that coordinates joint movements, servo tracking errors, acceleration dependent joint and link deflections and vibrations, both self-induced or forced, dynamic workpiece end-effector interactions, and cutting process induced vibrations (i.e. chatter). By their nature, these errors vary rapidly in time and primarily determine the repeatability of the multi-axis machine. Therefore these errors predominantly affect the local characteristics of a workpiece (surface roughness, undercutting of corners) rather than its dimensional accuracy [Spa 95].

The first three error sources mentioned are the so-called ‘quasi-static errors’. These errors are defined as “those errors of relative position and orientation between end-effector and workpiece that are slowly varying in time and are related to the structure of the multi-axis machine itself” [Hoc 80]. For machine tools these quasi-static errors account for the largest part (about 70%) of the errors attributable to the machine itself [Hem 73] [Hoc 80].

Since the positioning behaviour of multi-axis machines is deterministic (and therefore repeatable) machine error models can be constructed to describe the machine’s positioning behaviour coherently with respect to their error source [Bry 93]. By superposition of these models the overall positioning error of the machine can be obtained [Soo 93] [Spa 95] assuming no correlation effects. Such models can then for instance be used for accuracy enhancement by applying compensation techniques [Sch 93] [Spa 95] [Sar 95]. In this thesis machine error models are derived for describing the geometrical and thermally induced errors of multi-axis machines. Although a general method has been developed, the research presented has been applied to a machine tool. Modelling the effect of other error sources on the positioning behaviour of multi-axis machines is beyond the scope of this thesis. For these aspects see [Soo 93] [Spa 95] [Wee 95] [Hoc 02].

### 1.3 Measuring instruments and methods

For the measurement of the positioning behaviour of multi-axis machines many measuring devices are available. Such measurements can be used for different purposes like:

- Acceptance tests;
- Performance monitoring, quality control;
- Error reduction by compensation;
- Calibration;
- Error tracing.

For acceptance tests, measurements are executed on a multi-axis machine after its installation to verify whether the machine performs according to its

specifications, as initiated by Schlesinger in 1932 [Sch 32]. In principle this implies execution of specified (normally by the manufacturer of the machine) measurements by the owner or by certified institutions. Such a measurement results in a statement of acceptance or rejection of the machine.

Besides an initial acceptance test, multi-axis machines can also be subjected to measurements at certain time intervals. Such measurements or periodic inspections are then used to monitor the machine's performance during its use. In this case changes in the machine's positioning behaviour can be monitored and this information can for instance be used in decision-making processes. In this way, the quality of the machines used can be controlled.

So far the machine's positioning errors are just being measured. The information obtained can also be used to increase the machine's positioning accuracy by taking the (systematic part of the) measured errors into account. This implies that the machine's axis positions are being adjusted with certain compensation values (i.e. machine tools) or the stored axis positions are corrected afterwards (i.e. CMMs). Axis positions can be adjusted for instance by modifying the machine's controller, correcting axis setpoint values, or by simply adjusting the commanded machine coordinates [Spa 95]. In this way, the positioning performance of a multi-axis machine can be improved significantly [Sch 93] [Spa 95] [Sar 95]. This improvement depends on the ratio between the random and systematic (i.e. repeatable) part of the errors measured [Sar 95]. Small ratios indicate a relatively small random error with respect to its systematic error and large improvements in the machine's positioning behaviour (up to one order of magnitude) can be achieved in such cases.

Another possible reason to measure the machine's positioning behaviour is calibration to determine its accuracy. In this case the machine's positioning errors are measured in a prescribed and traceable way (i.e. traceable to the definition of the metre): measuring instruments used are related traceable to a higher (length) standard and the measuring procedure to be followed is prescribed by an official document (for CMMs i.e. ANSI/ASME B89.1.12M, ISO 10360, VDI/VDE 2617, JIS B 7440, machine tools i.e. ANSI/ASME B5.54, ISO 230) as provided by normalization institutions. Such measurements result in a calibration report of the machine of interest acknowledged by an official institution, which is valid for a certain period of time.

The measurement purposes mentioned so far are especially important for users of multi-axis machines. Multi-axis machine manufacturers on the other hand often require (specific) measurements for diagnostic purposes i.e. error tracing. In this case measurements are performed to locate the source(s) of a measured machine error and to quantify its contribution to the overall positioning error.

For measuring the positioning behaviour of a multi-axis machine, three methods have been reported:

1. Direct or parametric methods;
2. Artifact based (indirect) methods;
3. Indirect methods without artifacts.

The best known and widely accepted method for measuring the machine's positioning behaviour is the so-called direct or parametric method. In this case all the six axis error motions (three translational and three angular errors) are measured for each machine axis as well as the machine's squareness errors between these axes: the so-called ( $21^1$ ) parametric errors. Then these parametric errors are combined by means of a kinematic machine model, based on the machine's geometry to obtain the machine's relative positioning error. This method has been subject to extensive research in the past and is mainly used by machine manufacturers since it gives direct proof of mechanical accuracy of relevant machine components [Hoc 77] [Sar 95]. This method however possesses some practical disadvantages due to its complexity and the large number of measurements needed. Furthermore the measurement equipment required is expensive (laser interferometer and optics) and demands a skilled operator for analysing and performing the measurements properly. Mainly the related time expense, typically two days, makes this method expensive. This time is mainly used for preparing the measurement setup. It should be noted, however, that this method can be very accurate due to the impressive accuracy of a laser interferometer: the length measuring error equals  $10 \text{ nm} + 2 \cdot 10^{-7} \cdot \ell$ .

In the last decade(s) research in the field of accuracy analysis of multi-axis machines shifted to the second (and third) method mentioned. For this approach the machine's positioning behaviour is assessed by measuring (calibrated) artifacts, like for example hole plates, ball bars, step gauges etc., in the machine's working volume. This means that errors of a multi-axis machine are retrieved from differences between the measured and known dimensions of the artifact as measured on the machine subject to measurement. By using machine error models and estimation algorithms, the erroneous motions of each axis can be determined from the collected measurement data [Sar 95] [Soo 93] [Kun 90] [Kru 94] [Spa 95]. The major advantage of this method above the direct method is the reduced measuring time (typically a few hours) and related costs, including the instrumentation itself. In this thesis this approach will be used. In general a shift can be observed from modifying the machine's hardware (which is labour intensive) in the past to counteracting the machine's errors by means of measurement analysis and software.

For indirect methods, the use of an artifact to obtain information about the machine's positioning behaviour can also be substituted by a measuring instrument [Wan 00] [Jan 00] [Hoo 00]. A typical example is performing displacement measurements (i.e. 'tracking laser interferometry') along diagonals in the machine's workspace. In principle, the method is similar to the second mentioned one. Since a laser beam cannot be considered as an artifact, this distinction has to be made.

Many artifacts have been developed suitable for the artifact based method. These artifacts must at least have a good long-term stability and are preferably calibrated although not necessarily [Kru 94]. The following artifacts have been used and reported [Sar 95] [Kun 90] [Kak 93] [Kna 83]:

---

<sup>1</sup>For three prismatic axes for example there are  $3 \cdot 6 + 3 = 21$  parametric errors.

- 1D: Ball bars (with or without measuring system), gauge blocks, step gauges, ring gauges;
- 2D: Hole or ball plates, a square block, optical square;
- 3D: Tetrahedrons, ball cubes.

In Figure 1.2 some of the mentioned artifacts are shown on the workpiece table of a CMM.

The first artifacts mentioned all define a certain length in a different way. For a ball bar, for instance, its length is determined as the distance between the centre points of the precision balls attached at each end of the bar while for a step gauge, lengths are defined as the distance between parallel surfaces. Also ball bar systems equipped with a measuring system are available (for example the DBB110 (Double Ball Bar) of Heidenhain or the QC10 of Renishaw). Such a ball bar system contains a telescopic rod with a limited stroke and the distance between the ball centres is then detected by a measurement system (i.e. a linear encoder). For a ring gauge a certain length is defined by its diameter.

The uncertainty of the lengths defined this way increases with the size of the artifact, mainly due to growing uncertainty in its thermal expansion. Typical

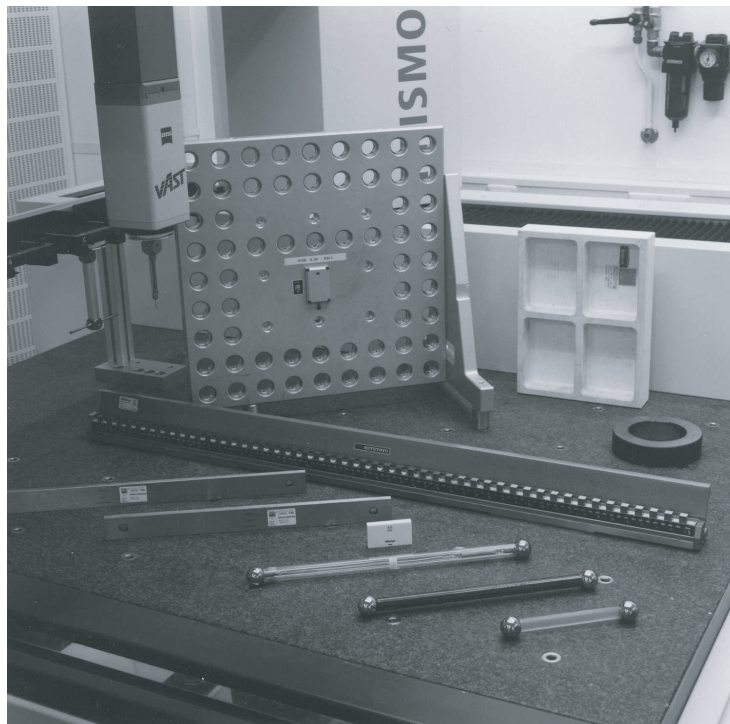


Figure 1.2: Typical artifacts on a CMM.

uncertainty values vary between  $0.02\ \mu\text{m}$  (small gauge blocks) and  $1\ \mu\text{m}$  (ball bars without measuring system) for artifact lengths up to 1 m.

Examples of two-dimensional artifacts are hole or ball plates. Such an artifact contains usually an orthogonal grid of holes/balls whose mutual positions are known accurately (length errors vary between  $0.1$  and  $1.0\ \mu\text{m}$ ) after a calibration procedure [Kun 90]. Finally the ball cube and a tetrahedron should be mentioned as the 3D artifacts available [Wal 97]. These devices contain a 3 dimensional framework with precision balls attached to it whose positions are being measured. The errors in defined lengths are typically  $1\ \mu\text{m}$ . A serious disadvantage of these 3D artifacts is their non-flexibility in use: the positioning of the bulky artifact on the workpiece table and the artifact size must fit the machine's working volume in all three dimensions.

When selecting a suitable artifact for assessing the machine's positioning behaviour a trade-off has to be made between the measurement effort and the machine's errors that can possibly be determined with that artifact. The latter is mainly determined by the spatial density of the measuring points available on the artifact in the machine's workspace. This density varies considerably between the artifacts mentioned. A ball cube for instance has a relatively low spatial measuring point density, mainly due to a poor accessibility of the balls present in the bottom plane, while for a step gauge very high measuring point densities can be achieved. Also the spatial measuring point density in the machine's working volume can be increased simply by performing several artifact measurements on different locations in the machine's workspace while varying its orientation. In this way high spatial measuring point densities in the machine's workspace can be achieved with relatively simple 1D measurements, which can be collected with relatively little effort. The latter explains that the majority of artifacts available are just one-dimensional.

In Figure 1.3 a photograph is shown of a telescopic Double Ball Bar (DBB) measurement performed on a five-axis milling machine. The length of the DBB can be adjusted with extension rods to fit the machine's workspace. For executing such a DBB measurement, the machine is commanded to move along circular paths while the DBB measures lengths at (discrete) points. Since the measuring stroke of a DBB is limited to 10 mm the measuring points have to be distributed on a semi-sphere with respect to the stand, which is positioned on the machine's workpiece table. By comparing the commanded length with the measured length (or radius) information about the machine's positioning behaviour can be obtained [Spa 95]. In this thesis telescopic Double Ball Bar (DBB) length measurements will be used for assessing the machine's positioning behaviour since this measuring device possesses advantages when comparing them to other artifacts. These advantages are:

- Measuring speed: lengths can be measured with a DBB in fractions of a second only, enabling application of high feedrates;
- Low measurement uncertainty: the DBB length measurement error is on submicron level after calibration (error  $\leq 1\ \mu\text{m}$ );



Figure 1.3: A telescopic Double Ball Bar (DBB) measurement on a five-axis milling machine.

- Traceability: a DBB can be calibrated to a certified laser interferometer on an optical bench with little effort (typically a few hours), see Appendix B;
- Good possibilities for automatic execution of DBB measurements;
- Simplicity: little specific knowledge is required for executing a DBB measurement.
- Flexibility: the DBB length can be adjusted with extension rods to fit the machine's workspace;
- Relatively low cost price:  $\leq 10.000$  €;
- Robustness due to its simple design.



## 1.4 Research objectives and content thesis

The research presented in this thesis investigates to what extent 3D length measurements can be used for accuracy analysis of multi-axis machines with a serial kinematic structure. The goal is to describe the machine's positioning behaviour throughout its entire working volume as resulting from its geometrical and thermal error sources. The information obtained can be used for acceptance tests of multi-axis machines, quality control of machines, software error compensation and error tracing purposes. Calibration of multi-axis machines to realize traceability of executed tasks is beyond the scope of this thesis, with exception of relatively simple tasks.

The basic philosophy in the analysis presented is that the positioning behaviour of multi-axis machines is deterministic, especially when equipped with a numerical controller (eliminating a human factor) [Soo 93] [Hoc 80] [Bry 93]. The effect of two major error sources on the machine's positioning behaviour is analysed: geometrical and thermally induced errors. For this purpose two separate machine error models are developed i.e. a geometrical error model and a thermo-mechanical error model. These models can for instance be used for software error compensation techniques to enhance the machine's accuracy. The effect of other error sources on the positioning behaviour of multi-axis machines are not considered in this thesis. For these aspects see [Soo 93] [Spa 95] [Wee 95] [Hoc 02].

The measurement time, necessary for collecting the 3D length measurements required for assessing the machine's positioning behaviour is reduced as much as possible in this research project, typically to a few hours only. Besides a limited measuring time also the measurement effort is minimized by developing user-friendly software modules. Consequently, little specialistic knowledge is required for executing 3D length measurements in the machine's workspace. Summarizing, the costs related to the execution of measurements is minimized by developing a fast, easy to handle and reliable measuring method.

Due to the advantages mentioned of employing a DBB, a measurement method has been developed which is suitable for industrial applications. It enables fast measurement possibilities in a flexible manner on the shop floor depending on the users needs i.e. quality control, error compensation or even error tracing (determine parametric errors) purposes to a limited extend. Furthermore the application of a DBB for assessing the machine's thermally induced positioning behaviour can be considered as being of a pioneering kind. Its major advantage over conventional thermal drift measurements is that application of a DBB in combination with a specially designed adapter enables measurement of the relative thermal drift of the end-effector with respect to the workpiece table on different locations in the machine's workspace in a single measurement setup. The latter implies a reduced measuring time and therefore decreasing cost rates related to analysing thermal behaviour of multi-axis machines.

In Chapter 2 a kinematic machine model is presented, suitable for describing the nominal positioning behaviour of multi-axis machines with a serial kinematic structure. This implies that this model describes the end-effector position and

orientation with respect to the workpiece (table) without the presence of any error. This model is completely defined by the nominal geometry and dimensions of the machine's structural loop.

Chapter 3 deals with geometrical errors of multi-axis machines and consists of two parts. The first part deals with the modelling procedure of geometrical errors of multi-axis machines. A model is presented which relates the actual positioning and orientation error of the machine to its current state and to some unknown parameters, describing the error components. In the second part the measurement of geometrical errors of multi-axis machines is discussed. A DBB measurement model is derived describing the relationship between the machine's positioning error and the resulting length deviation, as measured with a DBB. Also a measurement strategy is presented which prescribes the spatial distribution of the length measurements in the machine's workspace. The measurement data collected this way can be used for identifying the unknown error model parameters as presented in the first part of Chapter 4.

In Chapter 4 the identification of the model parameters is discussed together with the validation of the presented geometrical error model. First the identification of the error model parameters from DBB measurement data is discussed. For the estimation of these parameters least squares regression techniques have been used when optimising the error model. In the second part of Chapter 4 the validation of the geometrical error model is presented and this validation consists of two parts. First cross-validation measurements performed with a DBB are dealt with. Secondly, the machine's error components as described with the estimated parameters are compared with direct measurements (i.e. laser interferometry) of these error components.

Thermally induced errors of multi-axis machines are subject of Chapter 5. First (analytical) models are presented to describe the temperature distribution of machine parts, which are modelled as a plate structure, present in the machine's structural loop. This is realized by integrating sequentially updated element temperature time derivatives of a machine part. These derivatives are obtained by considering the heat flux in a machine part using conduction and convection coefficients (the effect of radiation is negligible) in combination with a limited number of temperature sensors. Secondly, the resulting thermo-mechanical deformation of the machine part is calculated by using formulas describing (stress-free) thermal expansion. Thirdly, the thermo-mechanical drift of the end-effector with respect to the workpiece is obtained by superposition of the machine part deformations present in the machine's structural loop. The predicted thermo-mechanical drift of the end-effector is then compared with length deviations measured by a DBB. In order to perform DBB measurements with a rotating spindle, an expansion free adapter has been designed and realised. Finally the validation of the thermal models is presented.

In the Chapter 6 conclusions are drawn together with recommendations for future research.



## Chapter 2

# Kinematic modelling of multi-axis machines

In this chapter a kinematic machine model is derived. The purpose of such a kinematic model is twofold. First it is used to describe the *nominal* positioning behaviour of a multi-axis machine. This means that all joints, links as well as their configuration are assumed to be error free. A static relation is derived between the end-effector's position and orientation with respect to the workpiece and the machine's axis positions. Secondly, the kinematic machine model will be used later on as a reference to model the propagation of errors induced at various machine parts. This implies that the machine's positioning errors due to geometrical as well as thermally induced errors are calculated as emanating from the machine's kinematic structure. This kinematic machine model can be applied to multi-axis machines composed of revolute and prismatic joints and links in an arbitrary serial configuration. In this thesis only the machine's kinematic chain from workpiece table to end-effector is considered regardless the fixation point of the machine to the world.

### 2.1 Link modelling

Any multi-axis machine with a serial kinematic structure can be considered to consist of a series of links connected together by (actuated) joints [Pau 81]. These links maintain a fixed relationship between the machine's joints and are modelled as a rigid body here.

In order to describe the relationship between links Cartesian coordinate frames are assigned to each link obeying the right-hand rule, see Figure 2.1. These frames are fixed to the link and the origin coincides with the enclosed joints. By considering the relative position and orientation of these two coordinate frames the link properties can be described. This implies in principle consideration of six degrees of freedom: three translations and three rotations.

The six degrees of freedom between these two local coordinate frames can

however be reduced using certain assumptions. Paul [Pau 81] for instance suggests that the orientation of a local coordinate frame should be chosen in such a way, that the local  $Z$ -axis coincides with the joint axis. With this assumption the description of the link properties can be reduced by considering the relative position and orientation of these two lines (i.e. the joint axes). This means that the minimum distance between these two lines and their angle, perpendicular on the minimum distance, have to be described [Mar 93].

Any link can be characterized by two parameters: the common normal distance  $a_n$  and the angle  $\alpha_n$  between the joint-axes in a plane perpendicular to  $a_n$ , see Figure 2.1. In general  $a_n$  is called the link length and angle  $\alpha_n$  the twist of the link [Pau 81]. The length of a link can be described by a vector

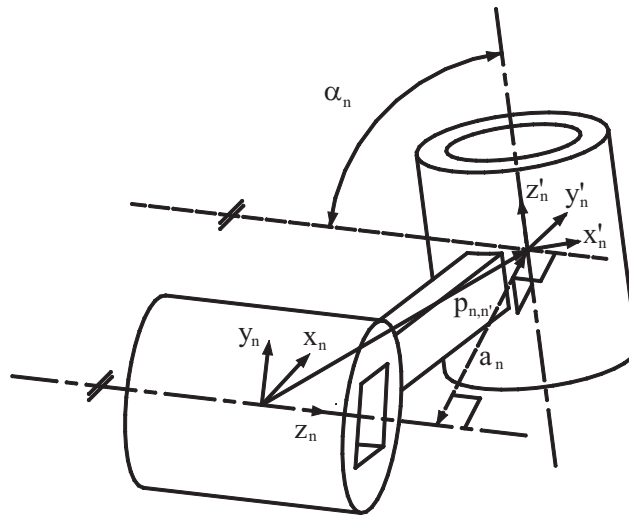


Figure 2.1: The length  $a_n$  and twist angle  $\alpha_n$  of a link  $n$ . Vector  $\mathbf{p}_{n,n'}$  describes the origin position of frame  $n'$  relative to frame  $n$ .

$\mathbf{p}_{n,n'}$  which starts at the origin of frame  $n$  and points to the origin of frame  $n'$ . The linkage twist angle  $\alpha_n$  can be accounted for by describing the relative orientation of frame  $n'$  with respect to frame  $n$  with rotation matrices  $\mathbf{R}_{n,n'}$  [Pau 81].

The majority of links found in existing multi-axis machines has a link twist angle equal to  $\pm 90^\circ$  due to an orthogonal configuration of the machine's axes. In such a case the description of the link parameters can be simplified considerably by assuming (convenient) frame orientations equal to the machine's coordinate frame. Although this frame orientation (used in this thesis) is just a choice from many equivalent possibilities, at least it should be stressed to use the selected frame orientation properly.

## 2.2 Modelling of joints

The links of a multi-axis machine are connected by joints. The number of joints is equal to the number of machine's axes and such a joint represents a prismatic or a revolute machine axis in this thesis (in some cases, it can be both [Ren 97]). The motion of the joint can be described by considering the assigned coordinate frames of the links that meet at that joint. For a rotational joint this implies a change in the relative orientation of these successive frames and a change in the relative position of the successive frame origins for a prismatic joint.

### 2.2.1 Revolute joints

In Figure 2.2 two linkages are drawn connected by a revolute joint. In this case the angle of rotation  $\theta$  is the joint variable. The direction of the joint axis (+Z, see Figure 2.2) is the direction along which the links rotate relatively. This

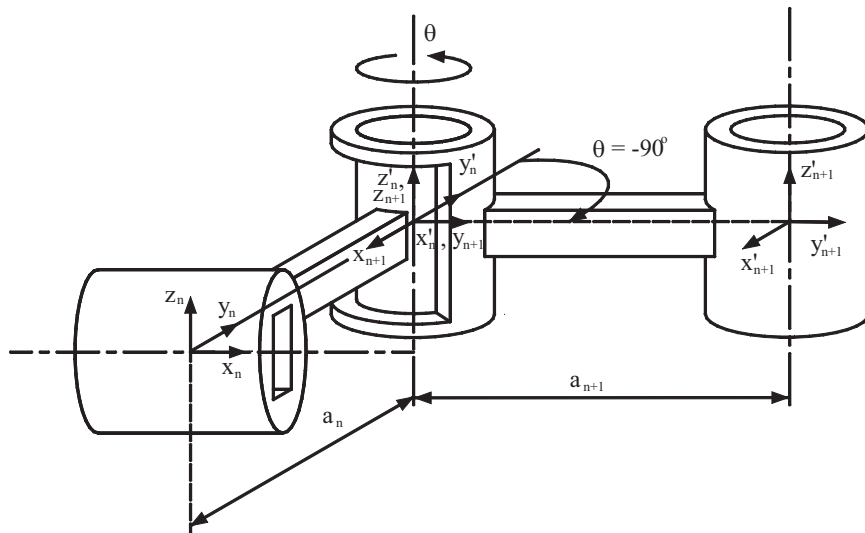


Figure 2.2: Two links connected by a revolute joint. Angle  $\theta$  is the joint variable affecting the proceeding frame orientations.

rotation can be described by considering the relative orientation of frame  $n + 1$  with respect to frame  $n$  at the respective joint. Therefore the following rotation matrix is introduced:

- Matrix  $\mathbf{R}_{n,n+1}(\theta)$  describes the orientation of coordinate frame  $n + 1$  relative to coordinate frame  $n$ .

This matrix describes the change in orientation of the successive frames from link  $n$  to link  $n + 1$ . For the opposite direction, the inverse rotation matrix has to be used which equals its transpose matrix:  $\mathbf{R}_{n+1,n}(\theta) = \mathbf{R}_{n,n+1}^{-1}(\theta) = \mathbf{R}_{n,n+1}^T(\theta)$  by definition [Mar 93][Str 88].

### 2.2.2 Prismatic joints

Links connected by a prismatic joint can translate along the direction of the axis. This implies that the distance between the origins of the link frames changes with the joint variable while the orientation of the connected link frames remains the same. In Figure 2.3 a prismatic joint is depicted. In this case one of the

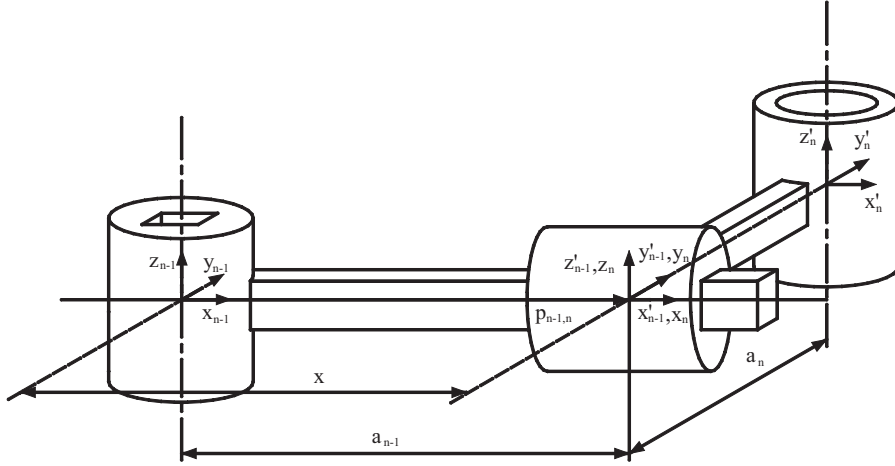


Figure 2.3: Links connected by a prismatic joint. Vector  $\mathbf{p}_{n-1,n}$  describes the origin position of frame  $n$  with respect to frame  $n - 1$  and its length changes with the joint variable  $x$ .

frame origins  $n - 1$  is fixed to the link (at the left hand-side, see Figure 2.3) and the other one to the prismatic joint, coinciding with the following coordinate frame origin  $n$ . The movement of the prismatic joint  $x$  can then be described by considering the relative position of successive frame origins. For this reason a vector  $\mathbf{p}_{n-1,n}(x)$  is introduced:

- Vector  $\mathbf{p}_{n-1,n}(x)$  describes the position of the origin of coordinate frame  $n$  relative to coordinate frame  $n - 1$ .

The length of vector  $\mathbf{p}_{n-1,n}(x)$  changes with the prismatic joint variable  $x$ . This way any prismatic joint movement can be described.

## 2.3 Machine configurations

Any multi-axis machine with a serial kinematic structure can be considered to consist of a number of links and joints. For the configuration or assembly of these links and joints, many possibilities exist. In Figure 2.4 some typical configurations of existing multi-axis machines are depicted. The configuration

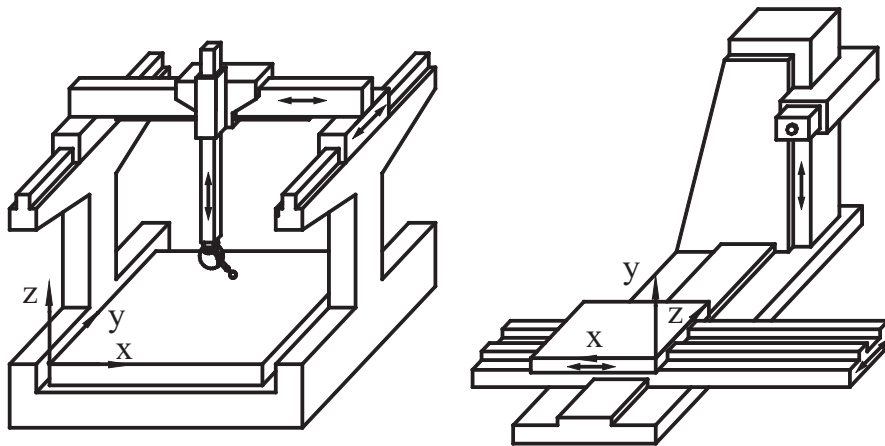


Figure 2.4: A moving bridge type CMM and a C-type milling machine.

of the machine's axis determines to a large extent the properties of a multi-axis machine. These properties therefore can differ significantly between several machine types due to a different sensitivity of the structural loop to various error sources. As a result, the machine's positioning accuracy depends among others on the machine type.

Besides the positioning accuracy also the accessibility of workpieces in the machine's workspace depends on the machine's configuration. A C-type (see right hand-side Figure 2.4) multi-axis machine for example offers good accessibility of workpieces (important for automation) although the positioning accuracy of a moving bridge type machine is generally better. Therefore the choice for a certain machine configuration depends on several factors (i.e. costs, accessibility, flexibility) not only on its positioning accuracy.

Due to the relative nature of tasks executed by multi-axis machines only the relative position of the end-effector with respect to the workpiece is relevant, not its absolute position in space. Therefore the machine's structural loop can be considered to be independent of the fixation of the machine to its environment. One end of the structural loop supports the end-effector (i.e. a probe, gripper, tool etc.) and the other end supports the workpiece. In between all the machine's joints and relevant links are present<sup>1</sup>. When constructing the

<sup>1</sup>Links between the machine's structural loop and its base for instance are not relevant.



machine's structural loop the following is required:

- Consider the relative location of the first machine axis as seen from the workpiece following successive machine parts;
- From this axis, consider the location of next axis etc.;
- Consider the end-effector location from the last machine's axis.

In this way any serial combination of revolute and prismatic axes can be described. In the next section this will be explained in more detail by means of an example.

For some machine configurations several chains seem to be present from workpiece to end-effector (see left-hand side Figure 2.4). Most of these chains however do not determine the end-effector position relative to the workpiece but support another axis. In the joints of such a chain, some degrees of freedom are released intentionally to avoid an over constrained machine construction. A typical example is a vertical support beam which is supported by an air-foot: it can only prescribe a certain height. Therefore the unique chain that determines the end-effector position relative to the workpiece must be considered when constructing a nominal machine model. This chain is also used by the machine itself when computing its end-effector position relative to the workpiece.

A special kind of machine configuration is a so-called Stewart platform or hexapod, receiving considerable attention recently [Tlu 99][Soo 97]. For such a machine the six linear axes are not connected serial but parallel. This results among others in complex geometric relationships between the six axis lengths and the end-effector position and orientation due to its design. The construction of a structural loop for this class of machines is beyond the scope of this thesis.

## 2.4 Nominal machine model

In this section a nominal machine model will be derived. This model describes the nominal position and orientation of the end-effector with respect to the workpiece (table)<sup>2</sup>. Since a (imaginary) workpiece is always fixed to the workpiece table (enforcing a fixed relationship between the local coordinate frames), the position of the end-effector with respect to the workpiece table will be considered here.

In order to demonstrate the kinematic modelling procedure presented, a five-axis milling machine will be modelled in this section. This machine is schematically depicted in Figure 2.5 and contains three translational axes and two rotary axes. The B-axis enables the workpiece table to rotate 360° in the horizontal XZ-plane and the C-axis has a range of ±60° enabling the tool to rotate in the vertical XY-plane. The range of the X-, Y- and Z-axis is 700 mm, 500 mm and 600 mm respectively resulting in a rather cubic shaped workspace of the multi-axis machine. Furthermore the machine's spindle can also be considered as a rotary axis but its angle of rotation is of no importance (unlike

---

<sup>2</sup>Another equivalent possibility is to use the tool point as point of view.

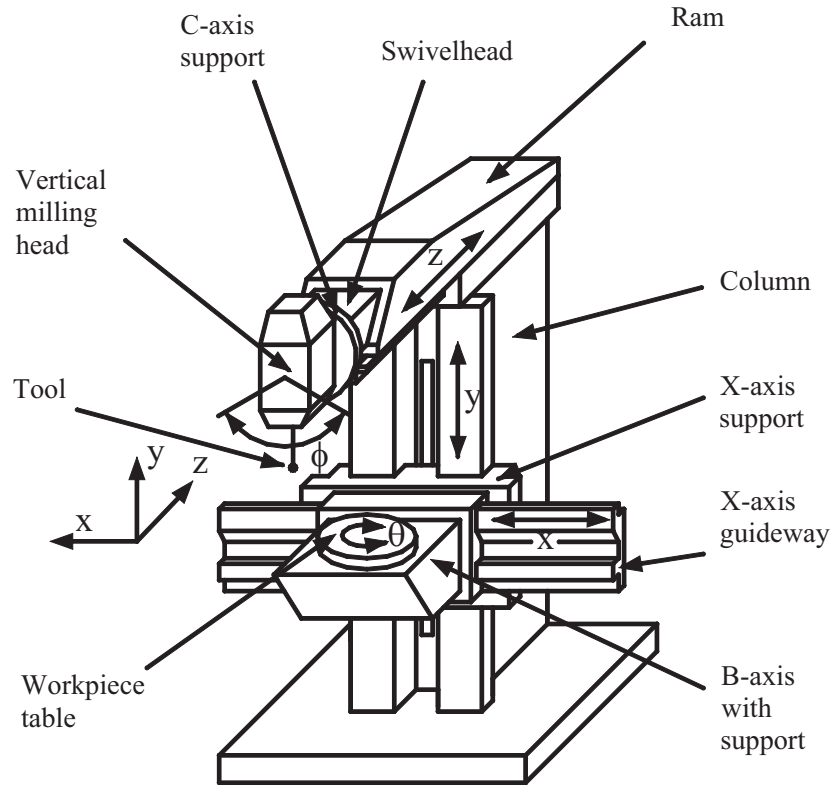


Figure 2.5: Schematic drawing of a Maho 700S five-axis milling machine and its main components with accompanying reference frame.

its rotatory speed) here and therefore the spindle unit itself is considered to be part of the vertical milling head.

In Figure 2.5 a coordinate frame is drawn on the left-hand side according to [ISO 841]. The orientation of this frame indicates how the workpiece table experiences movements of the tool on this machine.

The kinematic chain of the machine needs to be constructed by following the listed items of the previous section. This means that the relevant components between the workpiece and the end-effector have to be considered. For the Maho 700S milling machine this results in the following list:

- |    |                  |     |                        |
|----|------------------|-----|------------------------|
| 1: | Workpiece table; | 6:  | Ram;                   |
| 2: | B-axis support;  | 7:  | Swivelhead;            |
| 3: | X-axis guideway; | 8:  | C-axis support;        |
| 4: | X-axis support;  | 9:  | Vertical milling head; |
| 5: | Column;          | 10: | Tool.                  |

Due to the presence of the machine's axes, relative motions can be realised between these machine components. Some components however are connected rigidly. Regarding Figure 2.5 the (first) B-axis determines the orientation of the workpiece table relative to the B-axis support, the (second) X-axis changes the position of the B-axis support with respect to the X-axis guideway and the (third) Y-axis moves the X-axis support relative to the machine's column. Then the (fourth) Z-axis determines the position of the ram with respect to the column and finally the (fifth) C-axis rotates the vertical milling head relative to the C-axis support. In this way, several groups of machine components are identified and such a group will be modelled as one link according to Section 2.1. In general the number of links is equal to the number of machine's axes plus one.

In Figure 2.6 these links are drawn (as lines) with their local coordinate frames in a somehow exploded view where the joints have been omitted for clarity. The workpiece table is drawn with a dashed line. Since the local coor-

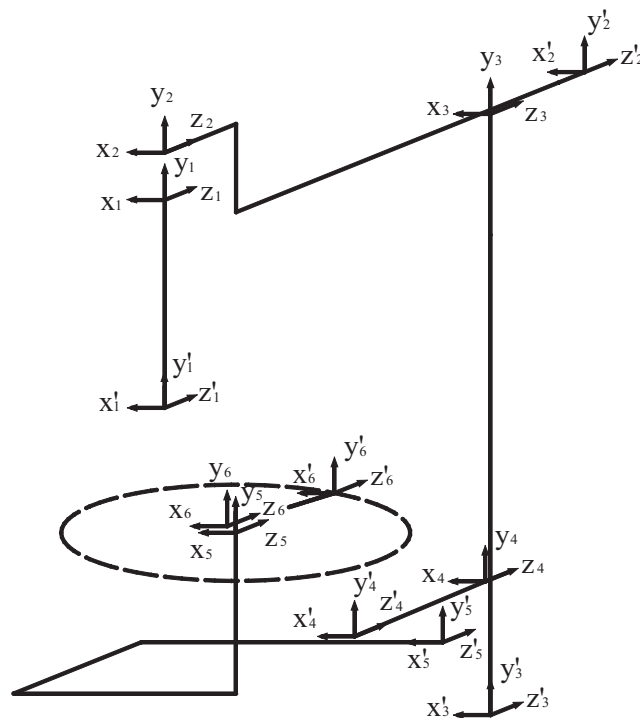


Figure 2.6: The links of a Maho 700S milling machine with local coordinate frames at each end of the link. The joints are omitted for clarity.

dinate frames all have the same orientation (by choice) due to convenient link twist angles (straight or inline), no rotation matrices are required for describing the link twist angle. Only the relative origin positions have to be considered in this case with vectors  $\mathbf{p}_{n,n'}$  as explained in Section 2.1. These vectors are obtained by using the dimensions of the specific machine components.

Regarding Figure 2.6 a part of a link is obviously present in the machine's kinematic chain but some part not and is therefore irrelevant. Examples of such redundant link parts are the backside of the ram and the part of the Y-axis below the B-axis support. Therefore only that part of a link has to be considered that is present in the machine's kinematic chain from workpiece table to tool.

In order to describe this chain, the machine's prismatic and revolute joints have to be considered next, see Section 2.2. The rotation angle  $\phi$  of the C-axis for instance can be described by considering the orientation of frame 1 with respect to frame 2, see Figure 2.5, 2.6. For the B-axis on the other hand this implies consideration of the orientation of frame 5 relative to frame 6 as a function of angle  $\theta$ . This results in the following rotation matrices:

$$\mathbf{R}_{2,1}(\phi) = \begin{pmatrix} \cos(\phi) & \sin(\phi) & 0 \\ -\sin(\phi) & \cos(\phi) & 0 \\ 0 & 0 & 1 \end{pmatrix}, \quad (2.1)$$

$$\mathbf{R}_{6,5}(\theta) = \begin{pmatrix} \cos(\theta) & 0 & -\sin(\theta) \\ 0 & 1 & 0 \\ \sin(\theta) & 0 & \cos(\theta) \end{pmatrix} \quad (2.2)$$

where matrix  $\mathbf{R}_{2,1}(\phi)$  describes a rotation along the local  $Z_2$ -axis and the rotation along the local  $Y_6$ -axis is described by matrix  $\mathbf{R}_{6,5}(\theta)$ . Since the remaining axes are connected by prismatic joints, the orientation of the other successive frames is identical:

$$\mathbf{R}_{3,2} = \mathbf{R}_{4,3} = \mathbf{R}_{5,4} = \mathbf{I}. \quad (2.3)$$

For describing the position of the machine's prismatic axes, the vectors describing the successive frame origins depend on the joint variable  $x$ ,  $y$  or  $z$ . In Figure 2.7 the machine's kinematic chain is drawn with vectors. This means in this case that vector  $\mathbf{p}_{3,2}$  depends on the  $Z$ -axis position, vector  $\mathbf{p}_{4,3}$  on the  $Y$ -axis position and vector  $\mathbf{p}_{5,4}$  is a function of the  $X$ -axis position, see Section 2.2. The length of the other vectors is constant. Since the tool vector is located at the end of the kinematic chain, the subscript is omitted. This tool vector is added directly to the proceeding vector representing the vertical milling head, denoted together as  $\mathbf{p}_1$ . Vector  $\mathbf{p}_1$  is defined relative to frame 1. Regarding

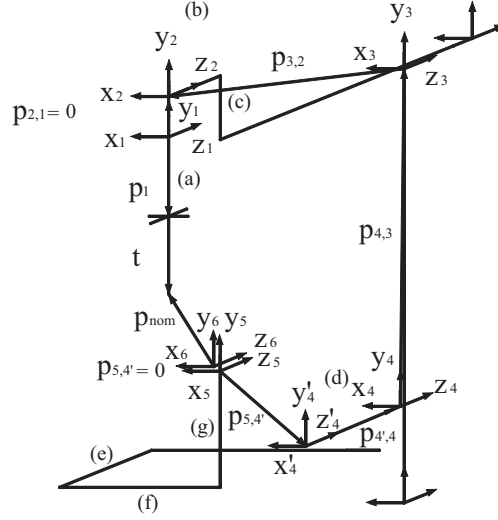


Figure 2.7: The kinematic chain of the Maho 700S described with vectors.

Figure 2.7 the following yields:

$$\mathbf{p}_1 = \begin{pmatrix} 0 \\ -a \\ 0 \end{pmatrix} + \mathbf{t}, \quad \mathbf{p}_{4',4} = \begin{pmatrix} 0 \\ 0 \\ +d \end{pmatrix}, \quad (2.4)$$

$$\mathbf{p}_{2,1} = \begin{pmatrix} 0 \\ 0 \\ 0 \end{pmatrix}, \quad \mathbf{p}_{5,4'} = \begin{pmatrix} f + x + o_x \\ -g \\ +e \end{pmatrix}, \quad (2.5)$$

$$\mathbf{p}_{3,2} = \begin{pmatrix} 0 \\ +c \\ z + o_z \end{pmatrix}, \quad \mathbf{p}_{6,5} = \begin{pmatrix} 0 \\ 0 \\ 0 \end{pmatrix}, \quad (2.6)$$

$$\mathbf{p}_{4,3} = \begin{pmatrix} 0 \\ y + o_y \\ 0 \end{pmatrix}, \quad (2.7)$$

where  $o_x$ ,  $o_y$  and  $o_z$  are offset values of the prismatic axes measurement systems. With these vectors the nominal tool position  $\mathbf{p}_{nom}$  relative to the workpiece table can be described stepwise. This means that the end point of the tool has to be described relative to frame 6 in this case.

Vector  $\mathbf{p}_1$  is defined with respect to frame 1. The following step is to describe this vector with respect to frame 2. This means that this vector has to be re-

oriented by multiplying this vector with matrix  $R_{1,2}(\phi)$ :

$$\begin{pmatrix} x_2 \\ y_2 \\ z_2 \end{pmatrix} = \mathbf{R}_{1,2}(\phi) \cdot \mathbf{p}_1. \quad (2.8)$$

The next step is to locate the origin position of frame 1 relative to frame 2. This is described by vector  $\mathbf{p}_{2,1}$  by definition<sup>3</sup>. By adding this vector to the re-oriented one, the end point of the tool relative to frame 2 becomes:

$$\begin{pmatrix} x_2 \\ y_2 \\ z_2 \end{pmatrix} = \mathbf{R}_{1,2}(\phi) \cdot \mathbf{p}_1 + \mathbf{p}_{2,1}. \quad (2.9)$$

This procedure has to be repeated until the (last) coordinate frame (no. 6) of the workpiece table has been reached:

1. Re-orient the tool vector for the next local coordinate frame by multiplying it with matrix  $\mathbf{R}_{n,n+1}$ ;
2. Add vector  $\mathbf{p}_{n+1,n}$  which describes the origin position of frame  $n$  with respect to frame  $n + 1$ .

Applying this on the chosen machine results in the following equations:

$$\begin{pmatrix} x_3 \\ y_3 \\ z_3 \end{pmatrix} = \mathbf{R}_{2,3} \cdot \begin{pmatrix} x_2 \\ y_2 \\ z_2 \end{pmatrix} + \mathbf{p}_{3,2}(z), \quad (2.10)$$

$$\begin{pmatrix} x_3 \\ y_3 \\ z_3 \end{pmatrix} = \mathbf{R}_{2,3}(z) \cdot (\mathbf{R}_{1,2}(\phi) \cdot \mathbf{p}_1 + \mathbf{p}_{2,1}) + \mathbf{p}_{3,2}(z), \quad (2.11)$$

$$\Downarrow \quad (2.12)$$

$$\begin{pmatrix} x_6 \\ y_6 \\ z_6 \end{pmatrix} = \mathbf{R}_{5,6}(\theta) \cdot \begin{pmatrix} x_5 \\ y_5 \\ z_5 \end{pmatrix} + \mathbf{p}_{6,5}. \quad (2.13)$$

This last relation describes the position of the end of the tool with respect to the workpiece table. Since most rotation matrices equal the identity matrix and some vectors  $\mathbf{p}_{n+1,n}$  are constant, this last expression can be written as:

$$\mathbf{p}_{nom} = \mathbf{R}_{5,6}(\theta) \cdot (\mathbf{R}_{1,2}(\phi) \cdot \mathbf{p}_1 + \mathbf{p}_{2,1} + \mathbf{p}_{3,2}(z) + \mathbf{p}_{4,3}(y) + \dots \dots + \mathbf{p}_{4',4} + \mathbf{p}_{5,4'}(x) + \mathbf{p}_{6,5}) \quad (2.14)$$

which is the equation sought.

The orientation of the tool (coordinate frame 1) with respect to the workpiece table (coordinate frame 6) is just the multiplication of all the successive rotation matrices:

<sup>3</sup>Since vector  $\mathbf{p}_{2,1}$  (and  $\mathbf{p}_{6,5}$ ) belongs to a rotary axis, it has no length.

$$\mathbf{R}_{6,1}(\phi, \theta) = \mathbf{R}_{2,1}(\phi) \cdot \mathbf{R}_{3,2} \cdot \mathbf{R}_{4,3} \cdot \mathbf{R}_{4',4} \cdot \mathbf{R}_{5,4'} \cdot \mathbf{R}_{6,5}(\theta). \quad (2.15)$$

At this point relations have been obtained for describing the nominal position and orientation of the tool with respect to the workpiece table. The method presented can be applied for modelling any multi-axis machine regardless of the number and serial sequence of translational and rotary axes.

Summarizing, rigid body kinematics in combination with a (sign) convention for the local coordinate frames is required for constructing such a nominal machine model. This however can be realized in many equivalent ways: the method presented is one of them and will be used later on this thesis.

## Chapter 3

# Modelling and measurement of geometrical errors

Geometrical errors of multi-axis machines are errors due to deviations between the actual and nominal dimensions and geometry of elements supporting the mechanical chain from workpiece to end-effector. This chapter deals with the modelling and measurement, based on length measurements, of this kind of errors of multi-axis machines with a serial kinematic structure.

### 3.1 Geometric error modelling

This chapter is divided into two interrelated sections. The first section deals with the modelling procedure of geometrical errors of multi-axis machines. This means that a geometrical error model is developed describing the relative positioning behaviour of the end-effector with respect to the workpiece. In this model the error components are described by parametric functions. The parameters present in these functions are later determined by fitting length measurement data, as will be discussed in Chapter 4.

In the second section, the measurement of geometrical errors is discussed using 3D length measurements performed throughout the machine's workspace. After dealing with the relevant measurement conditions for determining geometrical errors, a DBB length measurement model is derived. This model relates the measured length deviation to the positioning error of the machine. Furthermore a measurement setup is presented prescribing the spatial distribution of the length measurements to be performed. These measurements can be executed within three hours.

The geometrical error model proposed can be used for acceptance tests, quality control and (software) error compensation techniques of multi-axis machines



[Flo 98] [Flo 01]. Also possibilities for diagnostic purposes (i.e. error tracing) are available with this model [Flo 00] [Flo 01].

In order to obtain a geometrical error model, first the errors of a machine axis have to be considered, which is subject of the next section.

### 3.1.1 Axis errors

When a slide moves along its guideway, only one degree of freedom is supposed to be free while the other directions of translation and rotation are constrained by the construction. Often a closed loop feedback system is employed to control this motion numerically (i.e. CNC controlled machines). Besides the intended motion, also erroneous slide displacements and rotations do occur. Generally these deviations are small compared to the (controlled) motion or rotation of the axis. However, the positioning accuracy of the guideway system and/or multi-axis machine containing these axes can be affected significantly. These deviations are due to imperfections of the slide guideway system. Also the accuracy of the measuring systems used is of major importance. Besides the error motions of an axis itself, also the mutual alignment error between these axes (a squareness error) has to be taken into account when considering the positioning accuracy of a multi-axis machine. All these errors, the so-called parametric errors, are responsible for differences between the actual and nominal position and orientation of an end-effector relative to a certain reference.

The deviations of a slide guideway system can be divided in three translational and three rotational errors. In Figure 3.1 these error components are depicted according to the VDI 2617 guideline for a prismatic and a rotary axis (see also [DIN 66217] [ISO 841] for rotary axes). According to this definition the rotary axis around the X, Y or Z-axis is denoted respectively as A, B or C-axis. The first character denotes the axis of translation respectively rotation, the second one the type of error (t for translational, r for rotational) and the third one the direction along/around which the error is acting. These error components will be discussed briefly here including their conventional measurement technique, ending with squareness errors (not drawn in Figure 3.1). Extensive information about definitions, measurement procedures and conditions, suitable measuring instruments etc. can be found in [ISO 230-1].

#### Translational axis errors

The error motions of a translational machine axis (a Y-axis in this case) can be categorised as (see Figure 3.1):

1. Displacement, linearity errors (i.e.  $yty$ );
2. Straightness errors (i.e.  $ytx, ytz$ );
3. Roll errors (i.e.  $yry$ );
4. Pitch and yaw errors (i.e.  $yrx, yrz$ ).

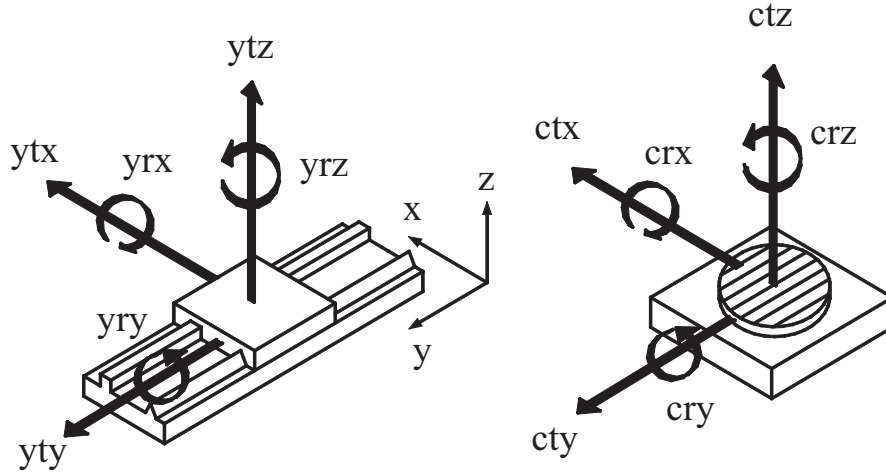


Figure 3.1: Errors of a prismatic (Y) and rotary (C) axis denoted according to VDI 2617 guideline.

The three translational errors of a prismatic axis can be divided into displacement and straightness errors. The displacement error is the error acting in the line of motion of the axis (i.e.  $yty$ ) and equals the difference between the actual and nominal axis position. If the measurement system axis coincides with the axis of movement (and assuming an infinite positioning resolution), this displacement error just equals the measurement system error or scale error. Due to the (hardware) construction of an axis however, often an offset distance is present between the axis of movement and the axis of measurement, determined in a plane perpendicular to the axis of motion. This distance is usually referred to as ‘Abbe offset’. Ernst Abbe realized that the displacement error is affected by unwanted angular motions of the axis moving elements (to the first order). If such an Abbe offset exists, the machine’s displacement error can be approximated by the product of the angular error with its Abbe offset, added to the scale error [Abb 1890]. For the measurement of this displacement error, a wide range of position measuring instruments are available e.g. laser interferometers [Sch 93], linear encoders.

Straightness errors are defined as lateral displacement errors of a slide guideway system perpendicular to the line of displacement with respect to a (arbitrary) straight line. Straightness errors of an axis are generally described with two error components perpendicular to each other and both perpendicular to the line of axis motion ( $ytx, ytz$  in Figure 3.1). Besides a laser interferometer with straightness optics, a straight edge (used as a straight reference) in combination with a displacement transducer can be used to measure a straightness error during axis motion. For the fixation of the straight edge and displacement transducer to the various elements of the axis, see [Soo 93]. Reversal techniques

can be applied to remove errors in the straight edge itself in order to increase the accuracy of the straightness measurement [Eva 96].

Besides translational errors, a slide guideway system possesses also small rotational error motions. A roll error is defined as a rotation error of an axis acting around the line of motion ( $ryr$  in Figure 3.1). In case of a horizontal axis this kind of error motion can be measured with two (electronic) levels each positioned at the two bodies, which are in relative movement (i.e. the slide and the guideway). The measurement of a roll error of a vertical axis is more troublesome but can be extracted from two vertical straightness measurements with a known and sufficient offset distance between these two measurements [Sch 93]. Roll errors cannot be measured with a laser interferometer.

Besides roll error motion, a slide guideway system possesses also pitch and yaw errors. These rotational errors occur perpendicular to the line of motion ( $rxr, yrz$  in Figure 3.1). Like straightness errors, these rotational errors can be described with two error components perpendicular to each other. This kind of error can be measured with a laser interferometer using rotation optics, electronic levels or with an autocollimator in combination with a plane mirror [Sch 93] [Sch 00].

### Squareness errors

A special kind of rotation error, a squareness error, will be discussed here. A squareness error represents the alignment error between two nominal orthogonal machine's axes and is expressed as a constant rotation angle by definition. According to the VDI 2617 guideline, such an error is denoted by a 'w' in between the characters denoting the machine's axes considered: the squareness error between the X- and Y-axis for example is denoted by  $xwy$ . The result of a squareness error is a lateral displacement linear with axis position, transforming a perfect square into a parallelogram<sup>1</sup>. In order to describe the squareness errors between the X-, Y- and Z-axis, denoted by  $xwy$ ,  $xwz$  and  $ywz$  respectively, rotational error components are used. This implies that a squareness error is described as the constant part of a specific rotational error component. The squareness error between a Y- and a Z-axis for example ( $ywz$ ) can be described as the constant part of error component  $zrx(z)$ :

$$zrx(z) = zrx'(z) + ywz \quad (3.1)$$

with  $zrx'(z)$  describing the Z-axis' pitch angle around the X-axis varying with axis position.

A squareness error can be measured using a laser interferometer (with a pentagon prism used as an optical square) but this is somehow troublesome due to the complex alignment procedure. The application of a calibrated square block in combination with displacement transducers is therefore preferable, resulting in two lateral displacement measurements with a known angle in between. The squareness error is then calculated as the angle between the least squares regression lines of the two measurements performed on the straight edge, since

<sup>1</sup>In the three-dimensional case, a cubic is transformed into a parallelepiped.

the axes are assumed as perfectly straight [ISO 230-1]. Reversal techniques can be applied to eliminate errors of the square block [Eva 96].

### Rotary axis errors

In Figure 3.1 a C-axis is depicted, which rotates along the Z-axis. Like for a translational axis, error motions of a rotary axis can be identified, see [ISO 230-1]. Typical examples of such error motions are, assuming the presence of a measurement system:

1. Scale errors (i.e.  $crz$ );
2. Tilt errors (i.e.  $crx, cry$ );
3. Axial errors (i.e.  $ctz$ );
4. Radial errors (i.e.  $ctx, cty$ ).

Periodic functions can for instance be used for describing the periodic (or synchronous) error motions of a rotary axis.

The scale error of a rotary axis is defined as the difference between the actual and nominal (actuated) rotation angle of the axis. Such a difference can be described with error component  $crz$  for the example shown in Figure 3.1. A scale error can be measured accurately with a autocollimator in combination with a calibrated polygon mirror [ISO 230-1] or with a laser interferometer.

Tilt errors are due to a change in the orientation of the axis of rotation (represented by its centreline) while rotating. Such an error can be described with error components  $crx$  and  $cry$ . Tilt errors can be determined by performing radial displacement measurements on different positions on the axis' centreline while rotating the axis. Another possibility is to perform axial displacement measurements on a flat surface (mounted on the rotation axis) with a certain distance from the axis' centreline while rotating the axis [ISO 230-1].

Axial errors result in a displacement of the rotated surface along the axis' centreline. Generally such an error consists of a constant part (axis displacement) and a periodic part, responsible for axial slip during rotation. Such an axial error can be determined by measuring the axial displacement of the rotary axis with a displacement transducer, performed on the axis' centreline.

Besides translational errors in axial direction, a rotary axis also possesses errors in a plane perpendicular to its centreline. Such a radial error can be described with error components  $ctx$  and  $cty$ . This kind of errors can be determined by performing displacement measurements in radial direction while rotating the axis.

Finally a squareness error can be considered as describing the constant orientation error of the axis' centreline with respect to another machine's axis. In [ISO 230-1] such errors are formally referred to as coaxiality and/or errors in parallelism dependent on the configuration of the axes and the specific measurement procedure. Such an error can be regarded as a constant tilting error. To describe such a squareness, coaxiality or parallelism error (for instance  $cwx$ ), error components  $crx$  and  $cry$  can be used, both modelled as a constant.

### 3.1.2 Error component functions

In principle the error components discussed in the previous section are not known. These error components are not necessarily constant but can vary with axis position. Therefore parametric functions will be derived here for describing this dependency. In this thesis only the error component functions of translational axes are presented; the formulation of the rotary axis error component functions is beyond the scope of this thesis.

These error component functions contain unknown parameters (i.e.  $\beta$ ) that will be determined from measurement data later on, as will be discussed in Chapter 4. The following parametric functions have been considered for describing the unknown error components of a multi-axis machine, see Appendix C. The choice of these functions is based on the ability of the functions to describe the behaviour of the error components with axis position:

1. Ordinary polynomials;
2. Piecewise polynomials (splines);
3. Orthogonal polynomials;
4. Fourier functions.

In Appendix C the application of piecewise polynomials, orthogonal (Legendre) polynomials and Fourier functions for describing error components is discussed. Summarizing, several parametric functions can be applied for describing the error components of a multi-axis machine with each their own characteristics. Here ordinary polynomials have been used for modelling the error components of a milling machine. When using alternative error component functions for this machine no advantages over applying ordinary polynomials have been observed: therefore ordinary polynomials are preferred and used due to their simplicity.

Squareness errors represent the alignment error angle between two machine's prismatic axes. The number of squareness errors of a multi-axis machine containing  $n$  axes equals:

$$\frac{n(n-1)}{2}$$

as obtained by considering the number of relevant combinations between the machine's  $n$  axes. By definition a squareness error is modelled as a constant angular error, to be described by a parameter. Considering a machine with three axes, say X, Y and Z, the following yields for its squareness errors:

$$i w_j(\beta) = \beta_{i w_j} \quad \begin{cases} i, j \in \{X, Y, Z\} \\ i \neq j \end{cases} \quad (3.2)$$

where parameter  $\beta_{i w_j}$  represents the squareness error angle between axis  $i$  and  $j$ . These error components are added to the corresponding rotational error component, varying with axis position according to Equation 3.1.

For describing the errors of the measurement system of a translational axis, ordinary polynomials can be used for example. This means that the scale error of for instance an X-axis (denoted by  $xtx$ ) can be modelled this way as:

$$xtx(x, \beta) = \sum_{j=1}^m \beta_{xtx_j} (x - x_0)^j \quad (3.3)$$

where  $x$  represents the nominal axis position,  $x_0$  the centre position of the X-axis and  $\beta_{xtx_j}$  unknown parameters, necessary for describing this error component. The regressor variables of the polynomials are centred to the middle of the machine's workspace in order to alleviate ill-conditioning of the design matrix when estimating the machine error model parameters  $\beta$  [Mon 92]. Due to the relative nature of tasks executed by multi-axis machines a constant term is omitted in the polynomial. If such a term would be added, it would represent a constant shift of the measurement system and this does not affect the positioning accuracy of a multi-axis machine: the entire workpiece will be milled or measured on a slightly different location in the machine's workspace equal to this shift.

The rotational error components ( $irj$  with  $i, j \in \{X, Y, Z\}$ ) are modelled in a similar way as the linearity error components.

Finally the application of ordinary polynomials for describing straightness errors has to be discussed. Since a straightness error represents the lateral displacement error of an axis with respect to a line, it cannot be described by a function linear with axis position due to its definition. Therefore the straightness errors are modelled as, with  $xty$  used as example<sup>2</sup>:

$$xty(x, \beta) = \sum_{j=2}^m \beta_{xty_j} (x - x_0)^j. \quad (3.4)$$

Although a lateral displacement measurement of an axis in general reveals a displacement linear with axis position, this is not accounted for by a straightness error component. Since such a displacement is the result of a misalignment error between the machine's axes, this effect is covered by the squareness error components.

At this point all the error components have been modelled with ordinary higher order polynomials with exception of the squareness errors, which are modelled by a constant. The selection of the polynomial order will be dealt with in Chapter 4 when optimising the machine error model.

### 3.1.3 Error propagation

In the previous section, the error components have been modelled with parametric functions. Here the influence of these error components on the positioning behaviour of a multi-axis machine will be considered. This means that relations are derived to compute the effect of an error component on the positioning and

<sup>2</sup>A constant term is omitted for the same reason as for the scale errors.

orientation error of the end-effector  $\xi_u$  with respect to the workpiece (table), see Figure 1.1. In this chapter this error vector is approximated by a geometrical error model, formulated in mathematical terms as:

$$\xi_u \approx \hat{\xi}_u = \begin{bmatrix} \hat{\xi}_u^t \\ \hat{\xi}_u^r \\ \hat{\xi}_u^u \end{bmatrix} = f(xtx(x), xty(x), \dots, ywz). \quad (3.5)$$

In this section, this function will be derived stepwise. As stated in the Introduction, the error vector  $\xi_u$  depends on the current state of the machine. When considering geometrical errors, this state is completely defined by the machine's nominal axis positions i.e.  $X, Y, Z, A, B, C$  and the vector describing the dimensions of the current end-effector, as stored in vector  $\mathbf{t}$ . Therefore the (geometrical) nominal state of a multi-axis machine is completely described by the following two vectors:

$$\mathbf{u} = (X, Y, Z, A, B, C),$$

$$\mathbf{t} = \begin{pmatrix} t_x \\ t_y \\ t_z \end{pmatrix}$$

with  $\mathbf{u}$  containing the nominal axis positions. In order to demonstrate the error propagation in multi-axis machines with a serial kinematic structure, a five-axis milling machine with axes  $X, Y, Z, B, C$  will be used as an example (see Chapter 2, Section 2.4).

The error components, as discussed in the previous section, are small compared to the nominal dimensions of the multi-axis machine. The magnitude of translational errors is typically  $0.1 - 100 \mu\text{m}$  and of rotational errors  $1 - 100 \mu\text{rad}$  for existing multi-axis machines. To obtain the effect of an error component on the machine's positioning error, rigid body kinematics are used, where only the first order terms are taken into account here. So for an orientation error  $\varepsilon$  of an axis the following approximation is applied:

$$\cos(\varepsilon) \simeq 1,$$

$$\sin(\varepsilon) \simeq \varepsilon.$$

The shortening  $\Delta\ell$  of an axis due to an orientation error  $\varepsilon$  equals  $\ell(1 - \cos(\varepsilon)) \simeq \frac{1}{2}\varepsilon^2 \cdot \ell$ . Due to small values of  $\varepsilon$  this shortening is usually negligible. For machining centres, the second order terms are generally much smaller than the resolution of the measurement systems employed (typically  $0.1 - 1.0 \mu\text{m}$ ) and therefore it is useless to take these higher order terms into account. Higher order effects are taken into account only when these terms cannot be neglected. When an extreme accuracy is required this might even be necessary, for instance when modelling a wafer-stepper/scanner.

In order to compute the influence of an error component on the relative end-effector positioning and orientation error, a distinction has to be made between translational and rotational error components. A translational error component on one hand is reflected directly in the relative end-effector position.

If a multi-axis machine contains at least one rotary axis, also the orientation of the translational error component with respect to the workpiece (table) has to be taken into account since the direction of the error can change relative to the workpiece.

For obtaining the contribution of a rotational error component on the machine's positioning error on the other hand a certain offset arm (an 'Abbe offset') has to be taken into account. The resulting displacement is then calculated by multiplying this rotation with its relevant offset arm as visualised in Figure 3.2 for an axis  $i$ . In this figure the resulting positioning error  $\xi_i^t$  is drawn (in ex-

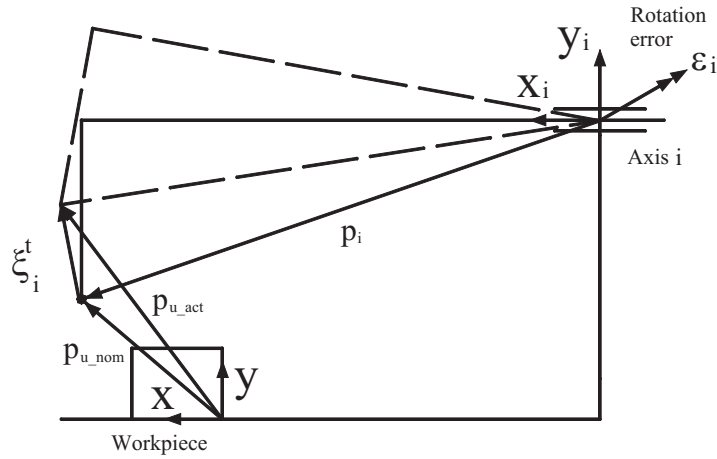


Figure 3.2: The effect of a rotational error component  $\epsilon_i$  with offset arm  $\mathbf{p}_i$  on the positioning error  $\xi_i^t$  of an axis  $i$ .

treme) for an orientation error  $\epsilon_i$ . The corresponding arm of rotation is denoted by  $\mathbf{p}_i$  and is defined with respect to the local coordinate frame  $i$ :  $\mathbf{p}_i$  starts at the joint of the axis and points towards the endpoint of the end-effector. Expanding this into the three-dimensional case, the resulting positioning error  $\xi_i^t$  due to an rotational error component  $\epsilon_i$  can be computed as the cross product between the arm of rotation and the rotational error components, both stored in a vector:

$$\xi_i^t = \begin{pmatrix} \xi_x \\ \xi_y \\ \xi_z \end{pmatrix}_i = \begin{pmatrix} \epsilon_x \\ \epsilon_y \\ \epsilon_z \end{pmatrix}_i \times \begin{pmatrix} p_x \\ p_y \\ p_z \end{pmatrix}_i = \epsilon_i \times \mathbf{p}_i. \quad (3.6)$$

In order to take the contribution of the rotational error components on the machine's positioning error into account, the offset arms have to be determined first. Besides these arms of rotation, also a rotation matrix definition is required necessary to describe the effect of rotary axes present in the machine's structural loop, since the relative orientation between local coordinate frames (see Figure 2.6 and 2.7) can change. Therefore the following definitions are stated:



- Vector  $\mathbf{p}_i$  describes the position of the end-effector relative to coordinate frame (joint)  $i$ ;
- Matrix  $\mathbf{R}_i$  describes the orientation of local coordinate frame  $i$  with respect to that of the workpiece table.

In Figure 3.3 these  $\mathbf{p}_i$  vectors are drawn for a five axis milling machine (see also Figure 2.6 and 2.7) including the local coordinate frames of the corresponding machine's axes. The error components are defined with respect to these local

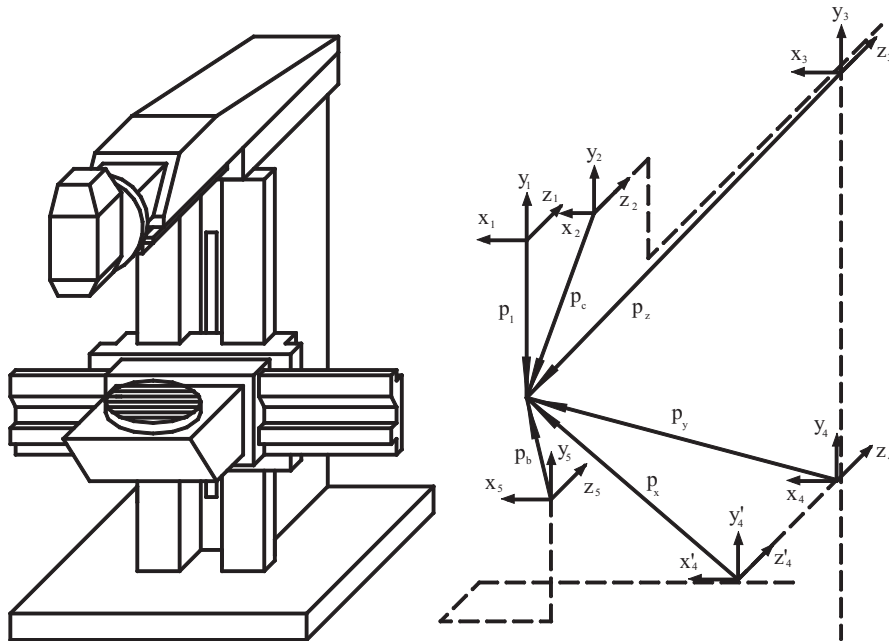


Figure 3.3: Five-axis milling machine with corresponding kinematic model containing vectors  $\mathbf{p}_i$ .

coordinate frames. The origin of such a local coordinate frame is located at the point where two machine's axes meet (i.e. at the joint, see Figure 3.3). This means that the error components of the C-axis are described relative to frame 2, the error components of the Z-axis with respect to frame 3 etc.

The vectors  $\mathbf{p}_i$ , shown in Figure 3.3 start at the origin of local coordinate frame  $i$  pointing towards the end of the tool. In order to describe such a vector  $\mathbf{p}_i$  with respect to the corresponding local coordinate frame (i.e. describe vector  $\mathbf{p}_z$  relative to coordinate frame 3) the 'preceding vectors' are re-oriented for successive coordinate frames, as will be explained here stepwise (see also Chapter 2, Section 2.4). For the mathematical description of these  $\mathbf{p}_i$  vectors,

the vectors  $\mathbf{p}_{i,j}$ <sup>3</sup>, as introduced in Chapter 2 Section 2.4, are used.

Vector  $\mathbf{p}_1$  is defined relative to frame 1 by definition and contains the tool vector  $\mathbf{t}$ . The next step is to describe this vector relative to frame 2. This can be computed by pre-multiplying vector  $\mathbf{p}_1$  with rotation matrix  $\mathbf{R}_{2,1}$ . Then vector  $\mathbf{p}_{2,1}$  is added, which is described relative to frame 2 by definition (and indicates the position of frame 1). This procedure is repeated until the respective local coordinate frame is reached. Due to the definitions of the rotation matrices  $\mathbf{R}_{i,j}$ <sup>4</sup>,  $\mathbf{R}_i$  and vectors  $\mathbf{p}_{i,j}$ ,  $\mathbf{p}_i$  the derivation of the vectors  $\mathbf{p}_i$  becomes straightforward. In order to generalize their formulation, all the rotation matrices  $\mathbf{R}_{i,j}$  and the vectors  $\mathbf{p}_{i,j}$  are considered as a function of the actual axis positions as stored in  $\mathbf{u}$  although this is not always necessarily true (i.e. most rotation matrices equal  $\mathbf{I}$  except  $\mathbf{R}_{2,1}$  and  $\mathbf{R}_{6,5}$  see Chapter 2, Section 2.4):

$$\begin{aligned}\mathbf{p}_c(\mathbf{u}, \mathbf{t}) &= \mathbf{R}_{2,1}^T(\mathbf{u}) \cdot \mathbf{p}_1(\mathbf{u}, \mathbf{t}) + \mathbf{p}_{2,1}(\mathbf{u}), \\ \mathbf{p}_z(\mathbf{u}, \mathbf{t}) &= \mathbf{R}_{3,2}^T(\mathbf{u}) \cdot \mathbf{p}_c(\mathbf{u}, \mathbf{t}) + \mathbf{p}_{3,2}(\mathbf{u}), \\ \mathbf{p}_y(\mathbf{u}, \mathbf{t}) &= \mathbf{R}_{4,3}^T(\mathbf{u}) \cdot \mathbf{p}_z(\mathbf{u}, \mathbf{t}) + \mathbf{p}_{4,3}(\mathbf{u}), \\ \mathbf{p}_x(\mathbf{u}, \mathbf{t}) &= \mathbf{R}_{4',4}^T(\mathbf{u}) \cdot \mathbf{p}_y(\mathbf{u}, \mathbf{t}) + \mathbf{p}_{4',4}(\mathbf{u}), \\ \mathbf{p}_b(\mathbf{u}, \mathbf{t}) &= \mathbf{R}_{5,4'}^T(\mathbf{u}) \cdot \mathbf{p}_x(\mathbf{u}, \mathbf{t}) + \mathbf{p}_{5,4'}(\mathbf{u}).\end{aligned}$$

At this point the corresponding arms of rotation of the rotational error components have been derived, necessary for computing the resulting relative displacement error of the tool according to Equation 3.6.

Due to the possible presence of rotary axes in the machine's structural loop, the orientation of the error components relative to the workpiece (table) frame can change. In order to take the effect of these rotary axes into account, the introduced matrices  $\mathbf{R}_i$  will be derived here. With these matrices, the error components can be re-oriented with respect to the workpiece (table). Due to the definitions of rotation matrices  $\mathbf{R}_{i,j}$ , the matrices  $\mathbf{R}_i$  can be obtained directly by multiplying the relevant matrices  $\mathbf{R}_{i,j}$  of the corresponding part of the machine's structural loop (beginning at the workpiece table):

$$\begin{aligned}\mathbf{R}_b(\mathbf{u}) &= \mathbf{R}_{6,5}(\mathbf{u}), \\ \mathbf{R}_x(\mathbf{u}) &= \mathbf{R}_{5,4'}(\mathbf{u}) \cdot \mathbf{R}_{6,5}(\mathbf{u}), \\ \mathbf{R}_y(\mathbf{u}) &= \mathbf{R}_{4',4}(\mathbf{u}) \cdot \mathbf{R}_{5,4'}(\mathbf{u}) \cdot \mathbf{R}_{6,5}(\mathbf{u}), \\ \mathbf{R}_z(\mathbf{u}) &= \mathbf{R}_{4,3}(\mathbf{u}) \cdot \mathbf{R}_{4',4}(\mathbf{u}) \cdot \mathbf{R}_{5,4'}(\mathbf{u}) \cdot \mathbf{R}_{6,5}(\mathbf{u}), \\ \mathbf{R}_c(\mathbf{u}) &= \mathbf{R}_{3,2}(\mathbf{u}) \cdot \mathbf{R}_{4,3}(\mathbf{u}) \cdot \mathbf{R}_{4',4}(\mathbf{u}) \cdot \mathbf{R}_{5,4'}(\mathbf{u}) \cdot \mathbf{R}_{6,5}(\mathbf{u}).\end{aligned}$$

These matrices describe the orientation of frame  $i$  with respect to the workpiece table frame (as indicated by no. 6 in Figure 2.6 and 2.7).

At this point, relations describing the influence of an error component on the machine's positioning behaviour can be derived stepwise. This means that an equation is needed describing how the error components of an axis  $i$  affect the position and orientation of the tool with respect to the workpiece table. In Figure 1.1 the tool positioning and orientation error is depicted and this vector is defined with respect to the workpiece table frame. The modelled positioning

<sup>3</sup>Vector  $\mathbf{p}_{i,j}$  describes the position of the origin of coordinate frame  $j$  relative to frame  $i$ .

<sup>4</sup>Matrix  $\mathbf{R}_{i,j}$  describes the orientation of coordinate frame  $j$  relative to frame  $i$

error due to the error components of an axis  $i$  is then denoted by  $\hat{\xi}_i^t$ . The error components however are defined relative to the corresponding local coordinate frame and therefore need to be re-oriented according to the workpiece table frame (by means of  $\mathbf{R}_i(\mathbf{u})$ ).

In order to derive the error propagation equation, the machine's positioning error  $\hat{\xi}_i^t$  is considered first. Consider the translational error components to be stored in an introduced vector  $\mathbf{e}_i(\mathbf{u}, \beta)$  and the rotation error components in a vector  $\boldsymbol{\varepsilon}_i(\mathbf{u}, \beta)$  belonging to axis  $i$ :

$$\mathbf{e}_i(\mathbf{u}, \beta) = \begin{pmatrix} itx(\mathbf{u}, \beta) \\ ity(\mathbf{u}, \beta) \\ itz(\mathbf{u}, \beta) \end{pmatrix}, \quad \boldsymbol{\varepsilon}_i(\mathbf{u}, \beta) = \begin{pmatrix} irx(\mathbf{u}, \beta) \\ iry(\mathbf{u}, \beta) \\ irz(\mathbf{u}, \beta) \end{pmatrix}$$

with  $i \in \{X, Y, Z, A, B, C\}$ . The machine's positioning error then can be considered to consist of two summed parts; one part results from the translational error components and the other part from the effect of the rotational error components, see Figure 3.2 and Equation 3.6:

$$\hat{\xi}_i^t(\mathbf{u}, \mathbf{t}, \beta) = \mathbf{e}_i(\mathbf{u}, \beta) + \boldsymbol{\varepsilon}_i(\mathbf{u}, \beta) \times \mathbf{p}_i(\mathbf{u}, \mathbf{t}). \quad (3.7)$$

This sum, describing the resulting positioning error, then has to be re-orientated from frame  $i$  to the workpiece table frame. The latter is computed by pre-multiplying this sum with the inverse of matrix  $\mathbf{R}_i$  (which equals  $\mathbf{R}_i^T$ ) as can be derived from its definition:

$$\hat{\xi}_i^t(\mathbf{u}, \mathbf{t}, \beta) = \mathbf{R}_i^T(\mathbf{u}) \cdot \{\mathbf{e}_i(\mathbf{u}, \beta) + \boldsymbol{\varepsilon}_i(\mathbf{u}, \beta) \times \mathbf{p}_i(\mathbf{u}, \mathbf{t})\}. \quad (3.8)$$

This equation describes the effect of the error components on the machine's relative positioning error  $\hat{\xi}_i^t$ .

The relative end-effector's orientation error  $\hat{\xi}_i^r$  due to axis  $i$  is equal to the rotational error components, taking their orientation into account in a similar way as for the machine's positioning error vector:

$$\hat{\xi}_i^r(\mathbf{u}, \beta) = \mathbf{R}_i^T(\mathbf{u}) \cdot (\boldsymbol{\varepsilon}_i(\mathbf{u}, \beta)). \quad (3.9)$$

Summarizing, the machine's relative positioning and orientation error due to the error components of an axis  $i$  are denoted as:

$$\hat{\xi}_i(\mathbf{u}, \mathbf{t}, \beta) = \mathbf{R}_i^T(\mathbf{u}) \cdot \begin{bmatrix} \mathbf{e}_i(\mathbf{u}, \beta) + \boldsymbol{\varepsilon}_i(\mathbf{u}, \beta) \times \mathbf{p}_i(\mathbf{u}, \mathbf{t}) \\ \boldsymbol{\varepsilon}_i(\mathbf{u}, \beta) \end{bmatrix}. \quad (3.10)$$

For obtaining the overall error vector  $\hat{\xi}$ , the contributions of all the machine's axes  $n$  are added by superposition since the magnitude of the error components is small compared to the nominal dimensions of the machine:

$$\hat{\xi}(\mathbf{u}, \mathbf{t}, \beta) = \sum_{i=1}^n \hat{\xi}_i(\mathbf{u}, \mathbf{t}, \beta) \quad (3.11)$$

resulting in a mathematical description of the tool positioning and orientation error with respect to the workpiece table.

Since the geometrical error model derived is linear in the unknown model parameters, this equation can be denoted in matrix notation, see Appendix D:

$$\hat{\boldsymbol{\xi}}(\mathbf{u}, \mathbf{t}, \boldsymbol{\beta}) = \mathbf{F}(\mathbf{u}, \mathbf{t}) \cdot \mathbf{Q}(\mathbf{u}) \cdot \boldsymbol{\beta} = \mathbf{H}(\mathbf{u}, \mathbf{t}) \cdot \boldsymbol{\beta} \quad (3.12)$$

where matrix  $\mathbf{H}(\mathbf{u}, \mathbf{t})$  is obtained by multiplying two matrices. Matrix  $\mathbf{F}(\mathbf{u}, \mathbf{t})$  computes the effect of an error component (i.e.  $\mathbf{e}_i, \boldsymbol{\varepsilon}_i$ ) on the machine's positioning and orientation error  $\hat{\boldsymbol{\xi}}$ . For translational error components, the corresponding matrix element equals 1 and for rotational error components, the arm of rotation  $\mathbf{p}_i$  is used. These arms depend among others on the machine's axis positions (i.e. stored in  $\mathbf{u}$ ) and the geometry of the end-effector (as stored in  $\mathbf{t}$ ). The second matrix  $\mathbf{Q}(\mathbf{u})$  contains the error component functions, see Equations 3.2-3.4 used for describing the error components (i.e.  $\mathbf{e}_i, \boldsymbol{\varepsilon}_i$ ). In this matrix the machine's axis positions ( $\mathbf{u}$ ) are present as variables.

## 3.2 Measurement of geometric errors

In this section, the measurement of geometrical errors will be discussed. First, the measuring conditions for assessing the machine's geometrical errors are considered. This means that the effect of other error sources on the machine's positioning behaviour (i.e. thermally induced errors, error due to finite stiffness of machine's structural loop) has to be minimized or cancelled if possible while performing measurements on the machine. Secondly, the application of length measurements for assessing the machine's positioning behaviour is considered. A measurement model is presented describing the relation between the machine's positioning error and the resulting length deviation, as measured by a length measuring instrument. Furthermore a measurement setup is proposed, prescribing the spatial distribution of length measurements to be performed in the machine's working volume in this section.

### 3.2.1 Measurement conditions

In order to measure the geometrical errors of a multi-axis machine only, it is important to cancel the effect of other error sources as much as possible.

Complete elimination of thermally induced errors is impossible but their effect on the machine's positioning behaviour can be minimised. The heat sources present should hereby be cancelled as much as possible in order to approximate the ideal situation (i.e. realize a 'cold' reference state) of a machine with a homogeneous thermal distribution of 20 °C. For a machining centre for instance, this mainly means that the main spindle should not rotate during the measurement of geometrical errors since this is a major heat source (friction in bearings and gear boxes, heating up of motor etc.). The heat generated by the servo motors on the other hand cannot be cancelled, because the machine must be able to move to certain measuring positions although the resulting

thermal distortion is limited compared to other heat sources. Another effective possibility to minimise thermal disturbances is to control the temperature of the environment, as often practised in metrology laboratories. In order to obtain a stationary temperature distribution in a machine (probably not homogeneous) the machine can also be left switched on for a period of time before performing measurements. Resulting positioning errors due to temperature differences with respect to the reference temperature of 20 °C can subsequently be compensated for by using formulas describing thermo-mechanical behaviour. Other ways of minimising thermally induced errors is using thermal invariant materials (i.e. invar, zerodur) and/or executing measurements in a short period of time in order to avoid changes in the temperature distribution of the multi-axis machine.

Besides thermo-mechanical effects, the machine's positioning behaviour is also affected by the finite stiffness of the machine's structural loop. Due to internal and external forces, the tool position and orientation is changed with respect to the workpiece table statically as well as dynamically. Machine deformations resulting from gravity forces on one hand are always present and cannot be eliminated. From a scientific point of view it might be interesting to separate positioning errors due to gravity effects from 'real' geometrical errors: errors resulting from geometrical imperfections of the machine axes including assembly errors (squareness errors). This however is not done for practical reasons: when for instance compensation for the measured positioning errors is performed, these separated effects have to be added first. For this reason, no effort is made to separate these errors: positioning and orientation errors due to dead weight forces (of the machine itself) are therefore considered as an implicit part of the geometrical errors. Besides the machine itself, also the workpiece is subjected to gravity forces, resulting also in deformation of the machine. Since machining centres can generally be loaded with heavy workpieces<sup>5</sup>, the resulting deflection of relevant machine components can be significant. With the term 'finite stiffness error', this type of error is meant in this thesis. This error can be examined by loading the machine with different masses on different positions while performing measurements. This kind of error however is beyond the scope of this research project. For these aspects see [Soo 93] [Spa 95]. Summarizing, static finite stiffness errors during geometrical measurements are eliminated by placing no additional loads on the machine. The mass of the measurement equipment itself is usually negligible.

Since the stiffness of the structural loop of a multi-axis machine is finite, also dynamic forces cause positioning and orientation errors. This kind of errors can be minimized by performing measurements of geometrical errors in a static way: read the instrument after machine vibrations have attenuated sufficiently. This means in practice that a certain waiting time has to be taken into account, typically (fractions of) a second.

When the slides of a multi-axis machine are at a certain (virtually fixed) position, vibrations caused by the servo-systems used for controlling the machine's axis positions, do occur. The amplitude of these vibrations however are generally small and can be neglected (or reduced to an acceptable level by proper

---

<sup>5</sup>A Maho 700S for example can be loaded with workpieces up to 500 kg.

tuning). Measurements with a dynamic laser interferometer on a milling machine (Maho 700S) for instance revealed vibrations with an amplitude of several tenths of a  $\mu\text{m}$  only.

By taking these remarks into account, geometrical errors of multi-axis machines can be assessed, since the effects of the other error sources on the machine's positioning behaviour have been minimised. In the following subsection, the measurement of geometrical errors itself will be discussed.

### 3.2.2 Length measurements with a Double Ball Bar

In this thesis length measurements are used for assessing the machine's positioning behaviour. For measuring lengths, a telescopic ball bar equipped with a measuring system is employed: a Double Ball Bar (DBB). In the Figure 3.4 a schematic drawing of a DBB length measurement of a five-axis milling machine is depicted. This measuring device contains two precision balls attached

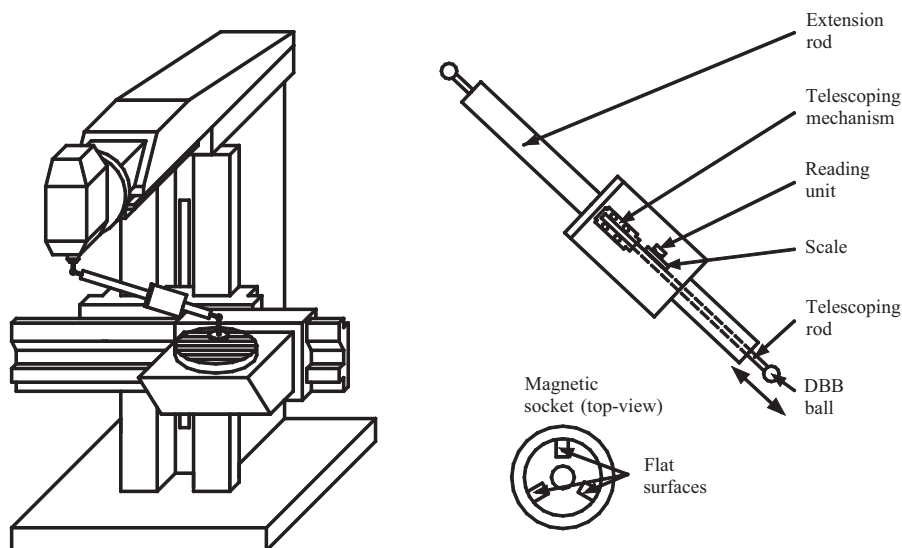


Figure 3.4: A DBB measurement on a five-axis milling machine.

at each end of the bar, see Figure 1.3 and its nominal length can be adjusted with extension rods to fit the machine's workspace. The length of a DBB is defined as the distance between the centre points of the DBB balls. One DBB ball is fixed to the DBB and the other ball is connected to a telescopic rod with a limited stroke of 10 mm. The integrated measuring system (a linear encoder, see [Dou 90]) can detect relative movements of the telescopic rod position with a resolution of  $0.1 \mu\text{m}$ . This measuring system contains an absolute reference mark (near the middle of the encoder) that has to be passed when initialising the length measuring instrument. Due to this reference mark the DBB can be

used as an absolute length measuring instrument after calibrating the DBB<sup>6</sup>. The calibration procedure of a DBB is presented in Appendix B. The length measurement uncertainty of this instrument is typically 1  $\mu\text{m}$ .

The DBB precision balls are mounted on the machine with two magnetic sockets: one ball is fixed to the tool and the other ball is mounted on the workpiece table by means of a stand. The magnet ensures contact between a DBB ball and three flat hardened surfaces present in the socket. This way, the position of a DBB ball in a socket is determined kinematically (not over-constrained) allowing relative rotations only.

Since the measuring stroke of the DBB used is limited to 10 mm, the measuring points have to be distributed on a semi-sphere with respect to the stand (or tool) in order to prevent serious damage of the instrument. Therefore the machine is commanded to move successively along circular paths which together generate a semi-spherical grid of measuring points. This implies that the length measurements can be considered as radius measurements of such a semi-sphere. With one DBB measurement, a collection of measuring points distributed on discrete points on such a semi-sphere is meant. Such a DBB measurement can be executed in five minutes typically.

Besides a DBB with a short measuring stroke (like the Heidenhain IK110 and the Renishaw QC10) also measuring ball bar systems with a longer measuring stroke (i.e. 100 mm) have been developed [Zie 94]. The distance between the attached balls is then measured using a laser interferometer. An advantage of this measuring instrument, referred to as Laser Ball Bar (LBB), over a DBB is that the measuring points do not necessarily have to be distributed on a sphere due to its extended measuring range. A LBB however is expensive and is therefore not used in this thesis.

If the machine's positioning error is zero, a perfect smooth semi-sphere is measured with a radius as commanded. Since the DBB is an absolute length measuring device, not only errors with respect to a spherical shape can be analysed, but also the radius itself can be evaluated. The following step now is to derive a relation between the positioning errors of the multi-axis machine and the output of the DBB measuring instrument. This relation will be derived here.

In the Figure 3.5 a semi-spherical DBB measurement is depicted schematically. The centre point  $\mathbf{c}$  of such a measurement is determined by the stand position, bolded on the workpiece table. This position however is not known accurately. Therefore this position  $\mathbf{c}$  is approximated by fitting a sphere through the measuring points and this approximation is denoted by  $\mathbf{w}$ : the distance vector between both points is represented by  $\gamma$ .

- $\mathbf{c}$ : centre point of semi-spherical DBB measurement;
- $\mathbf{w}$ : approximation of centre point  $\mathbf{c}$ ;
- $\gamma$ : estimation error of centre point position;

---

<sup>6</sup>In principle this calibration procedure has to be performed once. If the DBB length is modified with an extension rod however a new calibration is required.

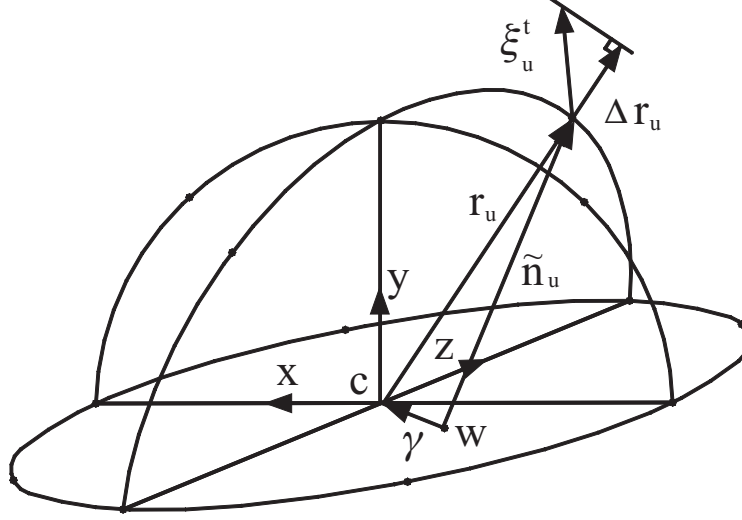


Figure 3.5: Schematic drawing of a DBB measurement.

- $\xi_u^t$ : positioning error in measuring point  $u$ ;
- $r_u$ : measured radius in measuring point  $u$ ;
- $\tilde{\mathbf{n}}_u$ : approximation of normal vector in measuring point  $u$ ;
- $\Delta r_u$ : measured radius deviation in point  $u$ .

In this way, the position of the DBB measurement centre point can be denoted as:

$$\mathbf{c} = \mathbf{w} + \boldsymbol{\gamma}. \quad (3.13)$$

This approximation error  $\boldsymbol{\gamma}$  is constant during a DBB measurement and can be regarded as a DBB measurement alignment error.

The following step is to analyse the position of the other DBB ball, attached at the tool of the machine. This position equals the nominal tool position added with the machine's positioning error  $\xi_u^t$  for point  $u$ :

$$\begin{aligned} x_u &= x_{u_{nom}} + \xi_{ux}^t \\ y_u &= y_{u_{nom}} + \xi_{uy}^t \\ z_u &= z_{u_{nom}} + \xi_{uz}^t \end{aligned} \quad (3.14)$$

Now the spatial positions of both DBB balls have been denoted. The shortest distance between these two points then equals:

$$r_u = \sqrt{(x_u - c_x)^2 + (y_u - c_y)^2 + (z_u - c_z)^2}. \quad (3.15)$$



However, not every variable in this expression is known: only the nominal tool position and the approximation of the centre point  $\mathbf{w}$  are available. By substituting 3.13 and 3.14 in the former formula, the following expression yields:

$$r_u = \sqrt{(x_{u_{nom}} + \xi_{ux}^t - w_x - \gamma_x)^2 + \dots + (z_{u_{nom}} + \xi_{uz}^t - w_z - \gamma_z)^2}. \quad (3.16)$$

The unknown variables in this equation, these are  $\gamma$  and  $\xi_u^t$ , are much smaller than the known variables<sup>7</sup>. Because of this, the radius in measuring point  $u$  can be approximated by linearisation to the unknown variables using first order Taylor polynomials:

$$\begin{aligned} r_u \simeq r_{u_{nom}} + \frac{\partial r_u}{\partial \xi_{ux}^t} \cdot \xi_{ux}^t + \frac{\partial r_u}{\partial \xi_{uy}^t} \cdot \xi_{uy}^t + \frac{\partial r_u}{\partial \xi_{uz}^t} \cdot \xi_{uz}^t + \dots \\ \dots + \frac{\partial r_u}{\partial \gamma_x} \cdot \gamma_x + \frac{\partial r_u}{\partial \gamma_y} \cdot \gamma_y + \frac{\partial r_u}{\partial \gamma_z} \cdot \gamma_z \end{aligned} \quad (3.17)$$

with:

$$r_{u_{nom}} = \sqrt{(x_{u_{nom}} - w_x)^2 + (y_{u_{nom}} - w_y)^2 + (z_{u_{nom}} - w_z)^2}. \quad (3.18)$$

Evaluating the partial derivatives by differentiating Equation 3.16 results in:

$$\frac{\partial r_u}{\partial \xi_{ux}^t} = \frac{x_{u_{nom}} - w_x}{r_{u_{nom}}}, \quad (3.19)$$

$$\vdots \quad (3.20)$$

$$\frac{\partial r_u}{\partial \gamma_z} = -\frac{z_{u_{nom}} - w_z}{r_{u_{nom}}}. \quad (3.21)$$

At this point, a linear approximation is obtained for the measured radius in measuring point  $u$  by substituting these partial derivatives in Equation 3.17:

$$r_u \simeq r_{u_{nom}} + \frac{x_{u_{nom}} - w_x}{r_{u_{nom}}} \cdot (\xi_{ux}^t - \gamma_x) \quad (3.22)$$

$$+ \frac{y_{u_{nom}} - w_y}{r_{u_{nom}}} \cdot (\xi_{uy}^t - \gamma_y) \quad (3.23)$$

$$+ \frac{z_{u_{nom}} - w_z}{r_{u_{nom}}} \cdot (\xi_{uz}^t - \gamma_z). \quad (3.24)$$

The next step is to derive an equation for the normal vector in measuring point  $u$  since the measuring axis of the DBB coincides with this normal vector. This normal vector with unit length 1 can be approximated by:

$$\mathbf{n}_u \simeq \frac{1}{r_{u_{nom}}} \cdot \begin{pmatrix} x_{u_{nom}} - w_x \\ y_{u_{nom}} - w_y \\ z_{u_{nom}} - w_z \end{pmatrix}. \quad (3.25)$$

<sup>7</sup>The order of magnitude of the nominal tool position and of the centre point coordinates are  $10^{-1}$  m while  $\gamma$  and  $\xi_u^t$  are of order  $10^{-5}$  m.

By defining the deviation of the radius as:

$$\Delta r_u = r_u - r_{u_{nom}}, \quad (3.26)$$

the following expression holds for the measured radius deviation as obtained by combining Equations 3.22 - 3.26:

$$\Delta r_u \simeq \mathbf{n}_u^T \cdot \begin{pmatrix} \xi_{ux}^t - \gamma_x \\ \xi_{uy}^t - \gamma_y \\ \xi_{uz}^t - \gamma_z \end{pmatrix} \quad (3.27)$$

or in vector notation denoted as:

$$\Delta r_u \simeq \mathbf{n}_u^T \cdot \boldsymbol{\xi}_u^t - \mathbf{n}_u^T \cdot \boldsymbol{\gamma}. \quad (3.28)$$

which is the equation sought. Note that vector  $\boldsymbol{\gamma}$  does not have a subscript since this centre point approximation error remains constant during a single semi-spherical DBB measurement while the other variables depend on the machine's axis positions.

Actually, this equation is quite straightforward. Since a DBB is a length measuring instrument, only the projection of the machine's positioning error  $\boldsymbol{\xi}_u^t$  on the measurement axis  $\mathbf{n}_u$  is detected. Therefore an inner product between the vectors  $\boldsymbol{\xi}_u^t$  and  $\mathbf{n}_u$  is present in the expression describing the measured radius deviation. The same yields for the approximation error of the DBB measurement centre point: this error affects the measured radius by the projection term  $\mathbf{n}_u^T \cdot \boldsymbol{\gamma}$ . The deviation in radius is then simply the difference between these two terms.

### Sensitivity DBB length measurements for error components

The positioning errors of a multi-axis machine distort the shape and size of the semi-sphere to be measured with a DBB. This distortion depends on the type of error component and will be discussed here, starting with linearity errors. In this analysis a very large number of measuring points within a DBB measurement is assumed for clarity, justifying terms like circles and spheres although the DBB length is measured at a limited number of discrete points on a semi-sphere.

A linearity error is a translational error which acts along a machine axis. Because of this, a circle of the measured semi-sphere can be transformed into an ellipse with its principal axes parallel and/or perpendicular to the machine axis, see Figure 3.6. In this figure, the relation between the machine's positioning error  $\boldsymbol{\xi}_u^t$  as a result of linearity error  $xtx$ , and the measured radius deviation is drawn. Since the positioning errors have been scaled up considerably for reasons of clarity<sup>8</sup>, the projection of the positioning error  $\boldsymbol{\xi}_3^t$  on the actual measurement axis  $\mathbf{n}_3$  is not exactly equal to the drawn radius deviation  $\Delta r_3$  of measuring point 3 and has therefore been omitted (otherwise see Figure 3.5). From this figure it is obvious that the sensitivity of length measurements for a

<sup>8</sup>The order of magnitude of the nominal radius equals the DBB length and is  $10^{-1}$  m while the machine's positioning errors are of order  $10^{-5}$  m.

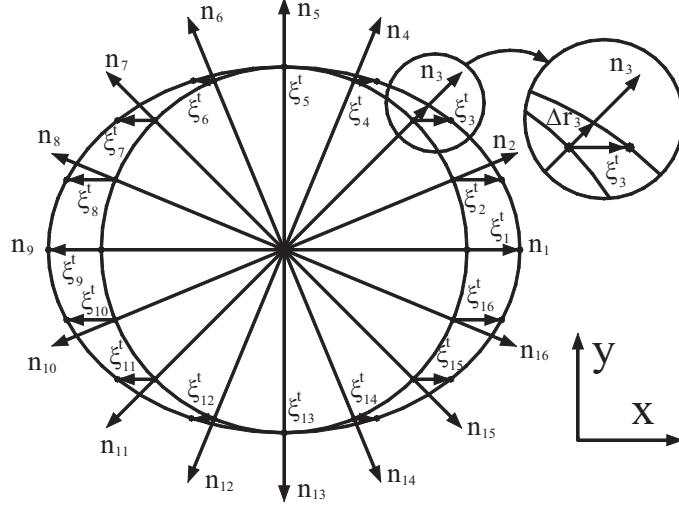


Figure 3.6: Sensitivity DBB measurement for linearity error  $xtx = \beta_{xtx1}(x - x_0)$ .

single linearity error is 0 when the orientation of the resulting positioning error is perpendicular to the measurement axis (points 5 and 13) and 1 when these orientations coincide (points 1 and 9): the measured radius deviation equals the positioning error.

The sensitivity of a DBB length measurement for positioning errors is obtained by differentiating Equation 3.28 to the components of  $\xi_u^t$ :

$$\frac{\partial \Delta r_u}{\partial \xi_{xu}^t} = n_x \quad (3.29)$$

$$\frac{\partial \Delta r_u}{\partial \xi_{yu}^t} = n_y \quad (3.30)$$

$$\frac{\partial \Delta r_u}{\partial \xi_{zu}^t} = n_z. \quad (3.31)$$

In point 5 on one hand, see Figure 3.6, the normal vector equals  $[0 \ 1]^T$  while the positioning error  $\xi_u^t$  only has a nonzero component in X-direction ( $\xi_x^t \neq 0$ ,  $\xi_y^t = \xi_z^t = 0$ ) so the sensitivity is zero since  $n_x = 0$ . For point 1 on the other hand, the normal vector is  $[1 \ 0]^T$  and therefore the machine's positioning error due to a  $xtx$  error component is reflected completely in the measured radius deviation. In Figure 3.7 some combinations of  $xtx$  and  $yty$  are drawn. By combining the linearity errors, this analysis can be extended into the three-dimensional case.

Besides linearity errors also squareness errors can transform a circle into an ellipse, but in this case with the principle axes  $45^\circ$  rotated relative to the

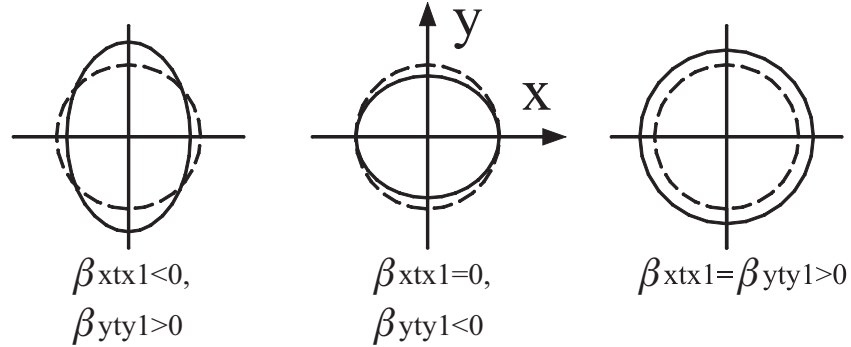


Figure 3.7: Effect of linearity errors  $xtx = \beta_{xtx1}(x - x_0)$  and  $yty = \beta_{yty1}(y - y_0)$  on a circular DBB measurement in a XY plane.

machine's axes. The orientation of these principle axes is determined by the sign of the squareness error. In Figure 3.8 such a squareness error is depicted. The sensitivity of the radius deviation for the positioning error components in X

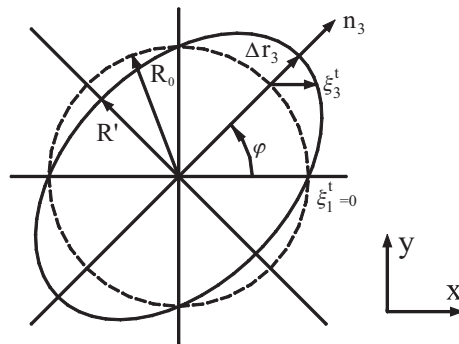


Figure 3.8: Effect of a squareness error  $xwy$  on a circular DBB measurement with radius  $R_0$ .

and Y direction due to a squareness error  $xwy$  in measuring point 3 for example can be denoted as  $[\frac{1}{2}\sqrt{2} \quad \frac{1}{2}\sqrt{2}]^T$ . This means that  $\Delta r_3 = \frac{1}{2}\sqrt{2} \cdot \xi_3^t$  in the drawn example. More specifically, it can be proved that the resulting ellipse radius  $R'$  as a function of angle  $\varphi$  can be expressed as (see Figure 3.8) [Sch 01]:

$$R' = R_0 \cdot \sqrt{1 + \varepsilon \sin(2\varphi)}$$

with  $\varepsilon$  denoting the squareness error angle.

Extending this analysis, the sensitivity of a measured radius deviation  $\Delta r_u$  to a geometrical error model parameter  $\beta_i$  used for describing an error component  $c_i$  (the error components are stored in a vector  $\mathbf{c}(\mathbf{u})$ , see Appendix D) can be obtained by differentiating the radius deviation to the components of the corresponding vectors. This can be expressed as:

$$\frac{\partial \Delta r_u(\mathbf{u}, \mathbf{t})}{\partial \beta_i} = \begin{bmatrix} \frac{\partial \Delta r_u(\mathbf{u}, \mathbf{t})}{\partial \xi_{xu}^t(\mathbf{u}, \mathbf{t})} \cdot \frac{\partial \xi_{xu}^t(\mathbf{u}, \mathbf{t})}{\partial c_i(\mathbf{u})} \cdot \frac{\partial c_i(\mathbf{u})}{\partial \beta_i} \\ \frac{\partial \Delta r_u(\mathbf{u}, \mathbf{t})}{\partial \xi_{yu}^t(\mathbf{u}, \mathbf{t})} \cdot \frac{\partial \xi_{yu}^t(\mathbf{u}, \mathbf{t})}{\partial c_i(\mathbf{u})} \cdot \frac{\partial c_i(\mathbf{u})}{\partial \beta_i} \\ \frac{\partial \Delta r_u(\mathbf{u}, \mathbf{t})}{\partial \xi_{zu}^t(\mathbf{u}, \mathbf{t})} \cdot \frac{\partial \xi_{zu}^t(\mathbf{u}, \mathbf{t})}{\partial c_i(\mathbf{u})} \cdot \frac{\partial c_i(\mathbf{u})}{\partial \beta_i} \end{bmatrix}. \quad (3.32)$$

The first row of this matrix represents the sensitivity of the measured radius deviation  $\Delta r_u(\mathbf{u}, \mathbf{t})$  to an error model parameter  $\beta_i$  evaluated for the X direction of the machine's positioning error  $\xi_{xu}^t$  for error component  $c_i$ . The other rows correspond to the sensitivity of the radius deviation, evaluated for the Y and Z direction respectively of the machine positioning error  $\xi_u^t$ . The distinction made for the X, Y and Z direction is necessary in order to differentiate the scalar value  $\Delta r_u(\mathbf{u}, \mathbf{t})$  to the (scalar) components of the positioning error vector.

Regarding the first row of this matrix, a product of three terms is present. The first term of this product, that is  $\frac{\partial \Delta r_u}{\partial \xi_{xu}^t}$  represents the projection of the machine's positioning error in X direction on the DBB measurement axis. The value of this partial derivative equals  $n_x$  and its value is between -1 and +1, see also Equation 3.31. The second part,  $\frac{\partial \xi_{xu}^t}{\partial c_i}$  describes the effect of an error component  $c_i$  on the machine's positioning error in X direction  $\xi_{xu}^t$ , see also Section 3.1.3. For translational error components (i.e. the 'itj' terms) on one hand this partial derivative equals  $\pm 1$  if the error component  $c_i$  acts in the machine's X direction, otherwise this term is zero. For rotational error components (i.e. the 'irj' terms) on the other hand, the term  $\frac{\partial \xi_{xu}^t}{\partial c_i}$  equals the component of the arm of rotation corresponding to the rotational error component  $c_i$ . The latter depends on the machine's axis positions (i.e.  $\mathbf{u}$ ) as well as on the dimensions and geometry of the end-effector (i.e.  $\mathbf{t}$ ). Finally the last term, that is  $\frac{\partial c_i}{\partial \beta_i}$ , depends on the derivative of the error component function to its parameters, see Equations 3.2-3.4 describing the dependency of an error component on axis position.

Summarizing: in order to be able to estimate an error component parameter from DBB measurement data, the product of these three partial derivatives must at least be non-zero for at least one row for some measuring points (i.e. large product values are desired).

This analysis has been performed for each error component. From this analysis the following is concluded:

- A DBB measurement is (or can be made) sensitive to each individual error component [Kna 83];

- The sensitivity of a DBB measurement to an error component in decreasing order is:
  1. Squareness errors;
  2. Linearity errors;
  3. Rotational error components;
  4. Straightness errors.

This means that positioning errors due to a linearity error do affect the measured radius deviation the most while the radius deviation is affected the least by a straightness error. This implies that in principle each individual error component can be determined from a single DBB measurement since each error component does affect the radius to be measured [Kna 83]. It also implies that the determination of a straightness error from radius deviation measurement data is affected more by measurement noise due its poor sensitivity then the determination of a squareness error for example.

So far, only one or a few error components have been considered at a time, responsible for the resulting positioning error of the multi-axis machine. In reality however, all the error components act simultaneously with each their characteristic influence on the machine's positioning behaviour. The determination of the error components in this case from the measured radius deviations is still possible but much more complicated. This is caused by the fact that it is impossible to distinguish certain error components from a single DBB measurement, even if the number of measuring points within a semi-spherical DBB measurement is infinite. In order to be able to determine all the error components from DBB measurements the measurement setup must satisfy certain conditions since multiple DBB measurements are required. This measurement setup is subject of the next subsection.

### 3.2.3 Design of measurement setup

Since length measurements only detect the projection of a positioning error on the measurement axis, see Equation 3.28, the components of the positioning error perpendicular on this measurement axis are lost for a single measuring point. Because of this reason it is important to distribute the measuring points throughout the machine's workspace in such a way, that the orientation of the measurement axis is varied in all possible directions. In this subsection measures are discussed in order to be able to determine/estimate all the error model parameters from DBB measurement data. The latter implies that multiple DBB measurements have to be applied. The measurement setup obtained in this way, prescribing the spatial distribution of the DBB measurements in the machine's workspace, should be regarded as a minimum constraint that must be met, not as a mathematical proof or as an optimal measurement strategy. The latter is impossible since no a priori knowledge is available about the error components of the machine considered. In [Que 98] it is shown that for a simple (virtual) machine with two axes, containing only three error components (i.e.  $x$ tx,  $y$ ty

and  $xy$ ) the optimal distribution of DBB measurements in its working plane depends on the value of these error components. Only when this knowledge is available, an optimal measurement strategy could possibly be derived. Nevertheless, a minimum required DBB measurement setup can be derived.

A DBB measurement is determined by several factors. When both DBB balls are connected to the machine, the structural loop is closed. This structural loop depends besides the machine tool itself on (see Figure 1.3 and 3.4):

- Tool geometry;
- DBB length;
- Stand position on the workpiece table.

Given these entities, the machine's structural loop is determined completely. The tool dimensions for instance determines among others how rotational errors of the ram are reflected (i.e. 'amplified') in the machine's positioning error, see also Equation 3.6. A roll error of the ram ( $zrz$ ) will contribute more to the positioning error for longer tools than for short tool lengths. The opposite is true for the rotational errors of the X-axis. The effect of the stand position on the workpiece table is comparable with that of the tool geometry: both (can) affect offset arms of rotational error components. This property will be used intentionally for separating and determining all the error components.

In order to make this clear, the machine's positioning error in Z-direction is written down using the error model derived. This error depends on several error components like  $ztz$  and  $zrx$ , which are both modelled linear with axis position (higher order terms are omitted for simplicity), see Equations 3.2-3.4:

$$\hat{\xi}_z^t(\mathbf{u}, \mathbf{t}, \boldsymbol{\beta}) = \dots + \beta_{ztz1}(z - z_0) + \beta_{zrx1}(z - z_0) \cdot (-a + c + t1_y) + \dots \quad (3.33)$$

In this equation,  $a$  and  $c$  are machine constants (see Figure 2.7) and  $t1_y$  stands for the length of the tool used. From this example it is clear that it is impossible to separate the translational error (parameter  $\beta_{ztz1}$ ) and the rotational error (parameter  $\beta_{zrx1}$ ) since the term  $(-a + c + t1_y)$  remains constant during a DBB measurement while the term  $(z - z_0)$  varies for each measuring point in the same way for both error components. Increasing the number of measuring points within a semi-spherical DBB measurement does not solve this problem and it is therefore useless. The only way to be able to separate the translational error from the rotational error is to include also a DBB measurement performed with another tool length, say  $t2_y$ , to the measurement data.

More specifically, regarding Equation 3.32 the first and third partial derivatives on the third row are the same for these two error components in this case: the normal vector equals  $[0 \ 0 \ 1]^T$  and the dependency of the error components on axis position is similar, see Equation 3.3. Therefore the second partial derivative, that is  $\frac{\partial \xi_{zy}^t}{\partial c_i}$ , must be changed in another DBB measurement for separating both error components considered: modify error component  $zrx$ 's arm of rotation. This can be realized by extending the vertical tool length in this case.

The influence of the stand position on the workpiece table is similar to that of the tool geometry and is reflected as a rigid displacement of the machine's coordinate  $z$  in the example shown, altering certain arms of rotation (see Equations 2.4-2.7). This means, regarding Equation 3.32 that the second term on a row (i.e.  $\frac{\partial \xi_{xu}^t}{\partial c_i}$ ) is altered when the stand is placed on another position on the machine's workpiece table. This proves the necessity of using multiple DBB measurements, performed with different tool geometries and stand positions, for determining all the machine's error components from length measurement data<sup>9</sup>.

Besides the tool geometry and stand position, a DBB measurement is also affected by the length of the DBB used. This length determines the distance between the measuring points with respect to the stand (i.e. the radius). This implies that this length determines the variation in the machine's axis positions (the term  $(z - z_0)$  in Equation 3.33) while executing a DBB measurement. Or more specifically, regarding Equation 3.32 the third term in each row  $\frac{\partial c_i}{\partial \beta_i}$  changes more for longer DBB lengths. So for separating the error components, it is advantageous to choose this DBB length as long as possible, taking the dimensions of the machine's workspace into account [Mon 97]. Since the machine's positioning error needs to be measured throughout the entire working volume with a limited amount of length measurements, the use of a relatively long DBB is also advantageous.

The items discussed can be summarised as follows for determining all error components from DBB measurements:

- The length of the DBB should be chosen as large as possible, taking the machine's working volume into account;
- Vary the position of the ball attached at the machine's end-effector as much as possible in X-, Y- and Z-direction;
- Vary the stand position as much as possible in X-, Y- and Z-direction;
- Using a large number of measuring points within a DBB measurement is of little use and time consuming. When increasing the number of measuring points, it is better to perform more DBB measurements under different conditions (by varying the stand position and/or the tool geometry) than increasing the number of measuring points within a semi-spherical DBB measurement.

For simple situations, the effect of the above mentioned measures can be quantified. For instance by considering the change in (co-)variance of estimated parameters this way: the parameter's (co-)variance decreases (as desired) when increasing the change in end-effector geometry. The same happens when increasing the DBB length. Another possibility is consideration of the change in condition number of the matrix used for estimating the parameters when

---

<sup>9</sup>The opposite is also true: as long as the stand position and tool geometry has not been varied in X-, Y- and Z-direction, the determination of all 21 error components is impossible.



modifying the DBB length, end-effector geometry, kind of measuring point distribution, etc. [Mon 92] [Mon 97] [Str 88]. Such an analysis however is rather specific: it is valid for a certain machine configuration with certain error components for a DBB measurement performed on a certain location with a certain tool etc. Therefore the measures necessary for determining all the machine's error components from DBB measurements are presented in a qualitative way.

In order to vary the position of the DBB ball attached at the tool, an offset adapter has been designed and realized. With this adapter, this position can be varied in the horizontal XZ plane with  $\pm 150$  mm. In Figure 3.9 such a DBB measurement is shown with an elevated stand. For modifying the tool length



Figure 3.9: DBB measurement with offset adapter and elevated stand.

a modular set of extension rods is used. With this set, the tool length can be extended up to 242 mm while the length of the shortest tool equals 115 mm. The magnitude of the extensions however is limited due to the lateral stiffness of the tool. The compliance measurement error introduced should be negligible to the entity to be measured: the machine's positioning error. This means that the measurement error as introduced by the tool extensions should be smaller than  $1 \mu\text{m}$ . This has been verified with experiments as shown in Figure 3.10 which displays the measurement setup for the most critical stiffness component of the extended tool. With the measurement setup depicted, the displacement



Figure 3.10: Measurement setup for determining the lateral stiffness of an extended tool.

of the extended tool is measured with a (hysteresis free) displacement gauge while loading (followed by unloading) the tool with a known lateral force using weights. The measured (lateral) stiffness of the tool is  $5.8 \times 10^6$  N/m. Since the measurement force of the telescoping DBB rod is below 0.4 N, the maximum measurement error as introduced by the extended tool equals:

$$u_{\max} \leq \frac{2 \cdot 0.40}{5.8 \cdot 10^6} = 0.13 \mu\text{m}$$

which is negligible with respect to the positioning error to be measured. A similar measurement setup has been used for verifying the stiffness of the offset adapter, which proved to be sufficient for an offset bar of 150 mm.

At this point, the measurement setup can be formulated for measuring the positioning errors of a multi-axis machine, where a five-axis milling machine serves as an example. Since the working volume of this machine equals  $500 \times 600 \times 700$  mm, a DBB length of 250 mm has been selected as most suitable. In Figure 3.11 a top-view of the machine's workspace is depicted where the numbered crosses indicate the positions of the stand. The measuring points are distributed on discrete points on these circles. With this measurement setup, the

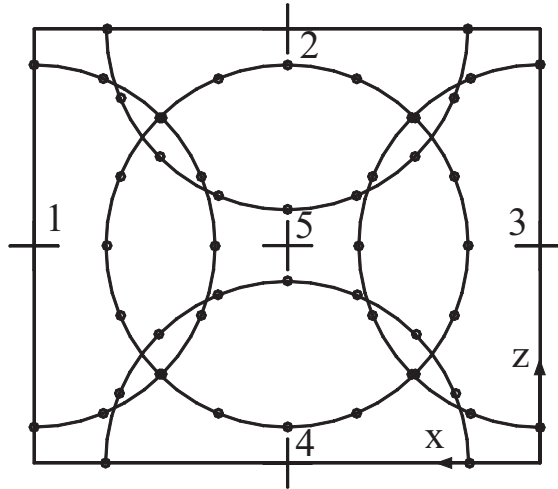


Figure 3.11: Top-view of applied DBB measurement setup in XZ plane. In this cross-section, the DBB orientation coincides with the machine's horizontal plane.

stand position has been varied as much as possible in the horizontal plane. The depicted setup consists of five DBB measurements. These five measurements are then performed at three different height levels by applying:

- a short tool (115 mm);
- extended tool with a length of 242 mm;
- an elevated stand to vary the stand position vertically with 100 mm (see Figure 3.9).

This measurement setup consist of 15 DBB measurements so far. Finally the offset adapter has been applied 4 times, where the tool point has been given an offset in the horizontal plane with  $\pm 150$  mm, resulting in a total of 19 DBB measurements.

In Figure 3.11 four DBB measurements (no. 1-4) have been positioned half way the axis range. Another possibility is to position these measurements at the corners of the machine's workspace since the stand position is then also varied as much as possible. The former setup however consists of more measuring points (compare a  $1/4$  sphere with a  $1/8$  sphere) while the time needed to perform these measurements is only marginally longer. Most time is used for preparing the DBB measurement setup. Also an approximation of the centre position of such a DBB measurement, positioned at a corner (a  $1/8$  sphere), is still possible but harder to obtain then when using a  $1/4$  sphere due to slower convergence of the approximation towards the centre point. Because of these reasons, DBB

measurements are not positioned at the corners of the machine's workspace but half way the axis range as depicted in Figure 3.11.

### Measuring point distribution within a DBB measurement

In the previous subsection, the design of the measurement setup has been discussed. So far the number and distribution of measuring points within a semi-spherical DBB measurement has been left open (at least a large number was assumed) and this will be discussed here. This means that a compromise has to be made between the information obtained about the machine's positioning behaviour for a certain number and distribution of measuring points and the costs related to execute such a DBB measurement i.e. the measuring time.

The most straightforward distribution of the measuring points within a semi-spherical DBB measurement is a homogeneous one. This means that a constant step angle is applied between the measuring points in the horizontal as well as in the vertical planes. Such a measuring point distribution is depicted in Figure 3.12. The number of measuring points of such a DBB measurement for a step

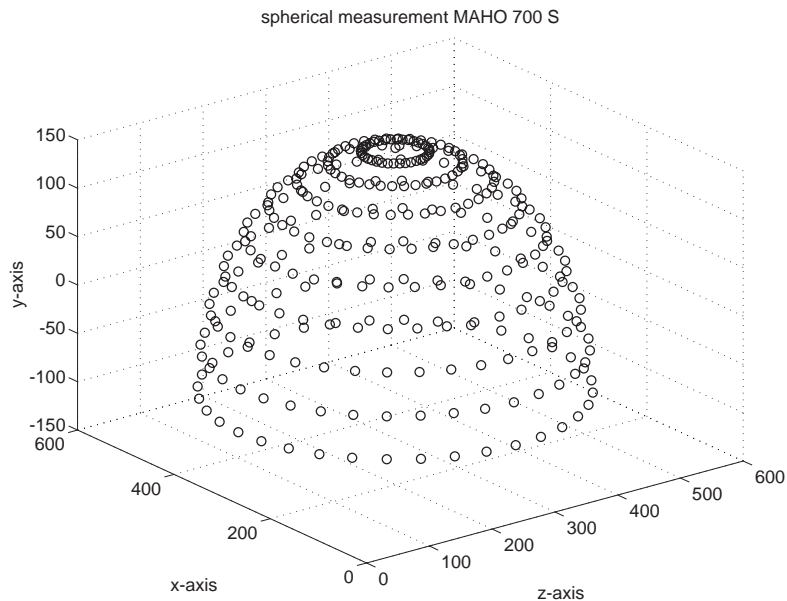


Figure 3.12: DBB measurement with homogeneous measuring point distribution.

angle  $\phi^\circ$  is then equal to:

$$\begin{aligned} nmp &= \frac{90}{\phi} \left( \frac{360}{\phi} \right) + 1; \\ &= \frac{32400}{\phi^2} + 1 \end{aligned}$$

where  $nmp$  represents the number of measuring points. Note that for obtaining a homogeneous measuring distribution, the fraction  $\frac{90}{\phi}$  must be an integer and that the number of measuring point increase rapidly (quadratically) when decreasing the step angle  $\phi$ .

When analysing the measuring point distribution of a DBB measurement three cases can be distinguished:

1. The DBB measuring axis coincides with one axis (X, Y or Z) of the machine (1D);
2. The DBB is oriented in a plane (XY, XZ or YZ) spanned by 2 machine's axes (2D);
3. The measuring axis of the DBB contains an X, Y and Z component (3D).

In the first case on one hand, the radius deviation measured is equal to that component of error vector  $\xi_u^t$  which coincides with the machine's axis. This implies that the other components of this error vector  $\xi_u^t$  do not affect the radius to be measured at all since these components are perpendicular to the measurement axis of the DBB: the sensitivity is 0 for these components. Because of this, the measured radius deviation is a function of a few error model parameters only, see Equation 3.33. A semi-spherical DBB measurement contains five such points, which can be regarded as most efficient for determining the machine's error model parameters  $\beta$  from length measurement data.

For the second and third case on the other hand the measured radius deviation is a combination of two or even three components of the positioning error vector  $\xi_u^t$  which on their turn are each a function of several error components. Therefore these measuring points are less efficient for the determination of the machine error model parameters and their number should therefore be limited. For these reasons the following measuring point distribution, a so-called 'bird-cage' distribution is applied as depicted in Figure 3.13 where most inefficient measuring points have been omitted. Such a distribution can be performed in less time and the amount of information obtained about the machine's positioning behaviour is comparable as for a homogeneous measuring point distribution, see also [Flo 97] and Appendix F.

### 3.2.4 Reversal Double Ball Bar measurements

In this subsection some aspects of the execution of DBB length measurements on a machining centre is discussed, see also Appendix E. These DBB measurements are all executed including a reversal measurement in order to be able to detect irregularities during measurement. This means that each measuring point is measured twice.

The axes of machining centres normally require frequent lubrication. For the milling machine (a Maho 700S) used for instance a lubrication pulse (lasting for several seconds) is executed every eight minutes when the machine moves continuously and for a non-moving machine once every three hours. This lubrication pulse is necessary to guarantee a certain lifetime of the machine but

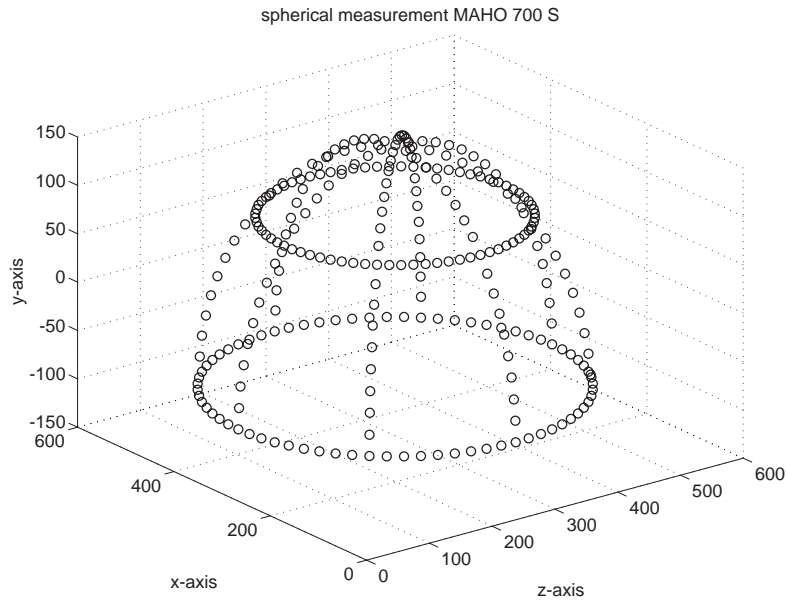


Figure 3.13: Applied measuring point distribution of a DBB measurement.

also affects the machine's positioning behaviour significantly (typically  $10\ \mu\text{m}$ ). Such a pulse is generated by a separated hydraulic pump system distributing oil to all the machine's axes by a flexible tube network. Obviously such a lubrication pulse should not occur during DBB measurements although this is hard to avoid completely. One way to eliminate this problem is to alter some machine constants (MC's) controlling the lubrication rates but this is not recommended since irreversible machine damage might result. Another way is to perform each DBB measurement cycle several times: since the measuring time of a DBB measurement cycle is a few minutes only the measuring points affected during lubrication can be detected (and rejected) simply. Mainly for this reason, each DBB measurement cycle is performed including a reversal measurement. In Figure 3.14 an example of such a reversal DBB measurement is depicted including the difference per measuring point. Obviously this measurement is free of lubrication pulses and can therefore be used for analysis of the machine's geometrical errors.

Including a reversal DBB measurement also has other advantages. First the accuracy of the radius deviation measured in a certain point is increased (by factor  $\sqrt{2}$  for Gaussian measurement noise) due to statistical averaging. Secondly, the first DBB measurement cycle can be compared to the reversal one. Since geometrical machine tool errors are highly systematic, this difference is usually small for each measuring point. This difference, as shown in Figure 3.14 has been computed for numerous DBB measurements and is rather constant: about

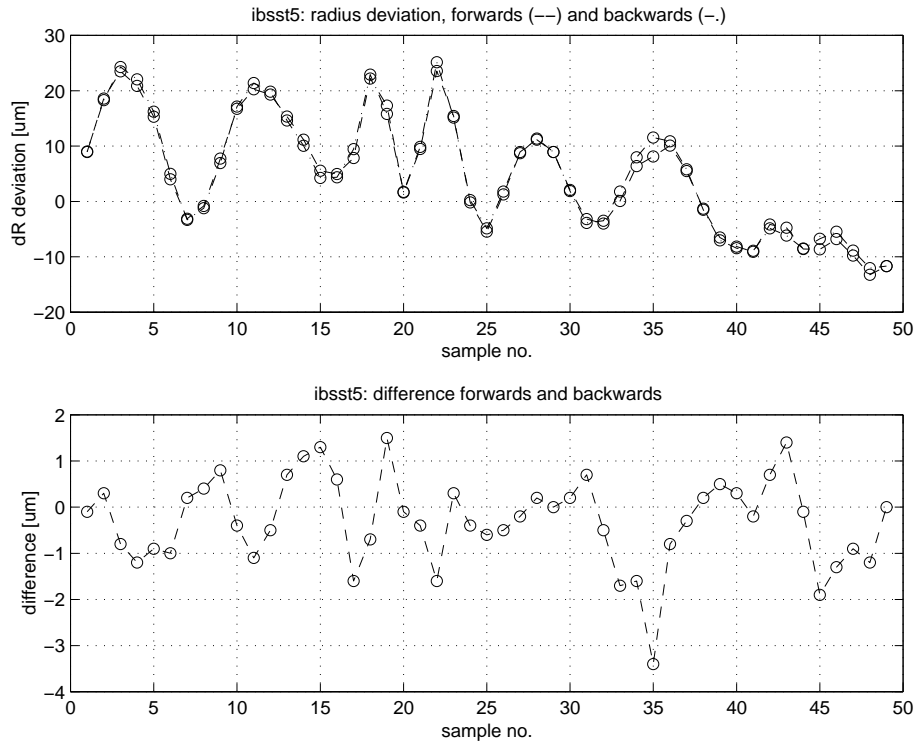


Figure 3.14: Example of a reversal DBB measurement with good repeatability. The figure at the bottom displays the small difference between the forward and backward DBB measurement.

$\pm 2 \mu\text{m}$ , independent of the deviations measured. This value is representative for the repeatability limit of the machine subject to measurement (when taking the previous remarks into account like cleaning etc.) and has been confirmed with other measurements i.e. laser interferometry. Apparently the machine considered cannot reproduce its tool position better than  $2 \mu\text{m}$  with respect to the workpiece table. When estimating error model parameters, this value should therefore be considered as a limit when reducing the radius deviations measured: smaller values (i.e. residual radius deviations) simply cannot be realised by the machine and must therefore be avoided.

### 3.3 Resume

In Section 3.1 a geometrical error model has been derived. In this model, the machine's error components have been modelled with ordinary polynomials, containing unknown parameters to be determined from DBB measurement data. Furthermore rigid body kinematics are used, using first order terms only, for

calculating the error propagation: the influence of the error components on the relative position and orientation error of the machine's end-effector with respect to the workpiece (table).

In Section 3.2 length measurements, performed with a DBB, have been discussed. First, the measurement conditions are presented for measuring the geometrical errors of a multi-axis machine. Secondly, a DBB measurement model has been derived. This model describes the relationship between the machine's positioning error and the resulting radius deviation. The unknown stand position has to be taken into account in this relation.

Subsequently, the sensitivity of DBB length measurements to the geometrical machine error model parameters has been discussed. Numerical simulations indicate that all machine error model parameters can (mathematically) be determined when applying the derived measurement setup, discussed in Section 3.2.3. It explains the importance to vary both DBB balls during a DBB measurement as much as possible. Using a large number of measuring points within a semi-spherical DBB measurement is just time consuming and therefore not useful since the measurement effort has been minimised in this research project. A so-called birdcage measuring distribution is proposed. Furthermore the nominal DBB length should be chosen as large as possible, taking the dimensions of the machine's workspace into account. Application of reversal DBB measurement is recommended.

In the next chapter, the determination of the geometrical error model parameters from the collected measurement data is discussed, followed by the validation of the geometrical error model proposed.





## Chapter 4

# Parameter identification and validation geometrical error model

In the previous chapter, a geometrical error model has been proposed together with a DBB measurement setup, prescribing the spatial distribution of length measurements in the machine's workspace. The next step is to determine the parameters present in the error model from the measurement data collected. For this purpose, least squares regression has been used and this is discussed first in the following section. The estimated parameters will subsequently be used to predict the machine's positioning error throughout its entire working volume.

The validation of the error model proposed is discussed later on and consists of two parts. First, the error model is cross-validated using DBB measurements. This means that intermediate DBB length measurements are performed in the machine's workspace (not used for estimating  $\beta$ ), using the geometrical error model with estimated parameters to predict the deviations in measured lengths (radius). Applying the error model for (software) compensation techniques implies that the residual (i.e. the measured minus predicted) radius deviations should be small for all measuring points.

Second, the error components of the geometrical error model are validated with direct measurements (i.e. laser interferometry). The latter means that the error component described by its function including the estimated parameter(s) is compared to laser interferometry measurements of the same error component. If this difference is small, the geometrical error model can be used for error tracing purposes as well. The latter means that statements can be made about the origin of the measured positioning behaviour of the machine considered, which implies quantification of the error components.

## 4.1 Estimating geometrical error parameters

In this section the estimation of the geometrical error model parameters (see Section 3.1) from DBB measurement data (see Section 3.2) will be discussed. Also the results obtained with the DBB method will be presented in this section. Our goal is to predict the machine's positioning behaviour in its entire working volume as good as possible by means of a geometrical error model. This means that the absolute difference between the measured and modelled (i.e. predicted) machine behaviour should be minimised throughout the entire workspace of the machine:

$$\min_{\beta} |\xi_u - \hat{\xi}_u(\beta)| \quad \forall \mathbf{u}. \quad (4.1)$$

Due to the projection of the machine's positioning error on the DBB measurement axis, however, this entity cannot be minimised directly since no measurement information is available about  $\xi_u$  itself. Hence Equation 4.1 has to be transformed first to an entity that can be minimised: the measured length (or radius) deviations in this case. The latter implies that the DBB measurement model derived has to be taken into account besides the geometrical error model when determining the error model parameters from DBB length measurement data.

Since the error model and DBB measurement model derived are linear in the model parameters, linear least squares regression techniques can be used for the estimation of the parameters [Mon 92]. This means in this case that the model parameters ( $\beta$  and  $\gamma$ ) are estimated in such a way that the sum of the squared differences between deviations of the measured and modelled length (or radius) is minimised for all lengths. It is assumed that if the measured length deviations can be predicted, the machine's positioning and orientation error can be predicted as well. This assumption will be validated in Section 4.2.

### 4.1.1 Least squares regression

In Section 3.1 a geometrical error model has been derived which describes the tool positioning error  $\hat{\xi}_u^t$  as a function of the machine's axis positions  $\mathbf{u}$ , the tool vector  $\mathbf{t}$  and a set of parameters  $\beta$  (of size  $p \times 1$ ) to be identified.

$$\hat{\xi}_u^t(\mathbf{u}, \mathbf{t}, \beta) = \mathbf{H}(\mathbf{u}, \mathbf{t}) \cdot \beta. \quad (4.2)$$

Since length measurements are used in this thesis for assessing the machine's positioning behaviour, the error model equation is substituted in the derived DBB measurement model, see Equation 3.28:

$$\Delta r_u \simeq \mathbf{n}_u^T \cdot \mathbf{H}_u \cdot \beta - \mathbf{n}_u^T \cdot \gamma \quad (4.3)$$

which applies for a measuring point<sup>1</sup>  $u$ .

At this point the measurement alignment parameters  $\gamma$  enter the equation describing the measured radius deviation  $\Delta r_u$  as well as the projection of the

---

<sup>1</sup>The dependency of  $\hat{\xi}_u^t$  and  $\mathbf{H}_u$  on  $\mathbf{u}, \mathbf{t}$  has been omitted for the sake of simple notation.

machine's positioning error  $\xi_u^t$  on the DBB measurement axis  $\mathbf{n}_u$ . The problem is to find such a set of  $\beta, \gamma$  that the squared difference between the deviations in the measured and modelled radius is minimised over all measuring points  $N$ :

$$J(\beta, \gamma) = \sum_{u=1}^N (\Delta r_{u\_meas} - \Delta r_{u\_model})^2.$$

In regression analysis, this sum is referred to as the 'Sum of Squared errors' (SSE) [Mon 92]. The minimisation of this sum to the model parameters will be explained stepwise.

Consider a DBB measurement  $j$  containing  $m$  measuring points. For such a measurement the relevant variables (see Equation 4.3) are stored in vectors and matrices by introducing:

$$\mathbf{y}_j = [\Delta r_1 \quad \Delta r_2 \quad \cdots \quad \Delta r_m]^T, \quad (4.4)$$

$$\mathbf{X}_j = \begin{bmatrix} \mathbf{n}_1^T \cdot \mathbf{H}_1 \\ \mathbf{n}_2^T \cdot \mathbf{H}_2 \\ \vdots \\ \mathbf{n}_m^T \cdot \mathbf{H}_m \end{bmatrix}, \quad (4.5)$$

$$\mathbf{Z}_j = [-\mathbf{n}_1^T \quad -\mathbf{n}_2^T \quad \cdots \quad -\mathbf{n}_m^T]^T, \quad (4.6)$$

$$\mathbf{y}_j = \mathbf{X}_j \cdot \beta + \mathbf{Z}_j \cdot \gamma_j. \quad (4.7)$$

In Equation 4.7 the deviations in the measured radius depend on two terms. The term  $\mathbf{X}_j \cdot \beta$  on one hand represents that part of the  $m$  radius deviations measured that can be explained by the positioning errors of the machine. The remaining term  $\mathbf{Z}_j \cdot \gamma_j$  on the other hand represents the effect of the alignment error of DBB measurement  $j$  on the radius deviations measured. The latter means that this term describes that part of the radius deviations measured of DBB measurement  $j$ , that can be explained by a rigid body (a sphere with a fixed radius) displacement. This displacement is mainly due to the unknown stand position on the workpiece table. This alignment error vector  $\gamma_j$  is constant during a DBB measurement and is therefore given a subscript  $j$  to indicate this. For  $l$  DBB measurements the following holds:

$$\begin{bmatrix} \mathbf{y}_1 \\ \mathbf{y}_2 \\ \vdots \\ \mathbf{y}_l \end{bmatrix} = \begin{bmatrix} \mathbf{X}_1 & \mathbf{Z}_1 & 0 & \cdots & 0 \\ \mathbf{X}_2 & 0 & \mathbf{Z}_2 & \cdots & 0 \\ \vdots & \vdots & \vdots & \ddots & 0 \\ \mathbf{X}_l & 0 & 0 & \cdots & \mathbf{Z}_l \end{bmatrix} \cdot \begin{bmatrix} \beta \\ \gamma_1 \\ \gamma_2 \\ \vdots \\ \gamma_l \end{bmatrix}. \quad (4.8)$$

Note that the dimensions of  $\mathbf{X}_l$  ( $m \times p$ ) and  $\beta$  ( $p \times 1$ ) are much larger than the size of the variables  $\mathbf{Z}_l$  ( $m \times 3$ ) and  $\gamma_l$  ( $3 \times 1$ ).

Since the error model parameters  $\beta$  have to be determined rather than the measurement alignment parameters  $\gamma_j$  the latter are estimated first. This can

## 64 Parameter identification and validation geometrical error model

be realized by using a projection matrix [Str 88] by introducing the following variables:

$$\mathbf{y}_j^* = \left( \mathbf{I} - \mathbf{Z}_j (\mathbf{Z}_j^T \mathbf{Z}_j)^{-1} \cdot \mathbf{Z}_j^T \right) \cdot \mathbf{y}_j, \quad (4.9)$$

$$\mathbf{X}_j^* = \left( \mathbf{I} - \mathbf{Z}_j (\mathbf{Z}_j^T \mathbf{Z}_j)^{-1} \cdot \mathbf{Z}_j^T \right) \cdot \mathbf{X}_j \quad (4.10)$$

In this way, Equation 4.8 is transformed into:

$$\begin{bmatrix} \mathbf{y}_1^* \\ \mathbf{y}_2^* \\ \vdots \\ \mathbf{y}_l^* \end{bmatrix} = \begin{bmatrix} \mathbf{X}_1^* \\ \mathbf{X}_2^* \\ \vdots \\ \mathbf{X}_l^* \end{bmatrix} \cdot \boldsymbol{\beta}, \quad (4.11)$$

which can be easily seen by premultiplying Equation 4.7 with the projection matrix  $\left( \mathbf{I} - \mathbf{Z}_j (\mathbf{Z}_j^T \mathbf{Z}_j)^{-1} \mathbf{Z}_j^T \right)$ . This implies that that part of the radius deviations measured has been removed from the measurement data, that can be explained by a rigid sphere displacement [Str 88].

Finally the error model parameters  $\boldsymbol{\beta}$  are estimated by least squares approximation [Mon 92]:

$$\mathbf{y}^* = \mathbf{X}^* \cdot \boldsymbol{\beta}, \quad (4.12)$$

$$\boldsymbol{\beta} = (\mathbf{X}^{*T} \mathbf{X}^*)^{-1} \cdot \mathbf{X}^{*T} \cdot \mathbf{y}^*. \quad (4.13)$$

This requires that  $(\mathbf{X}^{*T} \mathbf{X}^*)^{-1}$  must exist, or in other words: matrix  $(\mathbf{X}^{*T} \mathbf{X}^*)$  can be inverted only if  $\mathbf{X}^*$  has a full rank [Mon 92] [Str 88]. The latter depends on the structure of the error model as well as on the measurement setup applied. Since the dimensions of these matrices are quite large, Equation 4.13 has been analysed by means of numerous numerical simulations, which is subject of the next subsection.

### Numerical simulations

In order to verify the possibility of reconstructing the machine's positioning behaviour from length deviations measured, a numerical simulation module has been developed, consisting of two separated parts [Flo 97].

Given the error model parameters (e.g. generated with a random number generator), the resulting positioning error of the machine's end-effector can be computed using the error model. Subsequently, these positioning errors can be projected on the DBB measurement axis by specifying the stand position in the machine's workspace as well as the semi-spherical measuring point distribution. In this way, virtual DBB measurements can be generated (assuming that the error model is correct: the parameters present are identifiable).

The next step is to offer the virtual DBB measurements to the estimation algorithm, as derived in the previous subsection. The solution of this algorithm should resemble the entered error model parameters and obviously depends on

the simulated conditions. A simulation is called successful if the entered and solved error model parameters are identical.

The solution of the error model parameters  $\beta$  from length deviations (i.e.  $\mathbf{y}^*$ ) is determined to a large extent by the properties of matrix  $\mathbf{X}^*$ . The number of rows equals the number of measuring points and the number of columns resembles the number of error model parameters to be solved. Using the simulation module, the effect of the following items has been analysed:

- DBB measurement setup;
- Semi-spherical measuring point distribution;
- DBB length;
- Influence of measuring noise.

Regarding Equation 4.13 it is obvious that the number of measuring points must exceed the number of parameters to be solved: if not, the matrix  $\mathbf{X}^*$  cannot have a full rank. Furthermore, the number and location of semi-spherical DBB measurements determines mainly the number of parameters that can possibly be (distinguished and) solved. By applying the DBB measurement setup as discussed in Section 3.2.3, explaining the importance to vary the end-effector lengths as well as the stand position (vary the position of both DBB balls as much as possible in DBB measurements), all the error model parameters can be solved successfully. The opposite is also true: as long as the end-effector length and configuration and stand position has not been varied in X,Y and Z-direction, Equation 4.13 cannot be solved uniquely. By considering the three partial derivatives, see Equation 3.32, describing the sensitivity of radius deviations for the error model parameters, each simulation can be made successful. This proves that it is possible to retrieve the error model parameters  $\beta$  from deviations in length when the DBB measurement setup derived is applied, under the assumption of identifiability of the error model.

Besides the number of DBB measurements, also the distribution of the measuring points within a DBB measurement can be analysed. In this analysis, the two measuring points distributions shown in Figure 3.12 and Figure 3.13 have been compared by considering the condition number of matrix  $\mathbf{X}^*$ . This condition number represents the ratio between the smallest and largest singular value and should not be too small [Str 88], see Appendix F. Numerous simulations revealed that for an equal amount of measuring points the condition number is always larger (i.e. better) for a so-called birdcage distribution than for a homogeneous measuring point distribution, see Figure 4.1. In this figure the ratio between the smallest and largest singular value is depicted versus the number of measuring points, increased sequentially by reducing the step angle  $\phi^\circ$  in the respective measuring point (homogeneous versus birdcage) distribution. This difference is due to the omittance of less efficient measuring points in the proposed birdcage measuring point distribution, which therefore is preferable.

In addition, the influence of the nominal DBB length has been analysed by considering this condition number. It has been observed that this length

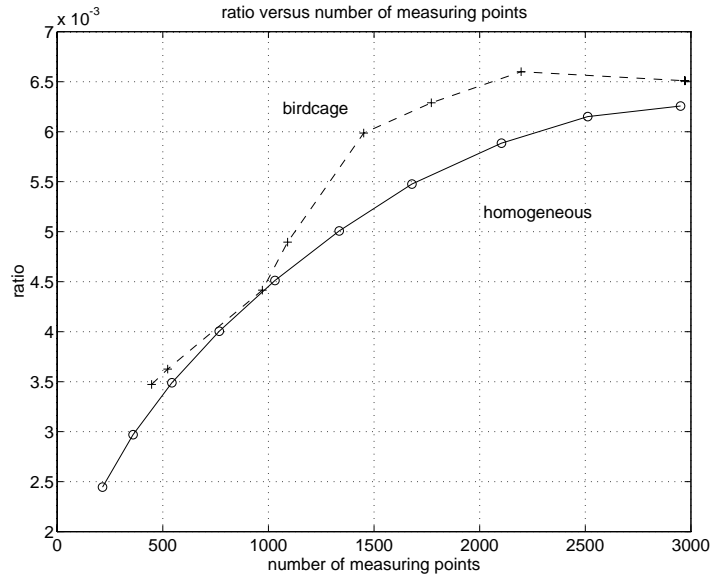


Figure 4.1: Influence measuring point distribution on the ratio between the smallest and largest singular value of the estimation matrix.

should be chosen as large as possible. This can be explained by the increase in variation of the regressor variables for long DBB lengths [Mon 97], facilitating the distinction between rotational and translational error components. Or more specifically: the term  $\frac{\partial c_i}{\partial \beta_i}$  changes more for longer DBB lengths (due to increased changes of  $\mathbf{u}$ ).

Finally measurement noise is added to the virtual DBB measurements. For the measurement setup derived, the resulting variations in parameter solutions seem to be proportional to the measurement noise. Reasonably measurement noise levels of several  $\mu\text{m}$  can be expected (i.e. DBB calibration error, influence of magnetic sockets in combination with DBB ball sphericity errors, etc.): the resulting distortions on the parameter estimates is limited to a small percentage of the simulated parameter value itself and is therefore not considered as problematic. This has been confirmed using Kalman filtering techniques [Mul 98]. This technique has been used since it enables quantification of the adaptation of the parameter solution (the Kalman gain) obtained by adding sequentially virtual DBB measurements.

Summarizing, machine error model parameters can be determined from DBB length measurements when taking the remarks made into account.

### 4.1.2 Geometrical error model optimisation

When applying Equation 4.13 to *real* DBB measurements performed on a five-axis milling machine (Maho 700S), problems with the variance of the parameter solution  $\beta$  have been observed: small variations in the error model (i.e. by adding/excluding certain parameters) and in the DBB measurement setup resulted in excessive variation of the parameter solution  $\beta$ . The parameters did not converge and the parameter variances were too large due to poor conditioning of matrix  $(\mathbf{X}^{*T}\mathbf{X}^*)$ . In this section the geometrical error model will be optimised in order to cope with these problems. This means in this case that the correlation between error model parameters has been investigated combined with the selection of the appropriate polynomial order of the error components, see Equations 3.2-3.4. The latter deals with the bias-variance dilemma.

#### Correlation

In linear regression the (co-)variance of estimated parameters is computed by [Mon 92]:

$$\text{cov}(\beta) = \frac{SSe}{N - (p + 3l)} \cdot (\mathbf{X}^{*T}\mathbf{X}^*)^{-1}, \quad (4.14)$$

$$\text{cov}(\beta) = MSe \cdot (\mathbf{X}^{*T}\mathbf{X}^*)^{-1} \quad (4.15)$$

with  $N$  indicating the total number of measuring points,  $p$  the number of error model parameters,  $l$  the number of DBB measurements and MSe represents the Mean Sum of squared errors. The value of MSe represents the average squared residual (this is the measured minus modelled) length deviation. In this thesis, the square root of this MSe value ( $\sqrt{MSe}$ ) will be used as an indication of the error model performance. This  $\sqrt{MSe}$  value represents the deviations in the remaining radius when applying the geometrical error model (e.g. for compensation purposes) and can be compared with the radius (length) deviations measured.

In order to judge whether parameter covariances  $\nu_{p,q}$  are significant, each covariance is scaled by using the corresponding variances  $\sigma_p, \sigma_q$ . This correlation coefficient  $r_{p,q}$  is defined as [Mon 92]:

$$r_{p,q} \simeq \hat{\rho}_{p,q} = \frac{\nu_{p,q}}{\sigma_p \sigma_q} \quad (4.16)$$

and its value lies between -1 and +1. Strong parameter correlations indicate that a mutual dependency between both parameters exists.

Computation of these correlation coefficients for the investigated machine (Maho 700S) reveals that rotational error components parameters are highly correlated with the straightness error components parameters ( $r_{p,q} > 0.8$ ). An explanation for this could be a relationship between these error components, assuming that the rotational error of an axis is proportional to the change of a straightness error with axis position. This relation depends on the kind of bearing of the machine axis. In Figure 4.2 the  $xxz$  error component is shown versus



the derivative of the  $xy$  straightness error, as measured by laser interferometry, showing a strong correlation. The rotational and straightness error component

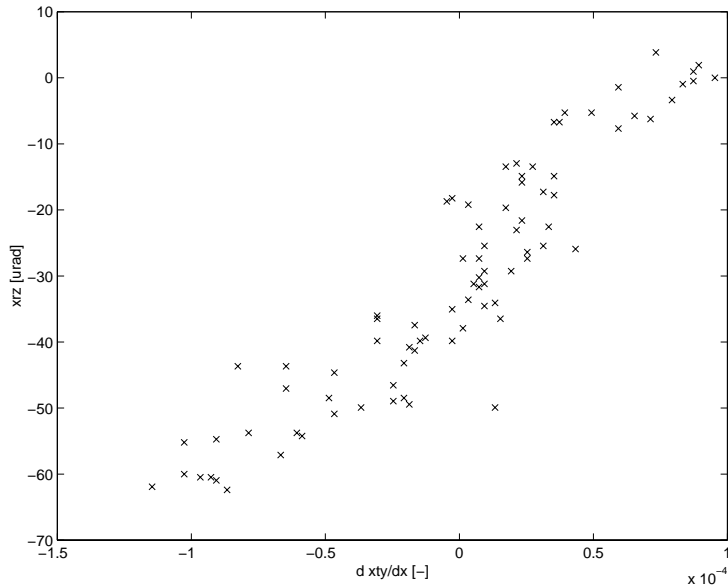


Figure 4.2: Correlation between error components.

parameters are strongly correlated. Although often observed in many machine configurations, this correlation is not necessarily present and can therefore generally not be assumed [Soo 93]. Consequently, this has to be verified when estimating the relevant parameters by calculating the correlation coefficients.

Due to the presence of these strong parameter correlations a selection has to be made between a rotational and a straightness error component to be included in the error model: including both results in excessive parameter variations. When comparing these two models, one can observe the reduction of the  $\sqrt{MSe}$  value due to a rotational and due to a straightness error component. This comparison reveals that including rotational error components in the error model reduces the  $\sqrt{MSe}$  value much more than including a straightness error component. Apparently the contribution of the rotational error components on the machine's positioning behaviour is much larger than for straightness errors. This is explained by the presence of relatively long arms of rotations, 'amplifying' rotational error in a machine considerably. Another explanation is the relatively poor sensitivity of DBB measurements for straightness errors, see Section 3.2.2 complicating the determination of a straightness error component (although theoretically possible) from DBB measurement data. For this reasons the straightness error components are omitted from the machine error model.

Furthermore strong parameter correlations were observed for the machine considered between the linearity errors (i.e. *iti*'s) and the rotational error com-

ponents of the same machine's axis. This correlation is due to the linear dependency of both error components on axis position as found in laser interferometry measurements performed on this machine. Comparison of models with and without linearity errors show that the contribution of the linearity errors is small compared to the contribution of the rotational error components: error models including the linearity errors reduces  $\sqrt{MSe}$  with  $0.2 \mu\text{m}$  only due to small values of the scale errors for the machine considered. For this reason only, error models without the linearity errors have been analysed as well. It should be stressed that cancellation of the linearity errors implies that the machine's scale errors are not included in the model anymore. This is justified only when the scale errors can be neglected with respect to the other error components.

### Selection of the polynomial order

In Section 3.1 error components have been modelled with ordinary higher order polynomial functions, see Equations 3.2-3.4. In order to find the appropriate polynomial order of these error component functions the contribution of a term in this function on the error model is considered. This means that the reduction of the  $\sqrt{MSe}$  value is compared for different error models (i.e. by including/excluding polynomial terms). This value is reduced as much as possible here without violating the repeatability limit of the machine (see Section 3.2.4) to avoid 'overfitting'. For the machine considered, positioning errors below  $2 \mu\text{m}$  simply cannot be realised and smaller values are therefore useless and must be avoided.

In Table 4.1 the  $\sqrt{MSe}$  value is computed for error components function sequentially extended with higher order terms, indicated by  $i$ . This implies that the Sum of Squared errors can only reduce when including higher order terms. Also a error model without the linearity error components has been considered. The error model reduces the radius deviations measured considerably for one

$i_{max}$	$\sqrt{MSe}$	$\sqrt{MSe}$ (without $iti$ 's)
0	11.05 $\mu\text{m}$	11.05 $\mu\text{m}$
1	2.24 $\mu\text{m}$	2.46 $\mu\text{m}$
2	1.34 $\mu\text{m}$	1.55 $\mu\text{m}$
3	1.26 $\mu\text{m}$	1.48 $\mu\text{m}$

Table 4.1: Model performance for extended error component polynomial functions applied to the Maho 700S milling machine.

or two parameters per error component function. Adding more parameters only marginally reduces the value of  $\sqrt{MSe}$  and is consequently of little use. Therefore the optimal number of parameters per error component function is between one or two, taking the repeatability limit of the machine into account ( $2 \mu\text{m}$ ). In addition, the contribution of including the  $iti$ 's error components in the error model is not significant due to a limited reduction of the  $\sqrt{MSe}$

## 70 Parameter identification and validation geometrical error model

value of  $0.2 \mu\text{m}$  only. Due to this small difference, the linearity errors are omitted from this error model.

The application of a (complex) error model with many parameters will usually result in smaller residuals (i.e. a small bias) than using rather simple error models. This however does not mean that complex models are better than simple ones due to a bias-variance dilemma [Gem 92]. This dilemma states

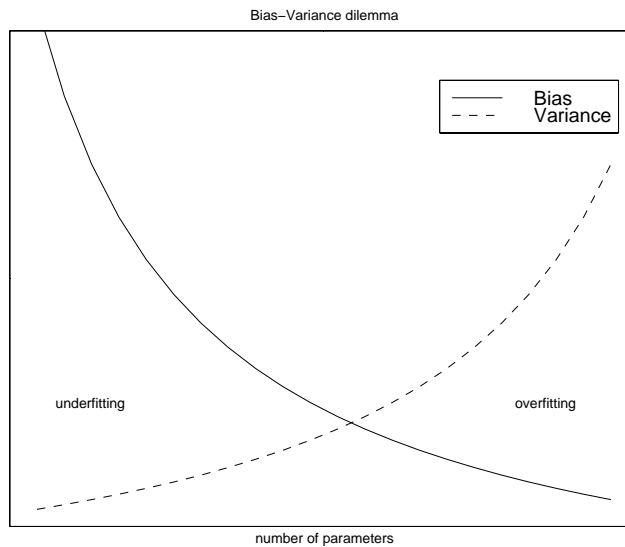


Figure 4.3: Bias-variance dilemma.

that for simple models on one hand the bias can be large, but the variance of the estimated parameters is small. For complex models on the other hand the bias can be small but the variance of the estimated parameters increases considerably due to overfitting. The latter implies that the model has lost its generalising properties: the model only works well for the measurement data used and loses its predictive power as desired. This bias-variance dilemma is visualised in Figure 4.3 where the abscissa represents the model complexity (i.e. amount of model parameters) and vertically the bias and variance of the parameters are depicted.

Since DBB measurement data are finite and contain a certain amount of noise, always a compromise has to be made concerning the bias error and the variance of the estimated parameters. This means, referring to Figure 4.3, that the left-hand side ('underfitting') as well as the right-hand side ('overfitting') has to be avoided. This way, reliable parameter estimations have been obtained: small modifications to the error model and/or to the measurement setup do not severely affect the value of the estimated parameters and their variance.

Finally, after removing (less significant) strongly correlated error model parameters the model is further tuned by modifying the polynomial order sub-

sequently for each error component individually. By analysing the  $\sqrt{MSe}$  reduction for each step, the appropriate polynomial order has been obtained: search for a low  $\sqrt{MSe}$  value with as less parameters as possible, without violating the machine's repeatability limit. A measure for this repeatability limit is assessed by considering the difference between successive (reversal) DBB measurements, see also Figure 3.14.

## Results

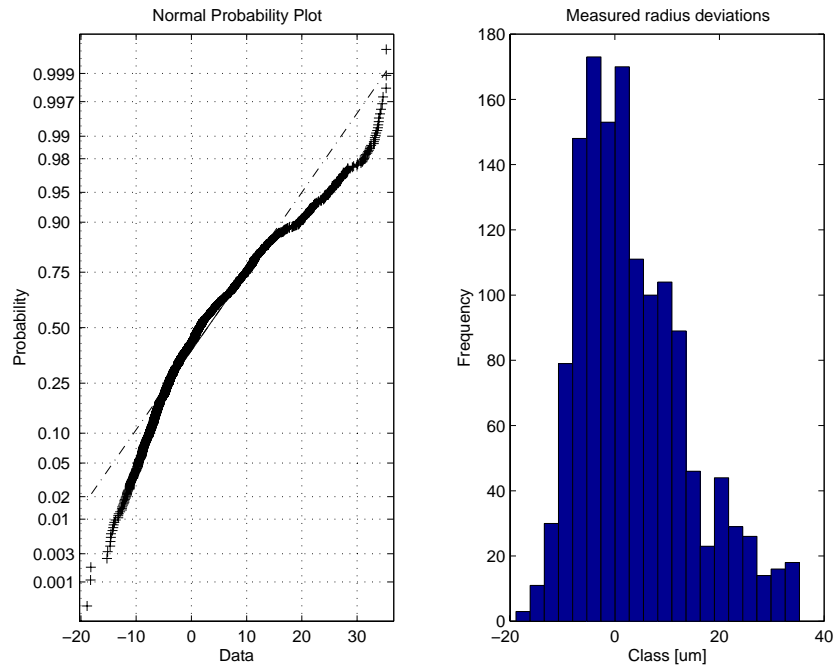
After estimation of the error model parameters, the geometrical error model can be used to predict the machine's positioning behaviour. For the estimation of these parameters 19 DBB measurement have been used (see Section 3.2.3) containing 1388 measuring points in total, performed on a five-axis milling machine (Maho 700S).

In Figure 4.4 the radius deviations measured, this is the measured radius minus the nominal (commanded) radius, for all lengths are depicted on a normal probability scale as well as in a histogram. Apparently, the majority of the radius deviations measured is too large and their distribution is far from normal. The largest radius deviation measured is about  $+35 \mu\text{m}$  and the average measured radius deviation equals  $+11 \mu\text{m}$ . By applying the geometrical error model, these radius deviations measured are transformed in the following residual radius deviations. Comparison of these figures (i.e. the abscissas of the histograms) reveals the capabilities of the error model to reduce the radius deviations measured.

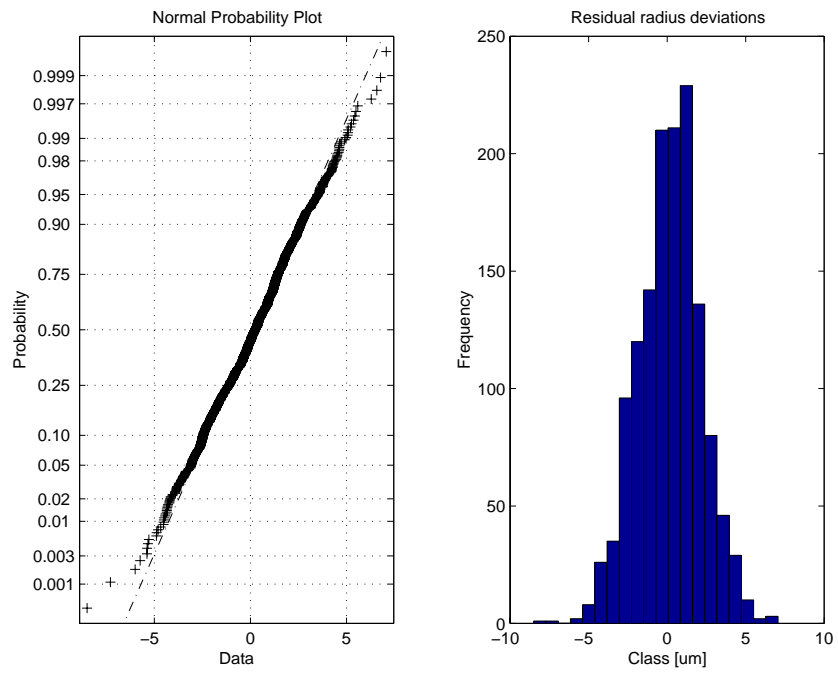
Obviously, the machine's positioning errors can be reduced significantly by using the error model: the radius deviations measured approach the repeatability limit of the machine. The average standard deviation of the residual radius deviation equals  $\sigma_{\Delta r_{res}} = 2.0 \mu\text{m}$ . A large improvement in the machine's positioning behaviour can be realised on the machine used for these experiments due to the small ratio between the random and systematic (i.e. repeatable) part of the radius deviations measured. For increasing ratios, the degree of improvement in the machine's positioning behaviour deteriorates. This ratio is machine specific.

In addition, the deviations in the residual radius follow a normal distribution, indicating that no deterministic information is left that could possibly be described by the error model. This is an important (residual) property when using least squares regression techniques [Mon 92] [Mon 97]. The average residual radius deviation equals  $0.3 \mu\text{m}$  and approaches the accuracy of the DBB used: the length measurement error of this device when comparing it with a (NKO) calibrated laser interferometer, see Appendix B.

Summarizing, in Section 4.1 the estimation of the model parameters (i.e.  $\beta$  and  $\gamma$ ) from DBB measurement data, using least squares regression techniques has been discussed. When estimating these parameters, the deviations in the measured radius are reduced as much as possible, taking the repeatability limit of the machine into account (to avoid overfitting). Due to strong parameter correlations, some error components (i.e. straightness error components) have



(a) measured radius deviation



(b) residual radius deviations

Figure 4.4: Experimental results obtained with a milling machine (Maho 700S).

been omitted from the error model. In this way stable parameter estimations have been obtained: small modifications to the machine error model and DBB measurements do not severely affect the value of the parameter solution obtained. Also the polynomial order of the error component functions is tuned to DBB measurements: search for a low  $\sqrt{MSe}$  value with as less parameters as possible. The latter deals with a bias-variance dilemma.

Finally the results have been presented. A significant improvement in the machine's positioning performance has been achieved: 95% of the residual radius deviations vary between  $\pm 4 \mu\text{m}$  only. Furthermore the residual radius deviations reveal a normal distribution.

## 4.2 Validation of the geometrical error model

The geometrical error model proposed is validated in two ways. First, the performance of the error model is cross-validated using DBB measurements. These measurements have been performed with another radius and on several locations in the machine's workspace and the error model is subsequently used to predict these measurements. Secondly, the estimated parameters, used for describing the machine's error components have been compared with direct measurements of the corresponding error component.

### 4.2.1 Validation based on DBB length measurements

In this section the cross-validation of the proposed geometrical error model is discussed using DBB measurements, performed on a milling machine (Maho 700S). For the estimation of the model parameters, a nominal DBB length of 250 mm has been used (see Section 3.2) while for the cross-validation measurements, a DBB length of 200 mm is chosen. In Figure 4.5 a top view of the machine's workspace is drawn, spanned by the machine's X- and Z-axis. In this figure, the DBB measurements used for estimation of the model parameters are drawn schematically (without discrete measuring points for clarity) with dashed arcs. The corresponding stand position is marked with a cross and these positions are indicated with numbers 1-5. In Figure 4.5 the cross-validation DBB measurements are represented schematically by solid circles. The corresponding stand positions are indicated with letters A-D. For these measurements a (short) tool with a length of 115 mm is used.

In Figure 4.6 the result of such a cross-validation DBB measurement is depicted. The deviation in measured radius is plotted versus the measuring point number of a semi-spherical DBB measurement, containing 81 points. By applying the geometrical error model to this DBB measurement, the deviations in radius are reduced significantly: the residual radius deviations are small compared to the radius deviations measured. The results of the other cross-validation DBB measurements are comparable to the displayed DBB measurement in Figure 4.6: 95% of all residual radius deviations are  $\pm 4 \mu\text{m}$  only.

These cross-validation measurements reveal that the error model derived, in combination with the DBB measurement setup proposed and parameter estima-

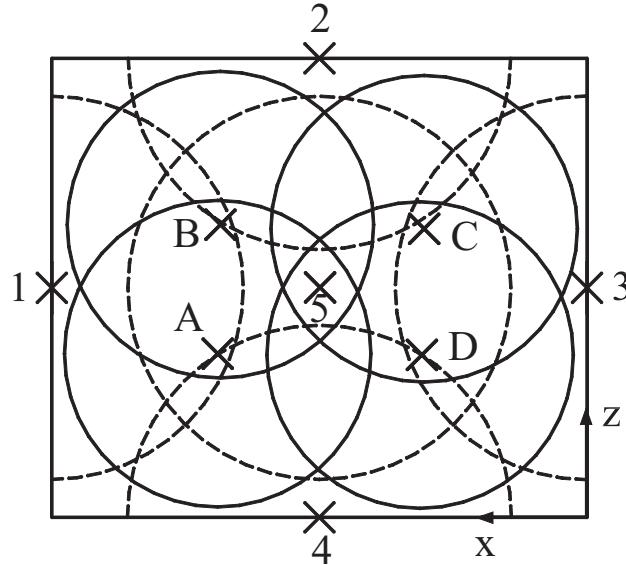


Figure 4.5: Top view cross-validation measurement positions in machine's workspace.

tion algorithm, is suitable for compensation techniques to enhance the machine's positioning performance. A significant reduction of the deviations in radius has been observed throughout the entire working volume of the machine. Furthermore the deviations in the residual radius approach the repeatability limit of the machine what must be considered as the upper limit of the achievable accuracy. Smaller values simply cannot be realised by this machine and have consequently no meaning.

In general, the degree of improvement in the machine's positioning behaviour depends on the ratio between the random (including unknown systematic errors) and systematic part of the measured deviations. For the milling machine used for these experiments this ratio is small ( $< 0.2$ ) resulting in a large accuracy enhancement. For CMMs in general this ratio is larger.

#### 4.2.2 Validation of the error components

In Chapter 3, Section 3.1 parametric error component functions have been presented, see Equations 3.2-3.4. In this section the estimated error components using DBB measurement data are compared to direct measurement of the same error component. For this validation, measurements performed on a milling machine (Maho 700S) are used.

For the direct measurement of error components a laser interferometer is preferably used due to its low measurement uncertainty in combination with a

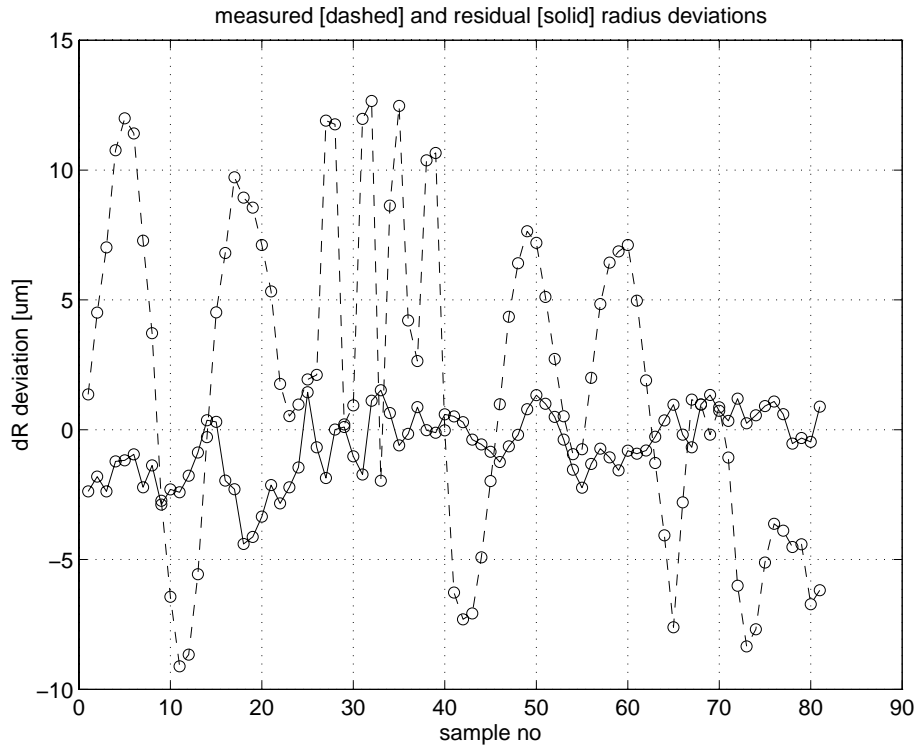


Figure 4.6: Cross-validation DBB measurement.

long measuring range (see also Section 1.3). For doing so, first the laser beam has to be aligned with the respective machine's axis whose error components are to be measured. In Appendix B the iterative alignment procedure of a laser beam with an axis is explained. After this alignment procedure, the relevant optical elements have to be mounted on the machine like a beam splitter, retro reflectors, turning mirror, adjustment devices etc. dependent on the kind (rotation, translation) and direction (horizontal, vertical) of the error component to be measured. Then small adjustments are necessary by translating and/or rotating certain optical elements in order to get an optimal beam strength before starting a measurement.

In Figure 4.7 a photograph is depicted, showing the measurement setup of a laser interferometry measurement on a milling machine, using rotation optics. More specifically, the rotational error of the Z-axis around the horizontal X-axis,  $zrx$  is measured this way. With this setup, the relative rotation of the (double) retro reflector (fixed to the milling head) with respect to the beam splitter (fixed to the workpiece table) is measured while moving the machine's axis successively to discrete measuring points distributed over its range. By performing this measurement including a reversal cycle, the respective  $zrx$  error





Figure 4.7: Direct measurement of error component  $zrx$  using a laser interferometer.

component can be determined.

In Figures 4.8 and 4.9 the results of three error components are compared: the line marked with ‘+’ is obtained using DBB measurements and the measurements obtained with direct measurements are indicated by ‘\*’. Due to the definition of the (centred) error component functions, the value of the error component is zero in the middle of the axis range: the  $2\sigma$  uncertainty in the estimated parameter indicates the slope error as drawn in Figures 4.8 and 4.9, not the value of the error component itself. These figures show the best ( $xrz$ ), a typical ( $yrx$ ) and the worst ( $zrx$ ) results obtained in this comparison. In general the error components revealed a good degree of resemblance: at least the trend and the order of magnitude of the error components is described correctly. The use of the estimated parameters to adjust the hardware of the machine (i.e. by grinding an axis guideway more ‘straight’) is, however, not recommended. The comparison of error component  $zrx$  as obtained with DBB measurements with the results of direct measurements (laser interferometry) for instance appears to be more troublesome, see Figure 4.9. This could be explained by the small (vertical) arm of rotation of this error component, complicating the determination of this error component with a DBB since it hardly results in a detectable displacement. For the same reason, the error in the estimated error component  $zrx$  does not affect the machine’s positioning behaviour seriously when using the geometrical error model. Due to the type of bearing of the Z-axis, the location of the rotational error introduced in the slide guideway system can shift forwards when the axis extends. Consequently, the actual arm of

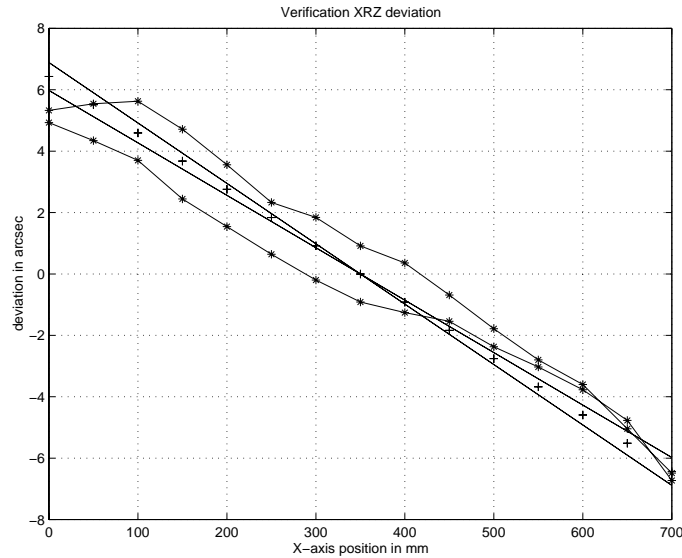
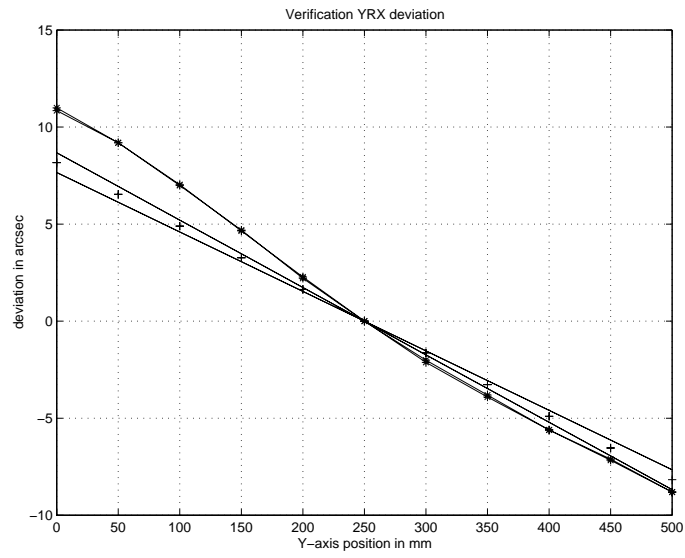
(a) Error component  $xrz$ 

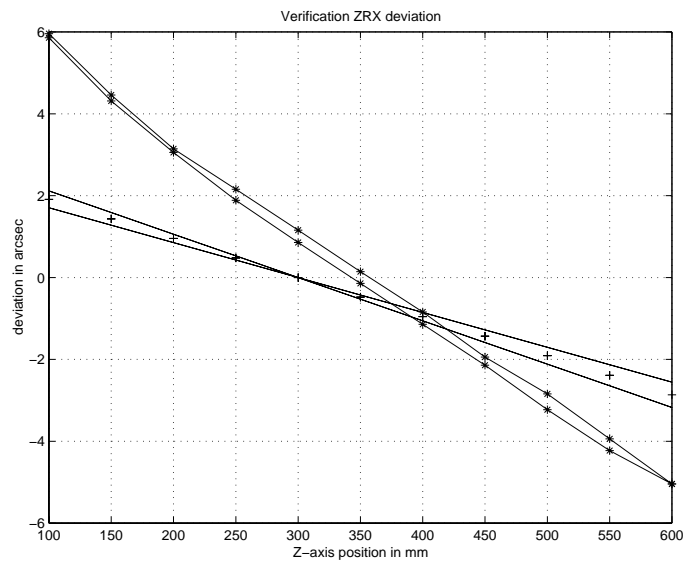
Figure 4.8: Validation measurement results of error component  $xrz$  of a Maho 700S milling machine, ‘\*’: measured, ‘+’: calculated.

rotation is shorter than the one used (see Section 3.1.3), resulting in an underestimated rotational error component  $zrx$ . The DBB measurement setup used, consisting of 19 DBB measurements, is especially suitable for purposes of error compensation (avoiding extrapolation); it could be adapted in such a way that certain error components can be determined better. The latter is not further investigated.

Summarizing, the method presented for assessing the machine’s positioning behaviour using DBB length measurements is suitable for error compensation techniques to enhance the machine’s accuracy (see Figure 4.4 and Figure 4.6). The possibilities of this method for determining error components (i.e. error tracing) are also present. Although in general a good degree of resemblance has been observed, the determination of an error component is most accurate using direct measuring techniques. The results obtained with the DBB method presented can therefore be used as a quick indication to search for significant error components. By performing DBB measurements frequently (for instance weekly), trends in the machine’s positioning performance and error components can be monitored and compensated for with little effort.



(a) Error component  $yrx$



(b) Error component  $zrx$

Figure 4.9: Validation measurement results of error components  $yrx$  and  $zrx$  of a Maho 700S milling machine, ‘\*’: measured, ‘+’: calculated.

## Chapter 5

# Thermally induced errors

The positioning behaviour of a multi-axis machine is affected to a large extent by the thermo-mechanical behaviour of its structural loop. Due to internal and external heat sources, the temperature distribution of a multi-axis machine changes in time. As a result the relative position and orientation of the end-effector with respect to the workpiece table changes. These thermally induced errors can deteriorate the positioning accuracy of a machine significantly, resulting in incorrect measurement results or geometry deviations of manufactured workpieces.

In this chapter a semi-analytical thermo-mechanical error model will be proposed used for describing the thermally induced positioning errors of a multi-axis machine with a serial kinematic structure. As a first approach, the machine's end-effector as well as the workpiece itself are disregarded and their thermo-mechanical behaviour is not included in this model. Such a model can be used for error compensation techniques to enhance the machine's accuracy and is primarily meant for machine tools. This model must be valid for any duty cycle of a machine, which may be located in a workshop.

This thermo-mechanical error model consists of 3 (sub-)models. First, the (instationary) temperature distribution of the machine parts present in the machine's structural loop is described. Secondly, a deformation model is proposed to calculate the resulting thermo-mechanical deformation of a machine part as a function of its temperature distribution. Thirdly, the relative position and orientation of the end-effector with respect to the workpiece table is obtained by superposition of the machine part deformations present in the machine's structural loop.

For validating the computed thermally induced relative drift of the end-effector, a specially developed measurement setup is used, employing a DBB. This means in this case that the radius deviations predicted (i.e. the predicted positioning error projected on the actual DBB measurement axis) are compared to measured radii. These validation measurements have been performed on a milling machine (Maho 700S).

In Section 5.1 a problem description is presented, which deals with mod-

elling thermally induced errors of multi-axis machines. After this introduction, a literature overview is presented in Section 5.2. Subsequently, in Section 5.3 a machine tool is divided into machine parts, using plates. The thermo-mechanical deformation of these machine parts is then discussed in Section 5.4. In order to compute these deformations, a temperature distribution is required. The description of such a temperature distribution is discussed in Section 5.5, explaining two methods. After combining the machine part deformations for obtaining the relative positioning error of the end-effector with respect to the workpiece table, subject of Section 5.6, the DBB measurement setup and procedure is presented subsequently in Section 5.7. Finally the validation of the thermal error models proposed is discussed in Section 5.8, followed by a resume in Section 5.9.

## 5.1 Problem description

Due to a changing temperature distribution of a multi-axis machine during operation, the relative position and orientation of the end-effector with respect to the workpiece (see  $\xi$  in Figure 1.1) changes in time. This is caused by thermally induced deformations of machine parts present in the machine's structural loop since the materials commonly used (i.e. steel, cast iron etc.) expand with temperature rise.

Since the machine parts deform thermally, including bending, rotational errors are introduced in the machine's structural loop. This structural loop is determined by the machine's configuration, the axis positions and the size and configuration of the end-effector. In order to compute the effect of these rotational errors on the machine's positioning accuracy (see also Section 3.1.3) the machine's axis positions (i.e.  $\mathbf{u}$ ) as well as the size and configuration of the end-effector (i.e.  $\mathbf{t}$ ) has to be taken into account. The thermally induced relative drift of the end-effector can therefore be expressed as:

$$\xi = f(\mathbf{u}, \mathbf{t}, t)$$

where  $t$  represents time. Experimental observations confirm these dependencies [Soo 93] [Spa 95].

Although the thermally induced positioning and orientation errors of a multi-axis machine change with time, there is no direct relationship between these two entities. It is the changing temperature distribution of the machine that is responsible for the resulting relative thermo-mechanical drift of the end-effector. These changes in temperature distribution are caused by changing heat flows in the machine. These heat flows can be imagined as vector entities, characterised by a magnitude and a direction. These changing heat flows are among others the result of a change in magnitude of internal and external heat sources present. Examples of internal heat sources are the spindle bearings, spindle motor, gearboxes, (hydraulic) pumps, axis actuators etc. The magnitude of these internal heat sources clearly depend for instance on the tool spindle speed, which can change frequently when using the machine in a workshop. In addition, the

magnitude of internal heat sources depend also on lubricant viscosity (which depends on temperature and lubricant type), on pre-load on bearings, oil level in gearboxes, type of gearwheel etc. [Sme 98]. Summarizing, the magnitude of the internal heat sources present in a multi-axis machine is varying in a complex way and results in changing heat flows in the machine's structural loop. Furthermore external heat sources can change in magnitude as well, like the effect of air temperature or cooling liquid for instance. Numerous measurements of the surrounding air temperature revealed that this air temperature is not constant in time nor place in workshop conditions [Wie 00].

Besides the magnitude of the internal heat sources, also the relative position of these heat sources with respect to the machine's structural loop are subject to changes when the machine moves its axes. Due to these movements the heat transfer rates between various machine parts is changed as well. Not only by another relative position of the heat sources with respect to the machine's structural loop, but also due to another local surrounding air temperature and altered heat flow resistances. The latter for instance depends among others on the machine's axis positions.

Summarizing, the thermo-mechanical behaviour of multi-axis machines is complex. When considering the modelling of thermo-mechanical behaviour of multi-axis machines with a serial kinematic structure, the following steps/items can be distinguished:

1. Dividing a machine tool into machine parts with a certain (simple) geometrical shape;
2. Description of the (instationary) temperature distribution of machine parts;
3. Calculation of the accompanying thermal deformation of machine parts based on its temperature distribution;
4. Calculation of the relative drift of the end-effector with respect to the workpiece table from thermally induced machine part deformations present in the machine's structural loop;
5. Validation thermo-mechanical error models by measuring the thermally induced errors in the end-effector position and orientation relative to the workpiece table.

These items will be discussed successively.

## 5.2 Literature overview

Thermally induced errors of multi-axis machines have been subject of extensive research [Bry 68] [Bry 90] [Wec 95]. In order to describe the thermally induced positioning behaviour of a multi-axis machine by means of a model, three methods can be distinguished:

1. Empirical models;
2. Analytical models;
3. Hybrid models.

Empirical models relate the measured drift of the end-effector with respect to the workpiece table to measured temperatures performed on various locations on the machine at certain time intervals. This relation can be expressed as:

$$\Delta \hat{\xi}(t) = \mathbf{C} \cdot \mathbf{x}(t) \quad (5.1)$$

where  $\mathbf{x}(t)$  represents a vector containing temperature sensor readings, varying in time and matrix  $\mathbf{C}$  contains coefficients to be determined experimentally. The coefficients in matrix  $\mathbf{C}$  can then for instance be determined using multi-variable regression analysis by fitting measurement data [The 91] [Spa 95] [Lee 02]. Other possibilities are the use of neural networks [Che 94] [Che 95] [Wec 98] [Deh 98], fuzzy modelling [Zho 99] or thermal modal analysis [Bue 96] to retrieve the relationship between the thermal relative drift of the end-effector and temperatures on the machine.

The thermally induced drift of the end-effector with respect to the workpiece table can be measured as depicted in Figure 5.1 [The 91] [Soo 93] [Spa 95]. A cylinder (or ball) is put in the machine's spindle and its relative displacement (and orientation when using a cylinder) is measured with 4 respectively 6 displacement transducers. In the picture displayed on the right-hand side six displacement transducers can be seen, used for measuring relative tool displacements. An additional displacement transducer is needed to compensate the relative tool displacement for diameter changes of the cylinder.

For heating up a machine tool, various spindle speeds are usually applied during such measurements. Besides a constant spindle speed (up to 6000 rpm for a Maho 700S) for a certain time also a spindle speed spectrum can be used where the spindle speed is varying in time (see also ISO 230-3). In Figure 5.2 an example of such a spindle speed spectrum is depicted according to DIN 8602. In this way, measurement data can be collected under different thermal conditions.

Although satisfying results have been reported when using empirical error models [The 91] [Spa 95] [Lee 02], this method possesses some drawbacks. First, the dependency of the machine's thermal drift on the machine's axis positions as well as the end-effector geometry is often omitted. Secondly, the optimal *set* of model coefficients (the elements of matrix  $\mathbf{C}$  in Equation 5.1) is hard to find, mainly due to overfitting problems since a large number of temperature sensors are generally available to be used in the thermal error model. Furthermore no physical information is used when constructing the thermal error model, deteriorating its reliability. In addition, such an empirical model is machine specific and must be generated separately for each machine.

Another approach to model the thermally induced positioning behaviour of multi-axis machines is by using physical relations describing the machine's thermo-mechanical behaviour. An advantage of this method over the empirical method is that such models are machine-type specific: machines belonging to



(a) Overview measurement setup



(b) Close up view of setup

Figure 5.1: Measurement setup for determining the thermally induced drift of the end-effector with respect to the workpiece table [The 91] [Soo 93] [Spa 95].

a specific type behave in the same way. Depending on the chosen input, one, two or three models are required for this purpose. First, a model is needed that determines heat flows in a machine, using ambient temperatures and operating conditions such as spindle speed, end-effector geometry and joint movements. Secondly, a model is required that relates the temperature distribution of the machine's structural loop to heat flows in the machine. Thirdly, the resulting thermo-mechanical deformation of machine parts present in the machine's structural loop needs to be modelled in order to determine the relative drift of the end-effector with respect to the workpiece table.

Generally a large amount of information about the machine is required for constructing an analytical machine error model. Finite element and finite difference techniques have been used by many researchers to model thermal errors, see [Sat 73] [Wec 75] [Oku 75] [Cam 76] [Att 79] [Jed 90]. In general these techniques are used to calculate both the temperature distribution and the resulting deformations. The inputs for these models are analytically or empirically determined heat flows. In some cases the measured temperature distribution is used as input since this temperature distribution is hard to predict, mainly due to uncertainties in the thermal boundary conditions [Bal 90] [Bry 90] [Soo 93] [Spa 95] [Wec 95]. The results obtained using this method reveal that the ma-



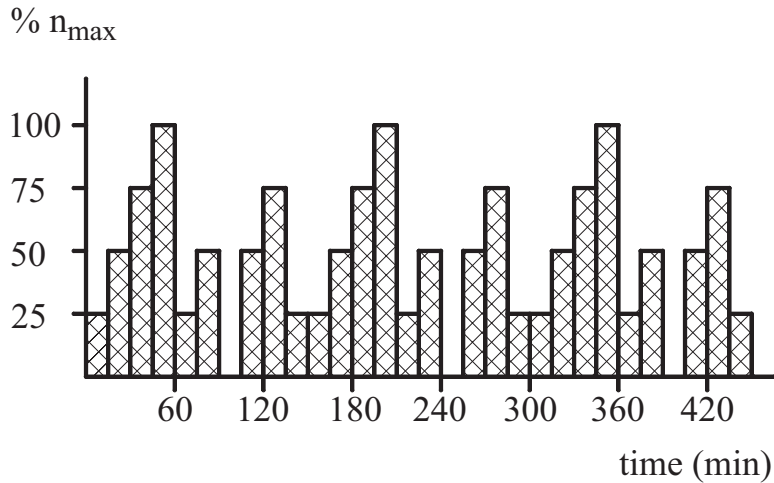


Figure 5.2: Duty cycle according to DIN 8602.

chine's thermo-mechanical behaviour can be described reliable in a rather qualitative way: the quantitative results are often disappointing [Bry 90].

Many thermal error models reported can not be considered as pure analytical nor empirical since both methods are used combined. The thermal distribution of a machine can for instance be modelled empirically (or measured) while the resulting machine deformations are determined analytically. The term 'hybrid' refers to this kind of models.

### 5.2.1 Research objective

In this research project a hybrid error model is desired that describes and predicts the thermo-mechanical behaviour of multi-axis machines, suitable for error compensation techniques. This model must be generated with relatively little effort, aiming for application in industry. This model is machine type dependent and must take the effect of internal heat sources present into account as well as the effect of the ambient air temperature on the machine's thermally induced positioning behaviour. Other external heat sources are not considered in this thesis for reason of simplicity like the heat generated by the cutting process or the use of cooling liquid for instance. For the measurement of the thermally induced drift a DBB is introduced and employed. This measuring instrument is also used for validation of the thermo-mechanical error model proposed.

### 5.3 Thermo-mechanical modelling of a machine tool

In this section, a kinematic model of a machine tool is constructed by dividing the machine into machine parts. These machine parts are bodies in the machine, that are separated by a machine's axis, or bodies which are connected (i.e. bolted) together. In this way, the complex geometry of a machine tool is simplified into simple geometrical shapes in order to facilitate the computation of thermally induced errors. By combining the machine part deformations computed, the relative drift of the end-effector with respect to the workpiece table can be computed. The construction of a machine tool can generally be

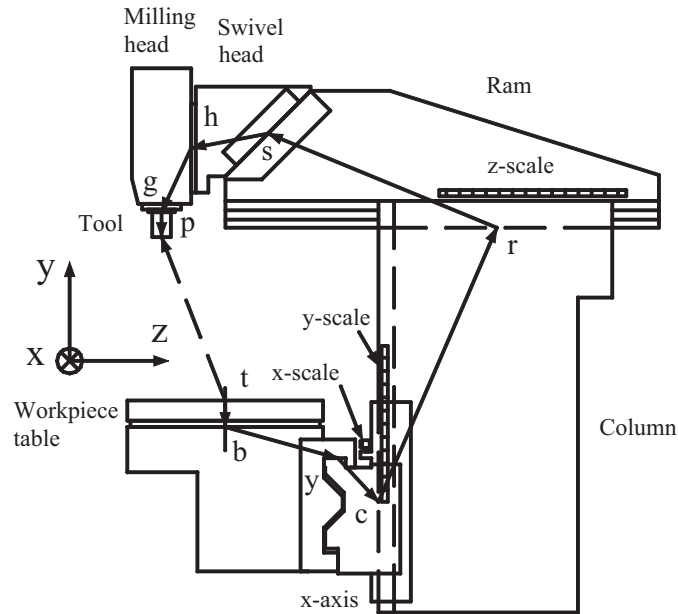


Figure 5.3: Machine model of milling machine (Maho 700S) in the vertical plane. The solid fat arrow line indicates the path used for computing machine part deformations: these are the successive vectors t-b, b-y, y-c, c-r, r-s, s-h, h-g and g-p.

modelled as a plate framework structure. This kind of structures are often used when designing a machine tool or a measuring machine since it combines a high stiffness with a relatively low mass unlike solid structures for example. The latter becomes relevant when considering the machine's dynamical behaviour for instance, which is generally important for this kind of machines. As a result, plate structures are widely used for constructing a machine's frame. This means that a machine part usually consists of two parallel plates, connected by

intermediate plates. In a first instance, such a machine part is modelled by one single plate, using symmetry in the vertical plane of the machine.

Subsequently, a machine tool is modelled by plates, which can move relatively due to axis movements. The machine's kinematic chain is divided into eight separated machine parts. Note that this flat plate-model is parallel to the YZ-plane.

The machine's scales are omitted in this model although their influence on the machine's thermal behaviour can be significant. The thermal expansion of the scales is treated separately as if it is stretching/shrinking the machine's working volume. Regarding Figure 5.3 this means that only the errors of the scale corresponding to the X-axis can introduce positioning errors of the machine in X-direction in the thermo-mechanical error model proposed.

In order to compute the thermally induced drift of the end-effector with respect to the workpiece table, the thermo-mechanical deformation of the 8 machine parts, as shown in Figure 5.3, has to be modelled first.

## 5.4 Thermal deformation of machine parts

Since the temperature distribution of machine parts is usually not homogeneous at 20 °C, the geometry of these machine parts changes due to thermal expansion. The machine parts are assumed to expand isotropic and freely: the resulting thermal expansion is not constrained by mechanical stresses induced by other machine parts. In this section, the calculation of the thermal deformation of a machine part based on its temperature distribution is discussed. The temperature distribution of a machine part is measured using a large number of temperature sensors (52) distributed over the machine's construction. The temperature distribution of a machine part is subsequently obtained by fitting (locally) linear gradients, using surrounding temperature sensor readings attached on the machine part [Bus 01]. This means that the temperature distribution considered can be expressed as:

$$T(y1, z1) = T_N + G_{y1} \cdot y + G_{z1} \cdot z$$

with  $G_{y1}$  and  $G_{z1}$  denoting the fitted linear gradient constants and  $y1, z1$  represent local coordinates of the machine part considered, see Figure 5.4.  $T_N$  represents the temperature at the middle of the line segment from  $i_0$  to  $i$ . The machine part deformations are subsequently computed by considering this line segment.

The basic equation used for calculating stress free thermal expansion of a body is usually expressed as:

$$\Delta\ell = \alpha \cdot \ell(T - 20\text{ °C}) \quad (5.2)$$

where  $\Delta\ell$  represents the thermal expansion [m],  $\alpha$  stands for the thermal expansion coefficient [ $\text{K}^{-1}$ ], and  $\ell$  is the nominal object length [m] (defined at 20 °C). The body temperature is denoted by  $T$  [°C].

Due to the plate framework construction of multi-axis machines, the thermal deformation of plates has to be described in this case. These plates are assumed to deform in their plane only: no deformations perpendicular to the plate's plane are considered. Due to the good heat conductive properties of the machine part material (steel, cast iron), no thermal gradients over the plate thickness are to be expected. As a result, a plate only deforms in its plane. This implies that two translational errors, acting in the plate's plane, have to be considered as well as one rotational error (thermally induced bending), acting perpendicular to the plate's plane.

In order to describe the thermally induced translational errors ( ${}_i T_{y1}$ ,  ${}_i T_{z1}$ ) and rotational error ( ${}_i R_{x1}$ ) between two points on a plate  $i$ , error components are introduced, see Figure 5.4. These error components are used to describe

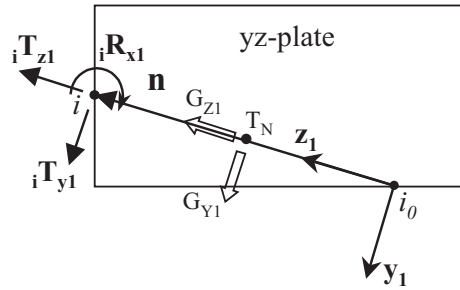


Figure 5.4: Temperature field and three error components of a plate  $i$  expressed in local coordinates.

the three thermal deformation modes of a plate in its plane by considering the elongation, the bending and transversal translation of the line segment between the points  $i_0$  and  $i$ . This line segment is described by a vector and its length is denoted by  $l_{zn}$ , which depends on the actual axis positions of the machine. By using local coordinates  $y1, z1$ , the following holds for the error components introduced [Bus 01]:

$${}_z T_{z1} = \alpha_N \int_0^{l_{z1}} (T(y, z) - 20) dz1 = \alpha_N (T_N - 20) \cdot l_{z1} \quad (5.3)$$

$${}_z R_{x1} = \alpha_N \int_0^{l_{z1}} G_{y1} dz1 = \alpha_N \cdot G_{y1} \cdot l_{z1} \quad (5.4)$$

$${}_z T_{y1} = -\alpha_N \int_0^{l_{z1}} \int_0^{l_{z1}} G_{y1} dz1^2 = 1/2 \cdot \alpha_N \cdot G_{y1} \cdot l_{z1}^2. \quad (5.5)$$

Due to the assumption of linear temperature distributions, the elongation  ${}_z T_{z1}$  of the line segment is completely determined by the average temperature over this line segment, which equals  $T_N$ .

Summarizing, the denoted error components are a function of the temperature  $T_N$  determined at the centre of the line segment, the local gradient  $G_{y1}$ ,

the coefficient of expansion  $\alpha_N$  and the length of the line segment  $l_{z1}$ . The latter depends on the axis positions X,Y,Z of the machine in order to evaluate the relevant line segment in a plate, used for calculations. This procedure is performed for each machine part.

In addition to the linear approach described, also a method has been derived for computing machine part deformations considering more complex temperature distributions, other than homogeneous and/or linear [Bus 01]. The description of the resulting thermal deformation of a machine part becomes difficult in such cases due to thermally induced stresses and strains present. These stresses constrain the thermal deformation to a certain extent and application of the Equations 5.3, 5.4 and 5.5 result generally in deformations of machine parts, which are over-estimated. Furthermore, the description of deformations of a machine part is not consistent anymore when using the linear approach presented: the computed deformations depend on the path used between two points of interest, used for computations. By introducing a so-called neutral point, a point for which thermal deformations are zero or minimal, to be used as a reference point for describing temperatures and deformations locally, the consistency problem can be solved. However, the effect of the thermal strains on the resulting thermo-mechanical deformation still needs to be taken into account. When comparing this approach with the presented linear one, small improvements have been observed in the capabilities of the thermo-mechanical machine error model to describe the measured relative drift of the end-effector with respect to the workpiece table [Bus 01].

## 5.5 Describing the temperature distribution of machine parts

In this section, methods are discussed to describe the temperature distribution of a multi-axis machine, while the machine is excited thermally by executing a certain duty cycle. For this purpose, the following two methods can be distinguished, using temperature sensors:

- Measuring the temperature of various machine parts and assuming linear temperature distributions between sensor positions;
- Applying models based on thermo dynamical theory in combination with a reduced number of temperature sensors.

The most straightforward way to describe the temperature distribution of a machine part is just to measure it, using temperature sensors attached to various machine parts. The temperature in between temperature sensors is subsequently obtained by linear interpolation, using surrounding temperature sensors. This method has been used as a first approach in this research project [Bus 01]. In Figure 5.5 the temperature sensor positions on the machine considered are displayed. The spatial density of the sensors in the upper half of the machine is increased when compared to the lower half since the temperature

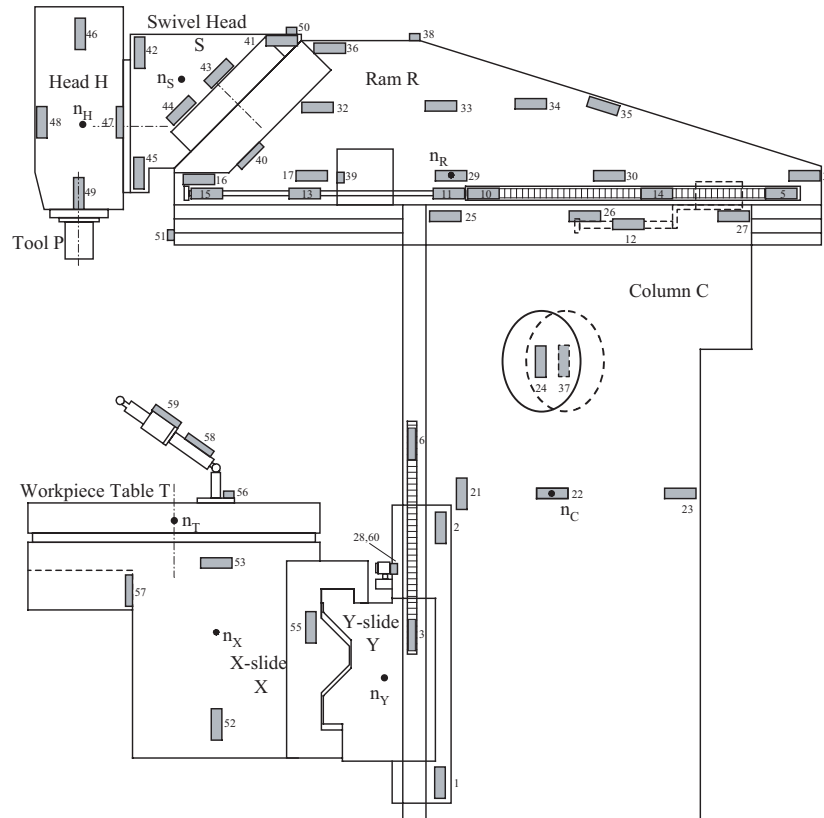


Figure 5.5: Temperature sensor distribution on Maho 700S milling machine.

distribution is more complex in that area of the machine due to the presence of internal heat sources. Despite the reliability and potential accuracy of this method, a considerable amount of temperature sensors is usually required for obtaining a reasonable description of the machine's temperature distribution. This is mainly caused by the assumed linear temperature distribution between sensor positions.

In order to limit the errors in the machine's temperature distribution, a large number of sensors is primarily used during this research project. In actual applications on a workshop floor, however, a reduced number of temperature sensors should be required by using previously obtained knowledge of the machine's thermo-dynamical behaviour.

Besides using temperature sensors, a temperature distribution can be measured by applying infrared thermography. The latter however is difficult and expensive and is preferably used in a qualitative sense rather than in a quantitative sense (due to complex instrument calibration and related temperature

uncertainty) [Ber 01].

Another possibility to describe the temperature distribution of a machine part is by using a model in combination with a limited number of temperature sensors. Usually such a model is used in order to reduce the number of temperature sensors required for obtaining a good approximation. This means that heat flows in machine parts have to be considered, necessary for determining certain temperature changes (i.e. temperature time derivatives:  $\frac{\partial T}{\partial t}$ ) in time. For these heat flows, three physical mechanisms are responsible which all result from temperature differences:

1. Conduction;
2. Convection (free and forced);
3. Radiation.

### Conduction

Conduction is the transition of heat through a substance (a gas, liquid or solid) without perceptible motion of the substance itself [Jan 88]. The amount of heat transport per unit area is considered to be proportional with the temperature difference per unit length and this heat flow  $q_{cond}$  is usually expressed as [Jan 88]:

$$\frac{q_{cond}}{A} = \frac{k}{L}(T_1 - T_2) \quad (5.6)$$

with  $A$  representing the cross sectional surface between two elements with temperatures  $T_1$  and  $T_2$  respectively. The distance between these elements is denoted by  $L$ . The constant of proportionality  $k$  represents the thermal conductivity of the substance, which depends on the material [Bir 60]. Applying Fourier's conduction law in three dimensions then results in [Bir 60] [Jan 88]:

$$\frac{1}{\alpha} \frac{\partial T}{\partial t} = \frac{\partial^2 T}{\partial x^2} + \frac{\partial^2 T}{\partial y^2} + \frac{\partial^2 T}{\partial z^2} + \frac{Q}{k} \quad (5.7)$$

with

$$\alpha = \frac{k}{c \cdot \rho}$$

where  $T$  represents temperature [ $^{\circ}\text{C}$ ],  $t$  time [s] and  $\alpha$  the thermal diffusivity of the material [ $\text{m}^2/\text{s}$ ]. The thermal conductivity coefficient is denoted by  $k$  [ $\text{W}/\text{mK}$ ],  $c$  stands for the specific heat [ $\text{J}/\text{kgK}$ ] and  $\rho$  for the density [ $\text{kg}/\text{m}^3$ ]. In Equation 5.7,  $Q$  represents a heat source [ $\text{W}/\text{m}^3$ ].

### Convection

Besides conduction, heat can be exchanged with the environment by means of convection. Convection is associated with fluid and/or gas motion [Jan 88]. This motion can be forced (for instance by a fan) and the resulting heat transfer is called 'forced convection'. When fluid/gas motion is due predominantly to

the presence of a thermally induced density gradient the heat transport is called ‘free’ or ‘natural convection’ [Jan 88]. In both cases the heat transfer rate per unit area is expressed as (Newton’s law of cooling):

$$\frac{q_{conv}}{A} = h_c \cdot (T_b - T_\infty) \quad (5.8)$$

where  $q_{conv}$  represents the heat flux [W],  $A$  stands for the area [m<sup>2</sup>] and  $h_c$  denotes the average convection heat transfer coefficient (or film conductance) [W/m<sup>2</sup>K].  $T_b$  is the body temperature and  $T_\infty$  represents the bulk temperature of the fluid/gas (the free-stream temperature). The average heat transfer coefficient  $h_c$ , however, is usually not known and is often determined experimentally.

### Radiation

The last heat transfer mechanism to be discussed is heat transport by means of radiation. The heat flux per unit area is proportional to the absolute temperature to the fourth power [Jan 88]:

$$\frac{q_{rad}}{A} = \sigma \cdot \varepsilon T^4 \quad (5.9)$$

where  $A$  denotes the radiating area [m<sup>2</sup>],  $\sigma$  represents the Stefan-Boltzmann constant [ $5.67 \cdot 10^{-8}$  W/m<sup>2</sup>K<sup>4</sup>] and  $\varepsilon$  stands for the emissivity coefficient [-].  $T$  represents the absolute temperature [K] of the radiating body.

### Heat sources

A serious problem for describing a temperature distribution analytically is the magnitude of the heat sources present in the model equations ( $Q$  in Equation 5.7). The magnitude of these heat sources changes considerably and is generally hard to predict. In this research project, no effort is made to determine the magnitude of these heat sources. A practical approach to circumvent this problem is to attach temperature sensors in close proximity to these heat sources. In this way the effect of the heat sources on the resulting temperature distribution can be taken into account indirectly. The position of these heat sources in a machine are generally known or can be identified experimentally.

#### 5.5.1 Approximation methods

The partial differential Equation 5.7 can only be solved analytically for certain geometries (i.e. an half-infinite plate, a sphere) with certain boundary conditions [Sme 98]. For geometries present in multi-axis machines such an analytical solution can generally not be determined. For this reason, several approximation methods have been developed like the Lumped Capacitance Method (LCM), Finite Difference Method (FDM), Finite Element Method (FEM), Boundary Element Method (BEM), Thermal Network Method (TNM) etc. [Sme 98]. With these methods, a machine or machine part is divided into elements, whose temperatures are computed. By combining the calculated element temperatures



using certain interpolation functions, a temperature distribution can be approximated. Such a model, which is machine type dependent, should be used in combination with some temperature sensors in order to limit the errors in the modelled temperatures.

Based on a preliminary study, a choice for the extended Lumped Capacitance Methods has been made, mainly due to the limited modelling effort required when compared to the other methods mentioned [Sme 98].

### 5.5.2 Extended Lumped Capacitance Method

One approximation method for describing temperature distributions is the extended lumped capacitance method [Jan 88] [Sme 98]. In this case, a machine or machine part (i.e. a plate) is divided into elements or so-called lumps. The accuracy of the method depends among others on the size of these lumps: smaller elements usually result in smaller modelling errors but the modelling effort is increased. Therefore a compromise has to be made concerning the element size.

A major assumption of the extended lumped capacitance method is that the internal element heat flow resistance is negligible. This means that there are no thermal gradients present in a single lump: the temperature distribution within a lump is homogeneous. This assumption has to be verified by computing the Biot number for such a lump. The Biot number is a dimensionless ratio of convection to conduction resistance to heat transfer [Jan 88]:

$$Bi = \frac{h_c \cdot L_c}{k} \quad (5.10)$$

where  $L_c$  represents a characteristic length [m], which is often obtained by dividing the element volume by its surface area [Jan 88]. The average heat convection coefficient is denoted by  $h_c$  and  $k$  stands for the thermal conductivity coefficient. It can be shown that if this Biot number is smaller than 0.1, the lumped capacitance method can be used with small approximation errors [Jan 88].

This Biot number has been computed for several geometries. For a solid square steel bar with dimensions  $200 \times 200 \times 1000$  mm for instance the Biot number equals 0.0125 [Sme 98]. For hollow structures and plates, this number is even smaller (i.e. an order of magnitude) since the characteristic length decreases considerably for such geometries. This kind of structures are mainly found in the (plate) frame construction of multi-axis machines. Due to the good heat conductivity of the material commonly present in a machine's structural loop (i.e. steel, cast iron: large  $k$ ) the assumption of a negligible internal heat resistance is met over the plate thickness.

As stated before, no heat sources are modelled since their magnitude is hard to predict. The effect of a heat source can be accounted for indirectly by placing a temperature sensor in close proximity to a heat source. This strategy has been used in this research project.

The next step is to consider the 3 heat transfer mechanisms: conduction, convection and radiation. Considering the relevant material properties, the ambient

temperature range and realistic machine part temperature ranges (20–60 °C), it can be concluded that conduction and convection are the dominating heat transfer mechanisms [Sme 98]. Heat transfer by radiation is often neglected when using the extended lumped capacitance method [Cha 87] [Inc 90]. Besides a relatively small heat flow rate compared to convection (typically 15% [Sme 98]) and conduction, this is mainly due to large uncertainties in the emissivity coefficients and its non-linear behaviour with temperature. These coefficients depends for instance on surface roughness, presence of grease and/or oxidation layers, paint layers, temperature, and are difficult to predict in practise. By linearising the radiation heat transfer equation over the stated temperature range, an approximation can be obtained [Sme 98]. This linearised equation can be incorporated into the equation describing convection heat transport, since both equations have then the same structure. The latter means that by increasing the average heat convection coefficient, radiation can be taken into account approximately [Soo 93] [Sme 98]. In this research project, heat transport by radiation is neglected: only heat transfer by conduction and convection has been considered.

After dividing a machine part in a number of elements or lumps, for instance according to a square grid, heat transfer relations have to be denoted for (convection) and in between (conduction) these elements, see Figure 5.6. The convective heat flow of a lump  $i$  with the ambient air is denoted by  $q_i$  and  $q_{i,j}$  represents the conductive heat flow between the lumps  $i$  and  $j$ . The lump temperature is denoted by  $T_i$ . This procedure can be considered as constructing a

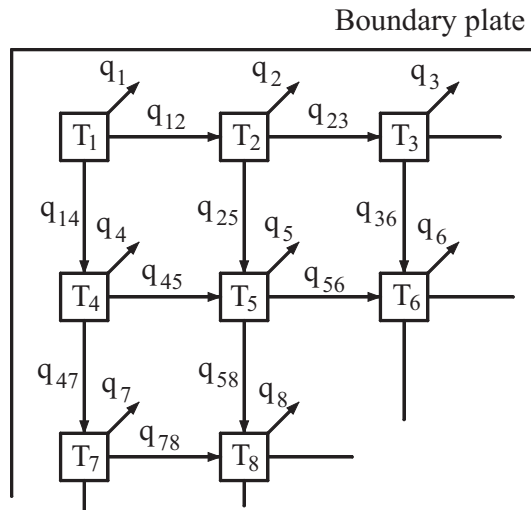


Figure 5.6: A plate divided into elements according to a square spatial grid. Conductive heat flows between elements and convective heat flows for each element have been denoted.

thermal circuit. With regard to this concept, a temperature difference  $\Delta T$  can be considered as the driving force or potential that causes heat to flow against a resistance [Jan 88]:

$$q = \frac{\Delta T}{R} \quad (5.11)$$

where  $q$  stands for the heat flow [W] and  $R$  represents a thermal resistance [K/W]. Applying this for conduction heat transfer results in the following thermal conduction resistance between 'neighbouring' elements ( $i$  and  $j$ ):

$$R_{i,j} = \frac{l_{i,j}}{k \cdot A_{i,j}} \quad (5.12)$$

where  $l_{i,j}$  stands for the distance between the respective elements (centre points) [m] and  $k$  stands for the material thermal conductivity coefficient [W/mK]. The area between these elements is denoted by  $A_{i,j}$  [m<sup>2</sup>]. For convection heat transfer on the other hand, the element-surrounding heat transfer resistance  $R_i$  is defined as:

$$R_i = \frac{1}{h_c \cdot A_i} \quad (5.13)$$

with  $h_c$  denoting the average heat convection coefficient [W/m<sup>2</sup>K] and  $A_i$  represents the contact area of the element with the ambient air [m<sup>2</sup>].

In order to determine the temperature change of an element or lump for entering and leaving heat flows, thermal element capacitances have to be determined. The thermal capacity  $C_i$  of element  $i$  can be computed as:

$$C_i = \rho \cdot V_i \cdot c \quad (5.14)$$

where  $\rho$  represents the element density [Kg/m<sup>3</sup>],  $V_i$  its volume [m<sup>3</sup>] and  $c$  stands for the specific heat [J/kgK].

At this point first order differential equations can be determined, describing the change in element temperature in time as a function of (convective and conductive) heat flows. The structure of such a differential equation of element  $i$  resembles:

$$C_i \frac{dT_i}{dt} = \frac{(T_j - T_i)}{R_{i,j}} + \dots + \frac{(T_i - T_\infty)}{R_i} \quad (5.15)$$

where the dots indicate conduction terms with other 'neighbouring' elements, omitted here for reasons of simplicity. The first term on the right-hand side of Equation 5.15 expresses the conductive heat flow while the last term represents heat transport by convection. Note that heat sources (i.e.  $Q$ ) are absent on the right-hand side of Equation 5.15. By dividing the right-hand side of Equation 5.15 by the elements' thermal capacity and integrating the resulting equation, element temperature changes are obtained. The number of differential equations equals the number of elements and these can be obtained with relatively little effort when expressed systematically.

Most effort, when using the extended lumped capacitance method, is needed for the determination of the coefficients present in Equation 5.15 like element

capacitances, thermal resistances (element distances and relevant areas). Estimation of these coefficients from measurement data is theoretically possible but difficult since all relevant heat flows must be considered quite exactly. Further research on this item is recommended for identifying and determining optimal coefficient values. So far, the coefficients have been determined by using material handbooks [Cha 87] [Inc 90] [Dub 93] and measurements/drawings of the machine to a limited extent. Due to large uncertainties in these values, these coefficients should not be considered as exact values but merely as an indication of them.

Since no heat sources are incorporated in the model equations, special attention is required for the placement of temperature sensors. The readings of such sensors are then used for computing or ‘updating’ the right-hand side of Equation 5.15 each time the sensor is read (each minute in this research project). If a measured temperature value is not available, a computed element temperature is used in Equation 5.15. Obviously, at least a temperature sensor has to be attached close to each heat source to account for its effect on the resulting temperature distribution indirectly. In general, these temperature sensors should be placed in such a way, that each relevant, occurring heat flow can be described. This means that the direction of each heat flow has to be considered, which always is initiated at a heat source. Therefore temperature sensors are placed on a machine part where a conductive heat flow enters or exits a machine part and at locations where heat sources are located.

The number of elements, used for dividing a machine part into a finite number of lumps, is chosen in such a way that the temperature between ‘neighbouring’ elements can be obtained by linear interpolation without introducing a significant interpolation error. Otherwise the number of elements is increased stepwise. All available temperature sensors are attached to the machine part considered during this modelling process, resulting in a high spatial temperature sensor density. The majority of these sensors are subsequently used as ‘checking points’ to verify the model performance at the respective location: only a few (i.e. 4) sensors are used for updating the right-hand side of Equation 5.15. In this tuning process, several duty cycles (i.e. spindle spectra) of the machine have to be considered in order to get a realistic impression of the model performance. This error in element temperature is simply obtained by comparing a computed value with a measured one. Summarizing the following iterative procedure has been used for dividing a machine part into elements/lumps using a square spatial grid:

1. Attach temperature sensors to a machine part, preferably with a high spatial density;
2. Measure air temperatures at some locations close to the machine part considered;
3. Divide a machine part in some (for instance 4) large elements;
4. Construct differential equations for each element (see Equation 5.15);

5. Determine the coefficients of the differential equations by evaluating elements areas, distances, etc.;
6. Compare the computed element temperatures with measured values for various duty cycles (including a varying spindle spectrum);
7. If the error in temperature exceeds a certain tolerance level increase the number of elements and repeat aforementioned procedure;
8. If the error in temperature can not be reduced by increasing the number of elements, select another temperature sensor or add a temperature sensor used for updating the right-hand side of Equation 5.15 when computing element temperatures and restart with the procedure.

This procedure has been applied to model the temperature distribution of some components of a milling machine (i.e. a Maho 700S). In this way, the temperature distribution of the workpiece table, the X-axis guideway and the machine's column has been modelled.

In Figure 5.7 some results are displayed for the modelled temperature distribution of the upper right edge of the machine's column (viewpoint as displayed in Figure 5.3). The machine's column has a significant contribution to the thermally induced positioning error of the machine since small bending angles result in considerable errors in position of the end-effector with respect to the workpiece table due to relatively long arms of rotation. The machine has been running at 6000 rpm for 5 hours followed by a 5 hour cooling down period.

Two temperature sensors are attached to the this machine part to be used by the lumped capacitance model: one is positioned in the upper left corner of the column and the other sensor is positioned more or less in the middle of the upper boundary. On these sensor positions, significant heat flows enter the machine's column from the ram. The heat flow that enters the upper left corner of the column is mainly generated by the machine's spindle bearings and gearboxes (located near the vertical milling head). The other heat flow mentioned is due to a gear box, near the main spindle motor and the resulting heat flow enters the column in the middle of the upper boundary. Furthermore, one sensor has been used for measuring the local air temperature. These three sensor readings are then used as *input* for the lumped capacitance model of the column. These sensor readings are used to update the right hand-side of Equation 5.15 by prescribing a measured temperature used as boundary conditions when solving the partial differential equations of the lumps. The corresponding lumps can subsequently be regarded as a heat source: the amount of energy entering the system considered equals  $C_i \cdot dT$ . For determining the value of the coefficients of the lumps, the following values have been used, using handbooks [Cha 87] [Inc 90] [Dub 93] and machine dimensions:

- Density cast iron ( $\rho$ ):  $7.3 \cdot 10^3$  kg/m<sup>3</sup>;
- Specific heat ( $c$ ): 420 J/kgK;
- Thermal conductivity coefficient ( $k$ ): 52 W/mK;

- Average convection heat transfer coefficient ( $h_c$ ): 10 W/m<sup>2</sup>K;
- Plate thickness: 20 mm.

The dimensions of the side of the column are 700 mm (width) and 1400 mm (height) and this column is divided into lumps according to a  $7 \times 7$  rectangular grid.

The remaining sensors are positioned all over the machine's column and these readings are then used to compare/check the computed temperatures with measured values. In Figure 5.7, the temperature is plotted versus the time in seconds of measurement for a temperature sensor attached at the upper right edge of the machine's column. The dashed line represents the measured temperature and the solid line indicates the computed values, using the extended lumped capacitance method applied to the machine's column. The maximum

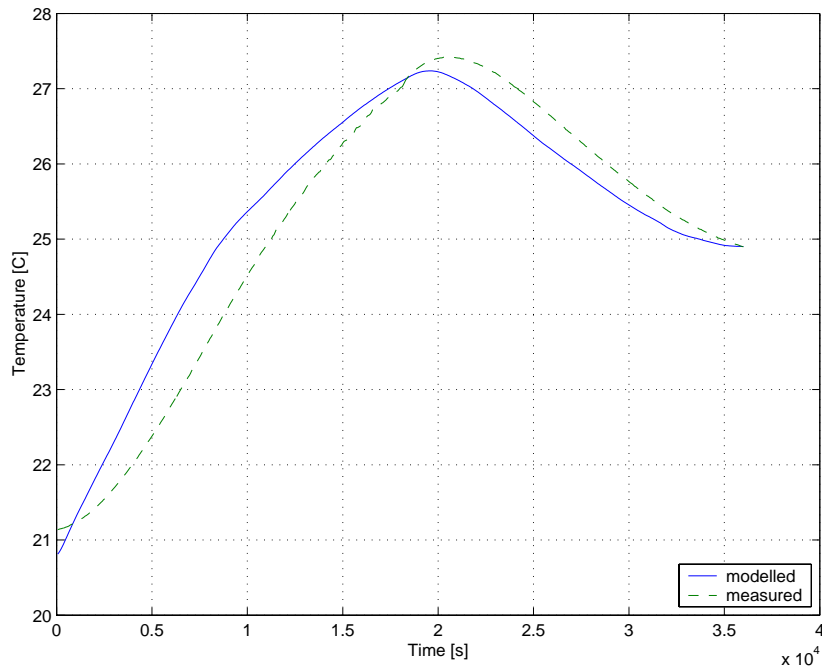


Figure 5.7: Modelled and measured element temperature for the upper right corner of the machine's column. The machine executed a duty cycle of 6000 rpm for 5 hours followed by a cooling down period.

error in predicted temperature for this sensor position considered here is about 1 °C. Considering the machine's column entirely, the error in predicted temperature at any location on this machine part does not exceed 3 °C for any duty cycle, using 3 temperature sensors. The temperature time derivatives of the modelled lump temperatures in the first hour of the experiment described is

relatively high, see Figure 5.7. This is caused by a fast increase in local air temperature, which has been measured for each experiment, see Figure 5.8. This demonstrates the significant effect of convective heat flows, which is relatively large over conductive heat flows, mainly in the beginning of an experiment. The

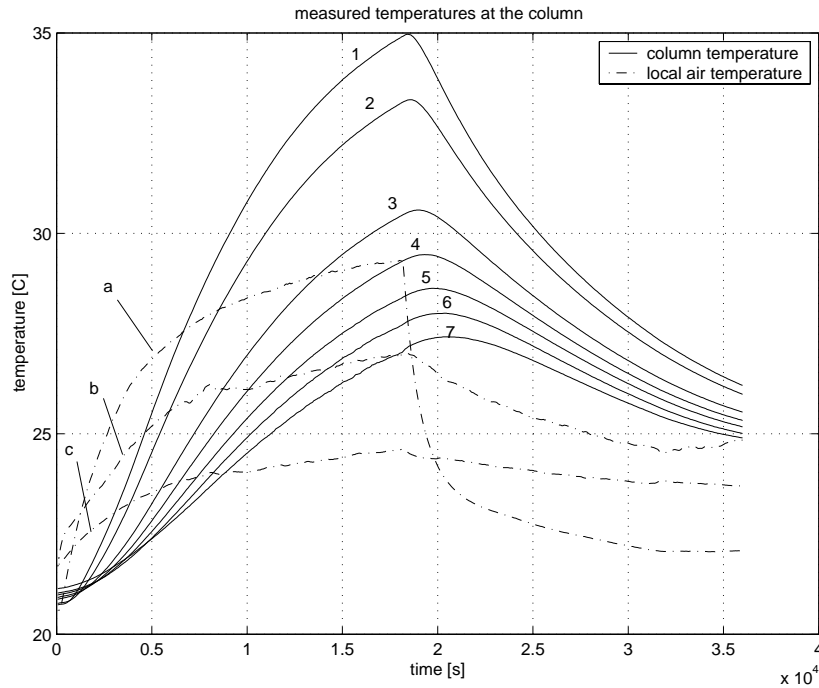


Figure 5.8: Measured temperatures during a 6000 rpm duty cycle. The solid lines represent body temperatures of the upper boundary of the machine's column (1: upper left corner, 7: upper right corner). The local air temperatures are indicated by dashed lines (a: at top, b: near the middle and c: at the bottom of the column).

temperature sensors (1-7) are attached equidistantly at the upper boundary of the machine's column.

The ram, swivelling head and vertical milling head are still subject to modelling and research.

A drawback of this method however is the need of skill and experience in order to get a good approximation of the temperature distribution. In some problematic cases, the error in temperature at a certain location can simply be reduced by using an increased number of temperature sensors used in the lumped capacitance model. This depends on the users demands and always a compromise has to be made between the related costs (i.e. the number of temperature sensors and related equipment) and the model accuracy required. The number of temperature sensors derived this way is probably not minimal

but at least the resulting temperature distribution can be described in a reliable way since information about the most significant heat flows has been considered and is incorporated in the derived model.

In addition, the effect of ambient air temperature on the accuracy of the results obtained was found to be large and difficult. This can be explained on one hand by the significant heat transfer rate by (free and forced) convection in a machine tool. A small absolute change of the temperature of the ambient temperature (for instance a 1 °C increase from 21 °C only) can consequently have a significant effect on the accuracy of the results obtained, since the relevant temperature difference between the machine part considered and the ambient temperature can be changed considerably (i.e. doubled for a machine part temperature of 20 °C). Also, assuming a single ‘air temperature’ might be convenient but is not correct. This ambient air temperature  $T_\infty$  has a local character and shows different trends in time on different locations with respect to the machine’s structural loop. In some cases, a considerable model accuracy improvement was obtained by adding a local ‘air sensor’ to the model instead of increasing the number of temperature sensors (attached at the machine part considered) to be used by the model. On the other hand, the large uncertainty in the average convection heat transfer coefficient  $h_c$  complicates the quantification of convective heat transfer rates.

## 5.6 Thermal drift of the end-effector

After computing the thermal deformations of the machine parts present in the machine’s structural loop the thermal drift of the end-effector with respect to the workpiece table has to be computed, based on these part deformations. This is realised by superposition of the deformations of the machine parts over the machine structural loop, assuming that each machine part can expand freely. The latter is assumed because the induced stresses and resulting (elastic) strains are difficult to quantify. As a first instance, the machine’s scales are not considered in the machine’s structural loop here for reasons of simplicity. The effect of thermal scale expansions has been considered separately from the machine’s structural loop although this is a simplification.

In Figure 5.3 a side view of a milling machine is drawn schematically. The machine part deformations, expressed in error components  ${}_i T_{y1,i}$ ,  ${}_i T_{z1}$  and  ${}_i R_{x1}$  are calculated over the drawn line segments, referring to a specific position of the machine’s axes. The error propagation is calculated conform geometrical errors (see Section 3.1.3). The thermally induced drift of the end-effector relative to the workpiece table is then obtained by combining the three deformation modes considered of each machine part over the machine structural loop by superposition, disregarding the scales. This superposition procedure can be used since the computed machine part deformations are much smaller than the nominal dimensions of the machine (part).



## 5.7 Measurement of thermally induced positioning errors by DBB

Conform geometrical errors, the thermally induced positioning errors are measured using a DBB. Since the spindle has to rotate relatively fast (up to 6000 rpm) the DBB ball can not be connected safely to the machine's spindle as practised for geometrical errors. For this reason, an adapter has been designed and realised. The thermal expansion of the adapter can be neglected due to its design, which is discussed in Appendix G. In Figure 5.9 a photograph of a 'thermal DBB measurement setup' is shown for assessing the machine's thermally induced positioning errors.



Figure 5.9: Photograph of a DBB measurement setup for determining thermally induced errors, using the developed adapter.

First a single semi-spherical DBB measurement is performed with an idle spindle. This DBB measurement, referred to as 'reference cage', lasts several minutes and is used to check if the stand is positioned properly in the centre of the programmed circular paths of the machine. Furthermore this measurement is used as a reference to determine the change in DBB length for each

single measuring point while the machine heats up and drifts. After the execution of this ‘reference cage’, semi-spherical DBB measurements are repeatedly performed at certain time intervals (for instance each 30 minutes) while the machine executes a duty cycle. The measured DBB length deviation  $\Delta\ell_k(j)$  for a single measuring point  $k$  at a time  $j$  is then defined as:

$$\Delta\ell_k(j) = \ell_k(j) - \ell_k(1) \quad (5.16)$$

with  $\ell_k(1)$  denoting the measured DBB length in measuring point  $k$  in the ‘reference cage’. Due to this definition, the DBB length instrument is used in a relative sense since the absolute DBB length is not relevant here. Note that geometrical errors, which do not change in time, present in the ‘reference cage’ are cancelled out this way.

In order to avoid thermally induced changes of the relative end-effector position during a single semi-spherical DBB measurement, the measurements have to be executed in a short period of time. Considering the large thermal time constants of the various (bulky) machine components, the machine’s thermal drift can be neglected within a DBB measurement. For this reason only 17 points are being measured, equally distributed with step angles of  $45^\circ$  with respect to the stand, see Figure 5.10. The time of execution of such a measurement is

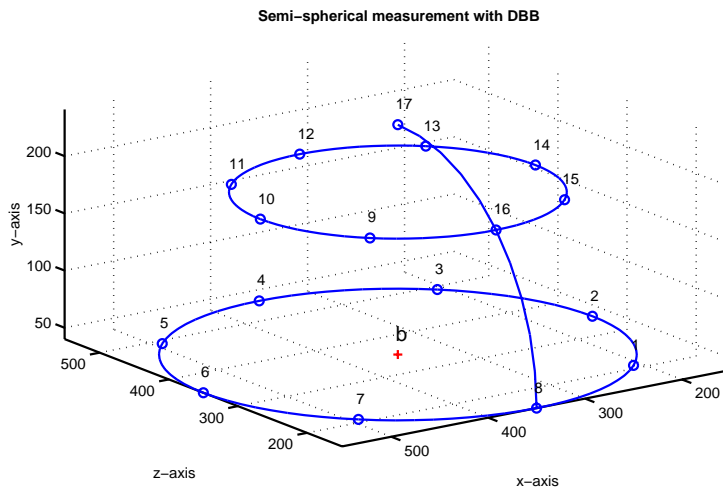


Figure 5.10: Applied measuring point distribution of a ‘thermal’ DBB measurement. The tool’s relative path is indicated by a solid line.

typically two minutes.

Due to the rotating spindle, the milling head is vibrating relative to the workpiece table. The vibrations, typically 100 Hz for 6000 rpm with an amplitude over several  $\mu\text{m}$  as determined experimentally, deteriorate the accuracy of the measured DBB length. By sampling the DBB readout  $n$  times for each

measuring point  $k$ , the effect of these vibrations on the determined DBB length can be alleviated by a factor  $\sqrt{n}$  (excluding systematic errors). During experiments, the DBB was sampled 9 times, decreasing the standard deviation of the average DBB length measurement by a factor 3 for each single measuring point.

Finally the measurement setup and strategy described has to be corrected for two effects: the thermal expansion of the DBB measuring instrument and of the stand, positioned on the workpiece table. The thermal DBB expansion at time  $j$  is calculated using:

$$d\ell_{DBB}(j) = \alpha_{DBB} \cdot \ell_{DBB}(T_{DBB}(j) - T_{DBB}(1)) \quad (5.17)$$

with  $\alpha_{DBB} = 12 \cdot 10^{-6} \text{ K}^{-1}$  representing the experimentally determined [Bus 01] thermal expansion coefficient of the DBB,  $\ell_{DBB}$  stands for the nominal DBB length (200 mm) and  $T_{DBB}(j)$  represents the DBB temperature at time  $j$ . The temperature of the DBB when executing the ‘reference cage’ is denoted by  $T_{DBB}(1)$ . The expansion of the stand is calculated in a similar way:

$$dl_{stand}(j) = \alpha_{stand} \cdot l_{stand}(T_{stand}(j) - T_{stand}(1)). \quad (5.18)$$

The thermal expansion of the stand is always pointing upward due to its rotation-symmetrical shape, perpendicular to the workpiece table. In vector notation, the expansion of the stand can be expressed as  $\mathbf{dl}_{stand}(j) = [0 \quad dl_{stand}(j) \quad 0]^T$ . The measured DBB length has then to be corrected according to:

$$\Delta\ell_{k,corrected}(j) = \Delta\ell_k(j) + d\ell_{DBB}(j) + \mathbf{n}_k^T \cdot \mathbf{dl}_{stand}(j) \quad (5.19)$$

with  $\mathbf{n}_k^T$  denoting the normal vector in measuring point  $k$ , coinciding with the DBB measurement axis.

In this way, the change in DBB length measured can be used as a measure for the thermally induced drift of the end-effector relative to the workpiece table. For a duty cycle of 6000 rpm for 6 hours followed by 7 hours cooling down, the following length deviations have been measured on a milling machine, see Figure 5.11. For the spatial distribution of these 17 measuring points, see Figure 5.10. In Figure 5.11 it is obvious that the deviations in the length measured depend on the orientation of the DBB. This figure is especially meant to analyse the change in magnitude of the deviation in the measured length in time. The spatial location of these measuring points is not that obvious but can be retrieved from this figure, also using Figure 5.10. The largest errors measured act in Z (points 4 and 8) and Y-direction, and the smallest deviations correspond generally to the machine’s X-direction (mainly due to symmetry).

The amplitude of the measured thermal drift of the tool (about  $\pm 100 \mu\text{m}$ ) is comparable to the thermal drift determined with a measurement setup, as displayed in Figure 5.1 of the same machine [Soo 93] [Spa 95]. Therefore the developed DBB measuring method can be considered as giving reliable measurement results.

When comparing both measuring methods, two main differences can be remarked. The conventional thermal drift measurement setup is performed on

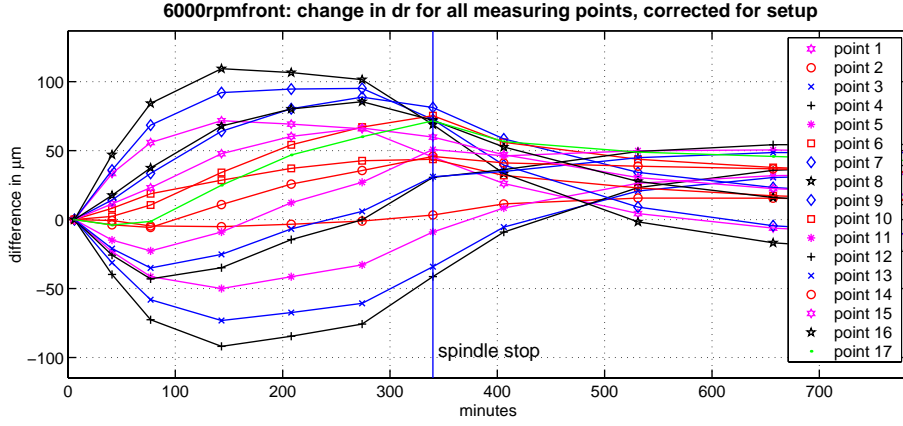


Figure 5.11: Measured thermal drift of the tool for the 17 measuring points plotted in time. The milling machine was running for about 6 hours at 6000 rpm.

the same location in the machine's workspace during a measurement cycle while for the DBB method developed, the machine is measured on multiple locations in its workspace<sup>1</sup>. This means that the dependency of the thermally induced relative drift of the end-effector on the machine's axis positions can be analysed with one single DBB measurement setup unlike the other method mentioned. On the other hand, only a component of the positioning error vector can be assessed directly with the DBB method for a single measuring point, dependent on the orientation of the DBB. However, in the previous chapters it has been shown that it is not impossible to reconstruct this positioning error vector from length deviations measured.

Besides measuring the thermal drift, the method developed can also be used for verifying the performance of a certain thermal error model used for error compensation purposes. The thermal drift measured is subsequently to be compared with the modelled drift for each measuring point at the corresponding time interval of measurement. The modelled change in DBB length at a time  $j$  of point  $k$  is calculated by projecting the modelled change in tool position on the DBB measurement axis and this can be expressed as (see also Section 3.2):

$$\Delta \hat{\ell}_{k, modelled} = \Delta \hat{\ell}_k(j) - \Delta \hat{\ell}_k(1) = \mathbf{n}_k^T \cdot (\hat{\xi}_k^t(j) - \hat{\xi}_k^t(1)) \quad (5.20)$$

where  $\mathbf{n}_k^T$  stands for the normal vector of measuring point  $k$ . The machine's positioning error when measuring the initial 'reference cage'  $\xi_k^t(1)$  is usually non-zero since the machine's temperature distribution is not homogeneously at 20 °C. The measured DBB length on the other hand equals zero by definition for

<sup>1</sup>For a zero DBB length, both methods are similar when omitting the relative orientation error of the end-effector.

each measuring point in the ‘reference cage’. In the next section, the validation of the proposed thermal machine error model is presented using the developed DBB measuring method.

## 5.8 Validation of the thermo-mechanical error model

In this section, the thermo-mechanical error model proposed will be validated, using DBB measurements. This means that the measured length deviation is compared to the predicted length deviation for a measuring point at a certain time. For predicting the length deviation, the thermo-mechanical error model presented is used. In order to realise this, the predicted positioning error of the machine is projected on the measurement axis of the DBB for each measuring point.

For expressing the performance of the proposed thermal error model, the modelling efficiency is computed [Spa 95]. This model efficiency calculates to what extent the thermally induced drift of the end-effector can be described by the model proposed as assessed by a DBB measurement performed at time interval  $j$ :

$$\text{modelling efficiency} = \left(1 - \frac{\text{mean residual}}{\text{average deformation}}\right) \cdot 100\% \quad (5.21)$$

where the mean residual is computed for ‘cage  $j$ ’ as the average absolute difference between the measured and modelled change in DBB length:

$$\text{mean residual} = \frac{\sum_{k=1}^m |\Delta \ell_{k,\text{measured}}(j) - \Delta \hat{\ell}_{k,\text{modelled}}(j)|}{m} \quad (5.22)$$

where  $m$  equals the number of measuring points in one cage, which equals 17. The average deformation of a DBB measurement  $j$  is expressed as the absolute value of the measured change in DBB length, averaged over the 17 measuring points in a DBB measurement  $j$ :

$$\text{average deformation} = \frac{\sum_{k=1}^m |\Delta \ell_{k,\text{measured}}(j)|}{m}. \quad (5.23)$$

A modelling efficiency of 100% indicates that the thermally induced DBB length changes measured can be described perfectly for all 17 measuring points present in the semi-spherical DBB measurement considered. If this efficiency is zero, this means that application of the thermo-mechanical error model does not contribute anything to the positioning accuracy of the machine tool. Negative efficiency values occur when the residual DBB length changes exceed the measured values.

For the validation measurements to be presented in this section, the temperature distribution of machine parts present in the machine’s structural loop is measured using 52 temperature sensors. The temperature distribution of a

machine part is then obtained by fitting (locally) linear gradients, using surrounding temperature sensor readings attached on the machine part [Bus 01].

Based on the temperature distributions measured on relevant machine parts, the resulting thermally induced deformations are calculated using Equations 5.3, 5.4 and 5.5. The positioning error of the machine's end-effector with respect to the workpiece table is subsequently obtained by superposition of the calculated deformations of machine parts, as indicated in Figure 5.3. The latter results in the positioning error of the machine's end-effector with respect to the workpiece table.

In Figure 5.12 the changes in DBB length measured is plotted with dots versus the measuring point number (1-17, see Figure 5.10) for a duty cycle of 6000 rpm. This figure shows the change in DBB length measured, two hours after the start of this experiment. In addition, it can be seen that the change in length measured depend on the orientation of the DBB. The predicted changes

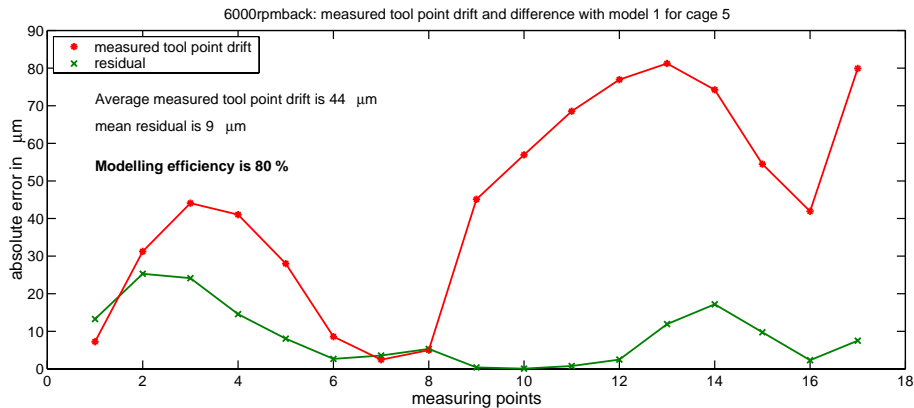


Figure 5.12: Measured and residual length deviations measured for a 6000 rpm duty cycle on a milling machine.

in DBB length are marked with crosses in Figure 5.12 for the 17 measuring points. For about 80% of the deviations in radius measured can be explained with the thermal error model for this specific DBB measurement at the time interval considered. The measured tool point drift equals  $44 \mu\text{m}$  and the mean residual radius deviation is  $9 \mu\text{m}$ . The stand was positioned at the back of the workpiece table during this experiment, still enabling the DBB to perform a semi-spherical DBB measurement. The largest residuals are found in the machine's X-direction. This is due to applying a near flat machine model in the YZ-plane: only the thermal expansion of the X-scale can be used so far to model the errors acting in the machine's X-direction. The performance of this model to predict the changes in length acting in the machine's Y and Z-direction is generally better.

Considering all DBB measurements performed successively during this experiment, where the machine is running 6000 rpm for 6 hours (DBB measure-

ments are executed each 30 minutes), including a 6 hour cooling period, reveal an average modelling efficiency of 64% [Bus 01].

In order to check whether the thermo-mechanical error model gives reliable results, also validation measurements have been performed on different locations in the machine's workspace (front, middle or back side of workpiece table by changing the stand position in Z-direction) and with other duty cycles (0, 3000 rpm, 6000 rpm and DIN 8602). The first measurement has been performed with an idle spindle and this measurement is mainly used to verify the effect of a changing ambient temperature on the results obtained in combination with the effect of heat sources which are not related to the machine's spindle (like axis actuators, hydraulic pumps etc.). In the other validation measurements, the thermal excitation of the machine is considerably increased by activating the machine's spindle, since this is the major heat source. The results of these validation measurements are depicted in Table 5.1.

name measurement	mean residual	average model efficiency
0rpm	3 $\mu\text{m}$	63%
3000rpmback	6 $\mu\text{m}$	65%
3000rpmfront	8 $\mu\text{m}$	53%
6000rpmback	14 $\mu\text{m}$	64%
6000rpmmid	15 $\mu\text{m}$	50%
6000rpmfront	18 $\mu\text{m}$	49%
DINback	8 $\mu\text{m}$	66%
DINmid	7 $\mu\text{m}$	57%
DINfront	6 $\mu\text{m}$	59%
Overall	9 $\mu\text{m}$	58%

Table 5.1: Mean residual values and average modelling efficiencies for various validation DBB measurements, performed on a Maho 700S milling machine.

Summarizing, about 60% of the thermally induced positioning errors of a milling machine can be explained by using the simple linear error model proposed. Therefore application of this model for error compensation purposes is useful. The performance of this model however is constrained by the large number of assumptions made.

Some additional studies have been performed [Bus 01], mainly to extend the presented approach to assess thermally induced errors of machine tools by considering more complex temperature distribution descriptions. In such cases, the modelling efficiency can be increased for about 10% [Bus 01] although some serious difficulties appear subsequently. One such problem for example is a consistent description of deformations of a machine part, since thermally induced stresses cannot be ignored then. Introduction of a so-called neutral point, a point for which thermally induced deformations are zero or minimal, to be used as reference point for defining machine part deformations, a consistent description can be generated for complex temperature distributions [Bus 01].

Despite its proven consistency, machine part deformations are generally still modelled too large since the constraining effect resulting from thermally induced strains is not included yet.

### 5.8.1 Validation of the lumped capacitance model

In Section 5.5.2 the extended lumped capacitance method has been applied for modelling the temperature distribution of machine parts. A result has been shown for the upper right edge of the machine's column, while the machine executed a 6000 rpm duty cycle for 5 hours. Loading the machine with a DIN 8602 spindle spectrum gives the following results for the same sensor position. The dashed line represents the measured temperature and the solid line indicates the computed values, using the extended lumped capacitance method. Considering the machine's column entirely, the error in predicted temperature

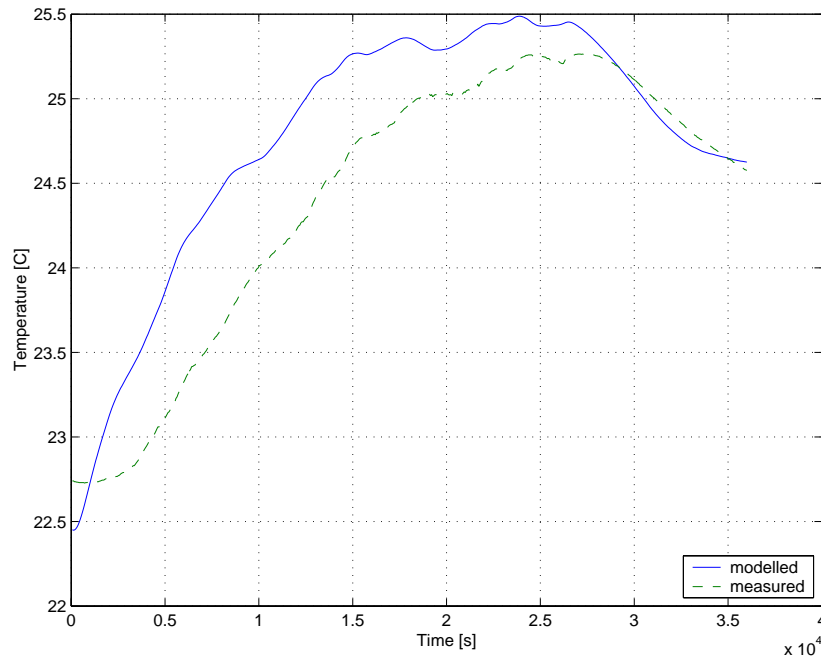


Figure 5.13: Modelled and measured element temperature for the upper right corner of the machine's column. The machine executed a duty cycle according to DIN 8602 followed by a cooling down period.

at any location on this machine part does not exceed 3 °C for any duty cycle, using 3 temperature sensors. Compared to the temperature measuring method, the number of 8 temperature sensors can be reduced to 3 sensors when applying the lumped capacitance model of the machine's column. Concluding, application of a lumped capacitance model for reducing the number of temperature



sensors required is useful. This reduction depends on the required accuracy of the lumped capacitance model and therefore always a compromise has to be made between these entities.

## 5.9 Resume

In this chapter, a hybrid thermo-mechanical error model has been proposed. This model can be used for error compensation techniques to enhance the machine's positioning behaviour and is primarily meant for machine tools.

In Section 5.1 the complexity of thermally induced positioning errors of multi-axis machines has been discussed, followed by a literature overview. In general, three methods can be distinguished for modelling this kind of errors. Such methods relate the measured relative drift of the end-effector with respect to the workpiece table to temperature sensor readings and empirical, analytical or hybrid models have been developed to describe this relationship.

Since the frame construction of a machine tool can generally be regarded as a plate framework structure, plates are used to model machine parts of a machine tool as discussed in Section 5.3. The effect of the thermally induced deformation of the machine's scales are treated separately from the machine's structural loop as if it is stretching/shrinking the machine's working volume.

After dividing a machine into simple geometries (plates), the thermal deformation of these plates is computed using equations describing stress free isotropic thermal expansion. Due to the use of plates, three deformation modes are distinguished for each machine part: elongation, bending and transversal translation. As a first approach, only linear temperature gradients have been considered. In this way, the effect of thermally induced stresses and strains has been circumvented, which generally constrain the resulting deformation to a certain extend. Additional studies have been performed to extend the approach described concerning more complex temperature distributions. Although application of such a model reveals a small improvement in the model performance to describe the measured relative drift of the end-effector with respect to the workpiece table, some problems related to thermally induced stresses and strains still remain.

In order to compute the thermally induced plate deformations, the temperature distribution of the machine part is required. Two methods have been discussed to obtain this temperature distribution in Section 5.5. The first method, which has been applied in this thesis, uses a relative large number of temperature sensors distributed over the machine's structure. These sensors readings are subsequently used to determine local linear gradients at the machine part considered.

Besides this approach, a thermo-dynamical model is presented, using the extended lumped capacitance method in combination with temperature sensors. Such a model is used to reduce the number of temperature sensors required otherwise for obtaining a good approximation of the temperature distribution of a machine part. This model, however, is not completed yet for some relevant

machine parts and could therefore not be applied to the entire machine.

After computing the three deformation modes of each machine part as defined in Figure 5.4, these deformations are combined by superposition to obtain the relative drift of the end-effector with respect to the workpiece table, as discussed in Section 5.6.

For measuring the thermally induced relative drift of the end-effector, a DBB has been applied in this thesis. In order to connect this length measuring device reliably and safely to the machine's milling head while the spindle is rotating fast, a near expansion free adapter has been designed and realised. By performing DBB measurements successively at certain time intervals while the machine executes a certain duty cycle, the relative drift of the end-effector with respect to the workpiece table can be determined. The major advantage of this new measuring technique is that measurements can be performed at different locations within the machine's workspace with a single measurement setup unlike reported methods, using a cylinder or a ball mounted in the machine's spindle. Measurements reveal that the thermally induced drift of the milling machine considered exceeds  $100 \mu\text{m}$ .

In Section 5.8 the validation of the thermo-mechanical error model proposed has been presented. Numerous measurements performed at different locations in the machine's working volume in combination with different duty cycles reveal that about 60% of the measured DBB length deviations can be described by the model proposed. The capabilities of this model to describe the measured deviations is limited due to the large number of assumptions made.

In addition, some validation measurements have been presented in order to validate the proposed lumped capacitance model to describe the temperature distribution of the upper boundary of the machine's column. These measurements reveal that the errors in the modelled temperature distribution, using two attached sensors and one air sensor, are limited to  $3^\circ\text{C}$  for any duty cycle of the machine considering the entire column. Therefore, it may be concluded that this lumped capacitance model can be used reliably to reduce the number of temperature sensors required. When setting up such a LCM model, always a compromise has to be made between the accuracy of the model and the number of temperature sensors to be used.



## Chapter 6

# Conclusions and recommendations

### 6.1 Conclusions

In this thesis it has been analysed to what extent 3D length measurements can be used for accuracy analysis of multi-axis machine with serial kinematic structures. The scope of this project is focused on geometrical and thermally induced errors of this kind of machines: the effect of other error sources (finite stiffness and dynamical behaviour of the machine's structural loop, the cutting process etc.) on the positioning accuracy of multi-axis machine's has not been considered here.

The choice for applying 3D length measurements over other measuring methods is motivated by the related costs of measurement, which is dominated by the time of measurement. Since length measurements can be performed in a short period of time with little effort, a major reduction of the costs related to perform measurements on a multi-axis machine has been realised as intended. Furthermore the costs related to the measurement equipment and manpower needed is reduced significantly as well. Based on the presented research the following conclusions are drawn, starting with geometrical errors and followed by the conclusions concerning thermally induced errors of machine tools. In addition the recommendations are presented in the next section.

#### 6.1.1 Geometrical errors

Concerning geometrical errors of multi-axis machine's, five reasons are mentioned to measure a machine's positioning behaviour: acceptance testing, quality control, error compensation, diagnostic purposes (i.e. error tracing) and calibration. The research presented hereby has been focused on the possibilities to realise (software) error compensation and error tracing techniques, based on telescopic DBB length measurements performed in the machine's workspace.

The core of the approach presented is the kinematic machine (error) model. This model is used for describing the nominal positioning behaviour of a multi-axis machine. Furthermore it is used as a reference to model the propagation of errors introduced at various machine parts, using rigid body kinematics. In this kinematic error model the error components are modelled with constants or with ordinary polynomials, containing some unknown parameters to be determined from measurement data.

A DBB length measurement model is derived which relates the positioning error of the machine to the length deviation measured of the measuring instrument. The unknown stand position has to be taken into account in this model. Since the DBB length measuring instrument is used as an absolute length reference, calibration of the instrument is required.

In order to be able to determine all the error model parameters, the spatial position of both DBB balls during a semi-spherical measurement has to be varied as much as possible. In this way, each parameter of the machine's error model can be identified from length measurement data. For this purpose, a measurement strategy, prescribing the spatial distribution of the length measurement in the machine's workspace has been presented. The length of the DBB should hereby be chosen as large as possible, taking the dimensions of the machine's working volume into account in order to realise a semi-spherical DBB measurement (or at least a significant part of it). Furthermore a reversal measurement is recommended for several reasons. On one hand to enable the user to detect possible irregularities during a measurement (lubricating pulses, dirt) and on the other hand to obtain an indication of the repeatability limit of the respective machine. The latter is used as an upper limit when performing error compensation techniques. In addition, it has been shown that using a large number of measuring points within a DBB measurement is of little use for the determination of the geometrical error model parameters. For this reason, a so-called birdcage measuring point distribution is proposed, where less efficient measuring points have been omitted to reduce the time required for executing a DBB measurement. The measurement setup proposed, containing 19 semi-spherical DBB measurements, can be executed within three hours only, using software modules developed in this research project. Conventional methods require a typical measurement time of two days in combination with advanced and expensive equipment, so a significant reduction of measuring time and related costs has been realised.

The parameters of the geometrical error model are estimated from DBB length measurements performed according to the measurement strategy proposed, using least squares regression techniques. The estimation of these parameters is generally complicated due to strong parameter correlations, which must be avoided in order to get a reliable solution. For this reason, straightness error components are omitted from the machine error model since the contribution of rotational error components is dominating over the contribution of straightness errors to the machine's positioning errors due to relatively long arms of rotation.

The error components are modelled with constants or higher order polyno-

mials containing some parameters, which have to be estimated. The polynomial order has been tuned by analysing the reduction of the sum of squared errors by adding/removing the error model parameter considered: search for a low  $\sqrt{MSe}$  value with as less parameters as possible. The latter deals with the bias-variance dilemma. The  $\sqrt{MSe}$  value should approach the repeatability limit of the machine from above: smaller values must be avoided because of overfitting problems otherwise.

The estimated geometrical error model parameters are subsequently substituted in the error model derived. Applying this model to predict the length deviations measured in the machine's workspace reveal that the amplitude of 95% of the residual length deviations are only  $\pm 4 \mu\text{m}$  throughout the entire working volume of the machine considered (a Maho 700S milling machine). These residuals are marginally larger than the repeatability limit of the machine considered. From this it can be concluded that the length measuring method presented, using a DBB, is suitable for error compensation techniques to enhance the positioning accuracy of a multi-axis machine significantly concerning geometrical errors with relatively little effort and related costs.

Due to the relatively low costs related to perform (automated) DBB measurements in terms of time, effort and equipment, the presented DBB method is also suitable for acceptance testing and periodic inspection of multi-axis machines.

Comparing the error components described with the estimated parameters, with direct measurements reveal that the results obtained are generally in good agreement. Therefore, the method presented, using a DBB, is also suitable for error tracing purposes. The estimated parameters can be used as an indication when searching for the origin of some errors of the machine like squareness or scale errors for instance.

### 6.1.2 Thermally induced errors

In this thesis a new and fast measuring method is introduced and evaluated for assessing thermally induced errors of a machine tool. With this new method, the machine's positioning error projected on the DBB measurement axis is measured on multiple locations in the machine's workspace, unlike conventional methods for which the machine's axes are idle. An adapter is designed and realised to connect a DBB safely to a milling head while the spindle rotates. Its thermal expansion is experimentally determined for various duty cycles and does not exceed  $\pm 2 \mu\text{m}$  due to its design. Comparing this error to the thermally induced positioning error of a machine tool (up to  $100 \mu\text{m}$  or even more for a Maho 700S) to be assessed, it can be concluded that the adapter developed meets its intended requirements well.

Considering the large thermal time constants of relevant machine parts, the choice of using a DBB for assessing positioning errors which are changing in time is advantageous, since a semi-spherical DBB measurement can be performed in typically a few minutes only. Consequently the thermally induced drift within a single semi-spherical DBB measurement can be neglected. The

thermally induced drift of the end-effector with respect to the workpiece table is subsequently determined by comparing DBB length measurements, performed at successive time intervals.

In order to be able to compensate thermally induced positioning errors of a machine tool, several interrelated models have been proposed for describing this kind of errors. These models are used respectively for describing the temperature distribution of relevant machine parts, to describe the thermal deformation of these parts and finally the calculated deformations of machine parts are combined in order to obtain the positioning error of the milling head with respect to the workpiece table.

As a first approach, the temperature distribution is measured using a large number (52) of temperature sensors, attached to various machine parts. The temperature distribution is then obtained by fitting linear gradients locally, using surrounding temperature sensor readings. Also a model, based on the extended lumped capacitance method, has been proposed for describing temperature distributions using a smaller amount of temperature sensors. This model however is still under development.

Based on the temperature distribution of a machine part, its thermal deformation can be computed using temperature differences, lengths, and expansion coefficients. For homogeneous and linear temperature distributions, the resulting deformations can be described correctly. For more complex temperature distributions, however, the resulting thermal deformation is affected by thermally induced stresses. Due to these stresses, the thermal deformation computed is generally over-estimated since these stresses constrain the machine part deformation to a certain extent. As a first approach, these problems have been circumvented by considering linear temperature gradients only. The latter however is a simplification in case of a machine tool.

The thermally induced drift of the machine's end-effector with respect to the workpiece table is obtained by superposition of the thermo-mechanical deformations of machine parts, present in the machine's structural loop. As a first approach, these machine parts are assumed to expand freely. Furthermore the effect of thermally induced scale errors is not included in the machine's structural loop but their contribution is added separately to the thermo-mechanical error model as if it is expanding/shrinking the machine's working volume.

Despite some assumptions (no consideration of complex temperature distributions and ignoring thermally induced stresses in and between relevant machine parts), the thermal error model proposed is capable of describing about 60% of the measured length deviations. For the validation of this thermal error model various duty cycles have been considered as well as multiple stand positions with respect to the workpiece table. Concluding, about 60% of the thermally induced positioning errors can be described with a rather simple thermal error model. The performance of this model is obviously constrained by the assumptions made.

## 6.2 Recommendations

Based on the presented research, the following topics are recommended, starting with geometrical errors:

- Compensate a machine tool for its geometrical errors by applying the geometrical error model derived. This can be realised either by implementing the model in the machine's controller to adjust setpoint values or by adjusting coordinates in the respective NC codes;
- Development of (user-friendly) software modules, necessary for applying the DBB method proposed to compensate geometrical errors of other types of multi-axis machines in industry. Since the code format of controllers of multi-axis machines is not properly normalised, the codes depend on the manufacturer. These different codes have to be implemented in software in order to apply the proposed method in industry;
- For improving the accuracy of the presented method (for instance for CMM applications) the accuracy of the length measurement requires improvement.

Concerning thermally induced errors of machine tools, the following recommendations are listed:

- Reduction of the number of temperature sensors used so far. This can be realised by applying the extended lumped capacitance model proposed or by using obtained knowledge more extensively when using a large number of temperature sensors;
- Consideration of complex temperature distributions, other than homogeneous or linear when computing machine part deformations;
- Analyse and quantify the effect of thermally induced stresses on the thermo-mechanical deformation of a machine part. The use of FEA techniques is hereby recommended since these techniques enable incorporation of thermally induced stresses and strains in computations concerning thermo-mechanical machine part deformations;
- Extend the modelling procedure of machine parts by using multiple plates instead of a single one, mainly to improve the performance of the thermal error model in X-direction;
- Study of thermally induced effects for specific operation tasks in order to reduce geometrical tolerance levels of workpieces;
- Investigate to what extent the thermally induced length deviations measured with a DBB can be used for tuning/optimising the thermal error model. So far, the DBB is only used as a length reference to quantify the difference between the measured and predicted positioning error in a measuring point.





# Bibliography

- [Abb 1890] E. Abbe. Meßapparate für Physiker. *Zeitschrift für Instrumentenkunde*, (10):446-448, 1890.
- [Att 79] M.H. Attia, L Kops. Calculation of thermal deformation of machine tools, in transient state, with the effect of structural joints taken into account. *Annals of CIRP*, 28(1):247-251, 1979.
- [Bal 90] A. Balsamo, D. Marques, S. Sartori. A Method for Thermal-Deformation Corrections of CMMs. *Annals of CIRP*, 39(1):557-560, 1990.
- [Ber 01] C. van den Bergh. *Reducing thermal errors of CMM located on the shop-floor*. PhD thesis, Katholieke Universiteit Leuven, Belgium, 2001.
- [Bir 94] K.P. Birch, M.J. Downs. Correction to the updated Edlen Equation for the refractive index of air. *Metrologia*, (31):315-316, 1994.
- [Bir 60] R.B. Bird, W.E. Stewart, E.N. Lightfoot. *Transport phenomena*. John Wiley & Sons, Wisconsin, 1960.
- [Bol 60] B.A. Boley, J.H. Weiner. *Theory of Thermal Stresses* Robert E. Krieger Publishing Company Inc., U.S.A. 1960.
- [Bry 68] J.B. Bryan. International status of thermal error research. *Annals of CIRP*, 16:203-215, 1968.
- [Bry 90] J.B. Bryan. International status of thermal error research. *Annals of CIRP*, 39(2):645-657, 1990.
- [Bry 93] J.B. Bryan. The Deterministic Approach in Metrology and Manufacturing. *ASME, Proceedings of the International Forum on Dimensional Tolerancing and Metrology*, Dearborne, Michigan, June 1993.
- [Bue 96] R. Bueno, J. Arzamendi, X. Almandoz. Thermoelastic instability problems in machine tools. In J. Jedrezejewski, editor, *Thermal behaviour, intelligent diagnostics and supervising of machining systems*, p34-43, Oficyna Wydawnicza Politechniki Wroclawskiej, Wroclaw, Poland, March 1996.

- [Bus 01] K.F. Bustraan. *Modelling the Thermomechanical Behaviour of Multi-axis Machines*. Master thesis, Eindhoven University of Technology, no. PE2001-063, August 2001.
- [Cam 76] A. Camera, M. Favareto, F. D'Aprile. Analysis of the thermal behaviour of a machine tool table using the finite element method. *Annals of CIRP*, 25(1):297-300, 1976.
- [Cha 87] A.J. Chapman. *Fundamentals of heat transfer*, 1987.
- [Che 95] J.S. Chen. Accuracy enhancement of multi-axis machine tools using real-time error compensation. *Proceedings of the 8th International Precision Engineering Seminar*, p249-252. Compiègne, France, 1995.
- [Che 94] L. Chen, M. Tsutsumi. Study on improving positioning accuracy of NC machine tools using a neural network. *Advancement of Intelligent Production* p241-246, Elsevier Science B.V., 1994. The Japan society of precision engineering.
- [Dea 92] Dea. Mill retrofit for CMM. *European Machining*, (2):59, 1992.
- [Deh 98] J. Dehaes. *Studie over de Thermische Beïnvloeding van de Bewerkingsnauwkeurigheid van een Freesmachine*. PhD thesis, Katholieke Universiteit Leuven, Belgium, 1998. (in Dutch)
- [Den 55] J. Denavit, R.S. Hartenberg. A Kinematic Notation for Lower Pair Mechanisms based on Matrices. *ASME, Journal of Applied Mechanics*, (77):215-221, 1955.
- [DIN 66217] DIN 66217, Koordinatenachsen und Bewegungsrichtungen für Numerisch Gesteuerte Arbeitsmaschinen, December, 1975.
- [Dou 90] E.O. Doubelin. *Measurement Systems, Application and Design*, Fourth edition, McGraw-Hill Publishing Company, 1990.
- [Dub 93] Dubbel. *Taschenbuch Für Den Maschinenbau* Springer-Verlag, 1993.
- [EA-4] EA-4/02 Expression of the Uncertainty of Measurement in Calibration. European Accreditation document, December 1999.
- [Eva 96] C.J. Evans, R.J. Hocken, W.T. Estler. Self-Calibration: Reversal, Redundancy, Error Separation, and 'Absolute Testing'. *Annals of CIRP*, 45(2):617-634, 1996.
- [Flo 97] G.H.J. Florussen. *Accuracy Analysis of Multi-axis Machines by Double Ball Bar Method*. Master thesis, Eindhoven University of Technology, no. WPA12.345, May 1997.
- [Flo 98] G.H.J. Florussen, F.L.M. Delbressine, P.H.J. Schellekens. Accuracy Analysis of Multi-axis Machines Using a Double Ball Bar. *Proceedings of the international Seminar on Improving Machine Tool Performance*, (2):533-543, San Sebastián, Spain, 1998.

- [Flo 00] G.H.J. Florussen, F.L.M. Delbressine, P.H.J. Schellekens. Error Component Determination of Multi-axis Machines from 3D Length Measurements. *Advanced Mathematical & Computational Tools in Metrology IV*, (53):88-97, Oxford, UK, 2000.
- [Flo 01] G.H.J. Florussen, F.L.M. Delbressine, P.H.J. Schellekens. Quality Control of Machine Tools by Length Measurements. *The 34th CIRP International Seminar on Manufacturing Systems*, p142-149, Athens, Greece, 16-18 May 2001.
- [Flo 01] G.H.J. Florussen, F.L.M. Delbressine, M.J.G. van de Molengraft, P.H.J. Schellekens. Assessing Geometrical Errors of Multi-axis Machines by three-dimensional Length Measurements. *Measurement*, (30):241-255, 2001.
- [Gem 92] S. Geman, E. Bienenstock. Neural networks and the bias/variance dilemma. *Neural Networks*, (4):1-58, 1992.
- [Gol 76] H. Golücke. *Ein Beitrag zur Meßtechnischen Ermittlung und analytischen Beschreibung systematischer Anteile der Arbeitsunsicherheit von Fertigungseinrichtungen*. PhD thesis, RWTH Aachen, 1976.
- [Gou 62] V.E. Gough, S.G. Whitehall. Universal Tyre Test Machine. *Proceedings of 9th International Technical Congress F.I.S.I.T.A.*, p117, May 1962.
- [Hem 73] C. Hemingray. Some Aspects of the Accuracy Evaluation of Machine Tools. *Proceedings of the 14th MTDR Conference*, p281-284, 1973.
- [Hoc 77] R. Hocken et al. Three Dimensional Metrology. *Annals of CIRP*, 26(2):403-408, 1977.
- [Hoc 80] R. Hocken and the Machine Tool Task Force. *Technology of Machine Tools: a survey of the state of art by the Machine Tool Task Force*. Machine tool Accuracy, Vol. 5, Lawrence Livermore National Laboratory, University of California, 1980.
- [Hoc 02] R. Hocken, P.H. Pereira. Modelling of Dynamical Errors of a Scanning Coordinate Measuring Machine. *Annals of CIRP 2002*, to be published.
- [Hol 98] C. Hollaar. *Regressie met behulp van orthogonale polynomen*. Internal project report, Eindhoven University of Technology, Juni 1998. (in Dutch)
- [Hoo 00] F.P. d'Hooghe, P.H.J. Schellekens, L.M. Levasier. Geometric calibration of CMMs using 3D length measurements. *Proceedings of the IMEKO 2000 International Measurement Confederation XVI*, Vienna, Austria, September 2000.
- [Inc 90] F.P. Incropera, D.P. de Witt. *Fundamentals of heat and mass transfer*. Third edition, 1990.

- [ISO 1] ISO 1. Standard reference temperature for industrial length measurements. ISO International Standard, April 1975.
- [ISO 841] ISO 841. Numerical Control of Machines - Axis and Motion Nomenclature. ISO International Standard, first edition, July 1974.
- [ISO 230-1] ISO 230-1. Test code for machine tools part 1: Geometric accuracy of machines operating under no-load or finishing conditions. ISO International Standard, second edition, July 1996.
- [Jan 88] S.W. Janna. *Engineering heat transfer*. S.I. Edition, Van Nostrand Reinhold Publishers, UK, 1988.
- [Jan 00] J. Janeczko, B. Griffin, C. Wang. Laser vector measurement technique for the determination and compensation of volumetric position errors. Part II: Experimental verification. *American Institute of Physics*, Vol. 71, no.10:3938-3341.
- [Jed 90] J. Jedrzejewski, J. Kaczmarek, Z. Kowal, Z. Winiarski. Numerical optimization of thermal behaviour of machine tools. *Annals of CIRP*, 39(1):379-382, 1990.
- [Kak 93] Y. Kakino, Y. Ihara, A. Shinohara. *Accuracy Inspection of NC Machine Tools by Double Ball Bar Method*, edited by Johannes Heidenhain GmbH. Carl Hanser Verlag, Munchen, Germany, 1993. ISBN 3-446-17430-3.
- [Kef 90] C.P. Keferstein et al. *Neue Meß- und Prüfkonzepte mit einem Präzisionsroboter*. VDI Berichte 836:139-152, 1990.
- [Kna 83] W. Knapp. Test of the three-dimensional uncertainty of machine tools and measuring machines and its relation to the machine errors. *Annals of CIRP*, 32/1:459-464, 1983.
- [Kre 88] E. Kreyszig. *Advanced Engineering Mathematics*. John Wiley & Sons, Inc, Canada, sixth edition, 1988.
- [Kru 94] J.P. Kruth, P. Vanherck, L. de Jonge. Self-calibration method and software error correction for three-dimensional coordinate measuring machines using artifact measurements. *Measurement*, Vol. 14:157-167, 1994.
- [Kun 90] H. Kunzmann, E. Trapet, F. Wäldele. A uniform concept for calibration, acceptance tests and periodic inspection of coordinate measuring machines using reference object. *Annals of CIRP*, 39/1:561-564, 1990.
- [Lee 02] J. Lee, S. Yang. Statistical optimization and assessment of a thermal error model for CNC machine tools. *International Journal of Machine Tools & Manufacture*. 42:147-155, 2002.
- [Mar 93] J.E. Marsden, A.J. Tromba, A. Weinstein. *Basic Multivariable Calculus*. Springer-Verlag New York, 1993. ISBN 0-7167-2443-X.

- [Mas 89] T. Masuda, M Kajitani. An automatic calibration system for angular encoders. *Precision Engineering*, 11(2):95-100, 1989.
- [Mon 92] D.C. Montgomery, E.A. Peck. *Introduction to Linear Regression Analysis, second edition*. John Wiley & Sons, U.S.A., 1992.
- [Mon 94] D.C. Montgomery, G.C. Runger. *Applied Statistics and Probability for Engineers*. John Wiley & Sons, U.S.A., 1994.
- [Mon 97] D.C. Montgomery. *Design and analysis of Experiments, fourth edition*. John Wiley & Sons, Arizona, U.S.A., 1997.
- [Mul 98] E. Mulder. *Development of a recursive Kalman filter algorithm for parameter estimations of a geometric machine error model*. Assignment report Mechatronica, Stan Ackermans Institute, August 1998.
- [Oku 75] K. Okushima, Y. Kakino, A Higashimoto. Compensation of thermal displacement by coordinate system correction. *Annals of CIRP*, 24(1):327-331, 1975.
- [Pau 81] R.P. Paul. *Robot Manipulators: Mathematics, Programming, and Control*. MIT, U.S.A., sixth edition, 1981.
- [Que 98] R. Quere, D.G. Deac. *Optimal Calibration in Precision Engineering*. Assignment report Wiskunde voor de industrie, Stan Ackermans Institute, December 1998.
- [Ren 97] M. Renkens. *Design of an Axially Controlled Spindle Unit for High Precision Diamond Turning*. PhD thesis, Eindhoven University of Technology, 1997.
- [Sar 95] S. Sartori, G.X. Zhang. Geometric Error Measurement and Compensation of Machines. *Annals of CIRP*, 44/2:599-609, 1995.
- [Sat 73] T. Sata, Y. Takeuchi, N. Sato, N. Okubo. Analysis of thermal deformation of machine tool structure and its application. *MTDR Conference Proceedings*, p275-280, 1973.
- [Sch 93] P.H.J. Schellekens, H.A.M. Spaan et al. *Development of Methods for the Numerical Error Correction of Machine Tools, BCR-project*. Final report, Bureau Communautaire de Référence, 3320/1/0/160/89/8-BCR-NL, Brussels, 1993.
- [Sch 00] P.H.J. Schellekens, H. Haitjema. *Meten en Signaalverwerking*, College diktaat 4C350, deel B, Eindhoven University of Technology, 2000. (in Dutch)
- [Sch 01] P.H.J. Schellekens. *Bijzondere Onderwerpen Precision Engineering*, Lecture notes College 4U740, Eindhoven University of Technology, 2000. (in Dutch)

- [Sch 32] G. Schlesinger. *Inspection Tests on Machine Tools*. Machinery Publishing Co. London, 1932.
- [Sme 98] B.C.H. Smeets. *Instationair thermisch gedrag van machines*. Assignment report no. PE98-003, Eindhoven University of Technology, 1998. (in Dutch)
- [Soo 93] J.A. Soons. *Accuracy Analysis of Multi-axis Machines*. PhD thesis, Eindhoven University of Technology, 1993.
- [Soo 97] J.A. Soons. Measurement and Analysis of Quasi-static Hexapod Errors. *Progress in Precision Engineering and Nanotechnology*, (1):356-359, Braunschweig, Germany 1997.
- [Spa 95] H.A.M. Spaan. *Software Error compensation of Machine Tools*. PhD thesis, Eindhoven University of Technology, 1995.
- [Ste 65] D. Stewart. A Platform with Six Degrees of Freedom. *The Institution of Mechanical Engineers, Proceedings*, No. 15, part 1:371-386, 1965-66.
- [Str 88] G. Strang. *Linear Algebra and its Applications, third edition*. Harcourt Brace Jovanovich Publishers, MIT, 1988.
- [The 91] F.C.C.J.M. Theuws. *Enhancement of Machine Tool Accuracy: Theory and Implementation*. PhD thesis, Eindhoven University of Technology, 1991.
- [Thu 99] J. Thlustly, J. Ziegert, S. Ridgeway. Fundamental Comparison of the Use of Serial and Parallel Kinematics for machine Tools. *Annals of CIRP*, 48/1:351-356, 1999.
- [Tön 01] H.K. Tönshoff, A. Schmidt, H.C. Möhring, G. Günther, E. Lübbbers. Transportable machining unit with hybrid kinematic structure for flexible maintenance of large metal forming tools. *The 34th CIRP International Seminar on Manufacturing Systems*, p7-10, Athens, Greece, 16-18 May 2001.
- [Ugu 95] A.C. Ugural, S.K. Fenster. *Advanced Strength and Applied Elasticity*. Third edition, Prentice Hall, U.S.A., 1995.
- [VDI 2617] VDI 2617, Blatt 3. VDI/VDE Richtlinien, Genauigkeit vom Koordinatenmeßgeräten, Komponenten der Meßabweichung des Gerätes. May, 1989.
- [Wan 00] C. Wang. Laser vector measurement technique for the determination and compensation of volumetric positioning errors. Part I: Basic theory. *American Institute of Physics*, Vol. 71, no.10:3933-3337.
- [Wal 97] F. Wäldele et al. *Workshop on Traceability of Coordinate Measuring Machines*. Project report: Traceability of Coordinate Measurements According to the Method of the Virtual Measuring Machine, PTB, October 9-10, 1997.

- [Wec 75] M. Weck, L. Zangs. Computing the thermal behaviour of machine tools using the finite element method - possibilities and limitations. p261-273, 1975.
- [Wec 95] M. Weck, P.A. McKeown, R. Bonse, U. Herbst. Reduction and compensation of thermal errors in machine tools. *Annals of CIRP*, 44(2):589-597, 1995.
- [Wec 98] M. Weck, U. Herbst. Compensation of Thermal Errors in Machine Tool with Minimum Number of Temperature Probes based on Neural Network. *Proceedings of the ASME*, volume 64, 1998.
- [Wec 02] M. Weck, D. Staimer. Parallel kinematic machine tool. *Annals of CIRP 2002*, to be published.
- [Wee 95] W.G. Weekers. *Compensation for Dynamic Errors of Coordinate Measuring Machines*. PhD thesis, Eindhoven University of Technology, 1996.
- [Wie 00] A.M. van der Wielen. *Thermische analyse Maho 700S*. Assignment report no. PE2000-048, Eindhoven University of Technology, 2000. (in Dutch)
- [Zho 99] E.P. Zhou, D.K. Harrison. Improving error compensation via a fuzzy-neural hybrid model. *Journal of Manufacturing Systems*, 18(5):335-344, 1999.
- [Zie 94] J.C. Ziegert. Measurement of machine tool parametric errors using the laser ball bar. *ASPE*, p76-79, October 1994.





# Appendix A

## Nomenclature, acronyms and symbols

### Abbreviations, acronyms

ASME	American Society of Mechanical Engineers
BEM	Boundary Element Method
BGM	Bond Graph Method
CMM	Coordinate Measuring Machine
DBB	Double Ball Bar
DIN	Deutsche Industrie Norm
DNC	Direct Numerical Control
EDM	Electrical Discharge Machining
FEA	Finite Element Analysis
FEM	Finite Element Method
FDM	Finite Difference Method
ISO	International Standard Organization
LBB	Laser Ball Bar
LCM	Lumped Capacitance Method
MC	Machine Constants
MSe	Mean Sum of Squared errors
NC	Numerical Control
NKO	Nederlandse Kalibratie Organisatie
PC	Personal Computer
SMD	Surface Mounting Devices
SSe	Sum of Squared errors
TNM	Thermal Network Method
VDI	Verein Deutsche Ingenieure

## Symbols

roman	description
$a_n$	length of link $n$
$A$	area
$Bi$	Biot number
$c$	material specific heat
$c_i$	thermal error model coefficient
$\mathbf{c}$	centre point DBB measurement
$C_i$	thermal capacity of lump $i$
$\mathbf{C}$	matrix containing thermal error model coefficients
$\mathbf{e}_i$	vector containing translational error components of axis $i$
$\mathbf{F}$	error propagation matrix
$G_{y1}$	local temperature gradient in $y1$ direction
$G_{z1}$	local temperature gradient in $z1$ direction
$h_c$	average convective heat transfer coefficient
$\mathbf{H}$	geometrical error model matrix
$i$	end point plate vector
$i_0$	start point plate vector
$\mathbf{I}$	identity matrix
$k$	thermal conductivity coefficient
$l$	number of DBB measurements
$l_{z1}$	length of plate vector in local coordinates
$l$	length
$l_{DBB}$	nominal DBB length
$\Delta l$	change in length
$\Delta l_k(j)$	measured change in length at time $j$ for point $k$
$\Delta \hat{l}_k(j)$	modelled change in length at time $j$ for point $k$
$L_c$	characteristic length
$m$	number of measuring points within a DBB measurement
$n$	number of joints/axes
$n_{max}$	maximum spindle speed
$nmp$	number of measuring points
$\mathbf{n}$	normal vector
$N$	total number of measuring points
$p$	number of geometrical error model parameters
$\mathbf{p}_i$	vector containing arm of rotation of axis $i$
$\mathbf{p}_{i,j}$	position vector frame $j$ relative to frame $i$
$\mathbf{p}_{u-act}$	actual position vector of relative end-effector position
$\mathbf{p}_{u-nom}$	nominal position vector of relative end-effector position
$q$	heat flow
$Q$	heat source
$\mathbf{Q}$	matrix containing error component functions
$r$	radius

---

$r_{i,j}$	correlation coefficient
$\Delta r$	radius deviation
rpm	revolutions per minute
$R$	thermal resistance
${}_i R_{x1}$	rotational error component of plate $i$ around $x1$ direction
$\mathbf{R}_i$	rotation matrix of axis $i$
$\mathbf{R}_{i,j}$	rotation matrix: orientation frame $j$ relative to frame $i$
$t$	time
$\mathbf{t}$	tool/end-effector vector
$T_i$	temperature at point $i$
$T_\infty$	air bulk temperature
$T_N$	temperature of machine part $N$
$\Delta T$	temperature difference
${}_i T_{y1}$	translational error component of plate $i$ in $y1$ direction
${}_i T_{z1}$	translational error component of plate $i$ in $z1$ direction
$\mathbf{u}$	state vector containing machine's axis positions
$V$	volume
$\mathbf{w}$	estimated position of centre point DBB measurement
$x$	position X-axis
$x_0$	half X-axis length
$\mathbf{x}(t)$	vector containing temperature sensor readings
$\mathbf{X}$	geometrical error model matrix
$\mathbf{y}$	vector containing radius deviations measured
$\mathbf{Z}$	measurement model matrix
<b>greek</b>	<b>description</b>
$\alpha$	thermal coefficient of expansion
$\alpha$	thermal diffusivity coefficient
$\alpha_n$	twist angle of link $n$
$\beta$	thermally induced bending angle
$\boldsymbol{\beta}$	vector contain geometrical error model parameters
$\boldsymbol{\gamma}$	estimation error vector centre point DBB measurement
$\varepsilon$	emissivity coefficient
$\boldsymbol{\varepsilon}_i$	vector containing rotational error components of axis $i$
$\phi$	rotation angle C-axis
$\nu_{p,q}$	covariance parameters $p, q$
$\rho$	density
$\hat{\rho}$	estimated correlation coefficient
$\sigma$	standard deviation
$\sigma$	Stefan-Boltzmann constant
$\theta$	rotation angle B-axis
$\boldsymbol{\xi}$	machine's positioning and orientation error vector
$\hat{\boldsymbol{\xi}}$	modelled positioning and orientation error vector
$\Delta \boldsymbol{\xi}$	measured change in positioning and orientation error vector
$\Delta \hat{\boldsymbol{\xi}}$	modelled change in positioning and orientation error vector

$\xi^t$	machine's positioning error vector
$\xi^r$	machine's orientation error vector
$\xi_i$	machine's positioning and orientation error vector due axis $i$

## Appendix B

# Double Ball Bar calibration

In this Appendix the calibration procedure of a DBB length measuring device is described. This means that the DDB length is compared to a length standard in this case: a laser interferometer on an optical bench. This laser interferometer is calibrated (with NKO certificate) and available at the Precision Engineering Laboratory, TUE. In this way, the traceability of the DBB length measuring instrument is realized as indicated in Table B.1. At the right hand side the relative uncertainty, that is  $\Delta l/l$ , of the standard is listed. A metre is defined (in 1983) as the distance travelled by light in vacuum during a period of  $1/299792458$  seconds.

Definition of the Metre:	$10^{-13}$ f
↓	
I <sub>2</sub> stabilized He-Ne laser:	$10^{-9}$ f
↓	
HP Laser interferometer:	$10 \text{ nm} + 2 \cdot 10^{-7} \ell$
↓	
Optical bench:	$5 \cdot 10^{-7}$ m
↓	
Double Ball Bar:	$10^{-6}$ m

Table B.1: Traceability scheme of DBB length measuring instrument to the metre.

Downwards the standard uncertainty increases due to errors introduced during calibration i.e. when comparing the standards.

The calibration procedure of the DBB as performed at the Precision Engineering Laboratory, TUE will be described here. For this calibration the following is required:

- A laser interferometer: laser head, beam splitter, turning mirror, 2 retro reflectors, air sensor, laser display;
- Optical bench: axis with travelling guide, measuring force controlling unit, several adjustment devices;
- a DBB: this device contains a telescopic rod and a linear encoder (resolution  $0.1 \mu\text{m}$ ). Furthermore a PC with specific DBB software is required to read the DBB length and a clamp for fixing the telescoping rod of the DBB during calibration.

The description of the preparation of the measurement setup can be found at the end of this Appendix.

In Figure B.1 a schematic drawing is depicted of the measurement setup for calibrating a nominal DBB length. The length of the DBB is defined as the distance between the centre points of the balls attached at each end of the DBB. During applications of a DBB for instance, this value is obtained by adding the scale readout to the nominal DBB length:  $L_{DBB} = L_0 + u_{DBB}$ . By resetting the laser interferometer while one DBB ball is positioned between the probing plates, as shown in the upper-half of Figure B.1, the DBB length can be compared directly with the reading of the laser interferometer when the DBB is put between the probing plates, as shown in the lower-half of Figure B.1. In this way, the diameter of the DBB ball is eliminated in the laser interferometer reading. This implies the assumption that both DBB balls do have the same diameter. After determining the DBB length this way, again one DBB ball should be measured again in order to check for irregularities during the measurement procedure: the laser reading must approach a zero reading closely (within a few tenths of a  $\mu\text{m}$ ). Considering this calibration procedure, the following relevant error sources can be identified:

1. Hertzian contact deformation of DBB balls;
2. Non-parallelity of probing plates;
3. Spherity errors of DBB balls;
4. Different DBB ball diameters;
5. Misalignment DBB with laser beam;
6. DBB length measurement system errors;
7. 'Abbe' errors;
8. Thermal expansion of DBB;

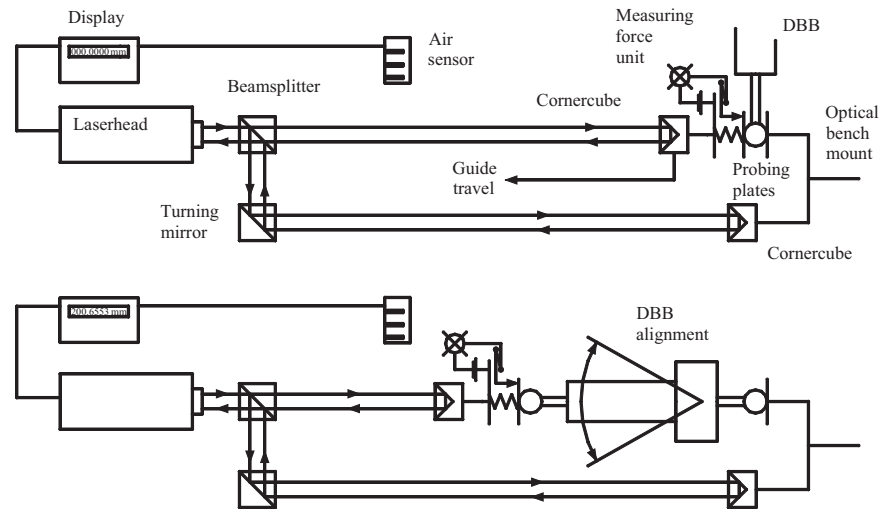


Figure B.1: Measurement setup for DBB length calibration with laser interferometer on an optical bench.

9. Environmental effects affecting the refractive index of air (temperature, humidity, CO<sub>2</sub> concentration).

In Figure B.1 a certain measuring force controlling unit is drawn schematically. This is a device to realize a constant non-zero contact measuring force when performing a measurement (i.e. by reading the laser interferometer display). This way the measurement force can be controlled, limiting the measurement error introduced otherwise due to Hertzian contact deformation. Due to this device, only variations in the measuring force can introduce a calibration error: the resulting DBB ball contact deformation is the same in both positions drawn in Figure B.1 and is therefore eliminated in the measurement procedure. The effect of measuring force variations of this unit is negligible to the effect of other error sources present.

The near flat probing plates used for sensing a DBB ball are not perfectly parallel. The error introduced equals the angle between these plate planes times the distance in ball position on these plates between the two calibration positions as displayed in the upper respectively lower half of Figure B.1. By aligning these plates the error can be limited to  $0.1 \mu\text{m}$ . These plates can for instance be set near parallel with adjustment screws by moving a ball in between the plates while reading the laser display. The calibration error is limited furthermore by measuring the DBB ball in both positions drawn in Figure B.1 on the same position on the aligned parallel probing plates.

The sphericity error of a DBB ball is typically  $0.1 \mu\text{m}$  or less. This error can



be estimated by rotating a DBB ball while sensing its diameter between the probing plates, using the laser interferometer. Since both DBB balls are sensed over the same ball diameter (along the measurement axis), DBB ball sphericity errors are not present in this calibration procedure. After carefully contacting the probing plates, the diameter of a DBB ball can be determined as well by comparing the instruments' value with the former one (referring to the upper-half of Figure B.1). DBB ball sphericity errors exceeding  $0.1 \mu\text{m}$  have not been observed.

Before reading the laser interferometer display during calibration (see lower-half Figure B.1) the DBB measurement axis has to be aligned with the measurement axis of the laser interferometer: the laser beam. This means that the orientation of the DBB must be varied somehow (with adjustment screw available on the travelling guide) until the maximum laser display reading is obtained: then the DBB is in line with the laser beam. Errors in this alignment procedure effect the measured length to the second order only. An alignment error of  $\alpha$  rad results in a shortening of a ball bar with length  $\ell$  equal to  $\frac{1}{2} \cdot \alpha^2 \cdot \ell$ .

The telescoping rod of the DBB must be fixed while determining the DBB's length (e.g. with a clamp) to avoid DBB contraction due to a measurement force. This clamp must be fixed at different positions on the telescoping DBB rod in order to determine the instruments' scale errors. Significant errors of the DBB's 10 mm linear encoder could not be observed with this measurement setup and are therefore neglected.

Since the laser beam is very close in line with the DBB measurement axis during calibration, angular motions of the travelling guide do not distort the DBB length measured. Due to this measurement setup the so-called 'Abbe' errors can be neglected.

The temperature of the DBB does not equal  $20^\circ\text{C}$  exactly and its temperature distribution is not homogeneous. Therefore an error due to the resulting thermal DBB expansion is present in a DBB calibration procedure. This is a major source of error and uncertainty while calibrating a length measuring device accurately. Besides DBB part temperature differences with respect to  $20^\circ\text{C}$ , the thermal coefficient of expansion is not accurately known when applied to a DBB. The thermal expansion of a DBB can be approximated by using:

$$\Delta\ell_{DBB} \simeq \alpha_{DBB} \cdot L_0 (T_{DBB} - 20^\circ\text{C}).$$

The largest source of uncertainty in this approximation is the thermal expansion coefficient used for the DBB, consisting of the balls, a telescoping rod, a linear glass encoder, an extension rod and a fixed ball housing. In theory this coefficient equals the weighted sum of the relevant material expansion coefficients present in the DBB's measurement loop ( $11 \cdot 10^{-6} \text{K}^{-1}$  resp,  $8 \cdot 10^{-6} \text{K}^{-1}$ ) according to its length of steel (240 mm) and glass (10 mm). Therefore the thermal expansion coefficient used for the DBB is mainly determined by the steel DBB frame and marginally by the glass encoder due to its small length in the DBB's measurement path.

Besides leaving the DBB ('switched on') for several hours in a temperature controlled metrology laboratory before calibration, gloves must be used

while performing calibrations. Body heat can significantly disrupt the calibration procedure described. Examples are heating up of the DBB and changing the temperature of the air present in the laser interferometers' optical path. Temperature (as well as humidity and CO<sub>2</sub> concentration) affects the refractive index of air and its distortions can be compensated for by using the Edlen formula to correct the actual laser wavelength. This formula quantifies the effect of temperature, humidity and CO<sub>2</sub> concentration on the refractive index of air [Bir 94]. These entities are determined by an air-sensor, which is part of the laser interferometer measuring instrument.

The error in nominal DBB length  $L_0$  marginally affects the calculated expansion of the DBB due to the small values of the product  $\alpha_{DBB}$  and  $\Delta T_{DBB}$ .

The listed errors are dominated by the uncertainties introduced by the DBB's thermal behaviour. Besides above-mentioned error sources, fast execution of the described calibration procedure furthermore limits the calibration error introduced otherwise, constraining the change of disturbances affecting length measurement.

The nominal DBB length, as obtained with this calibration procedure can be expressed as:

$$L_0 = L_{laser} - u_{DBB} + \Delta D + \delta\ell_{probing} - \delta\ell_{align} - L_0 \cdot \alpha(T - 20^\circ\text{C}) + \delta u_{scale}.$$

In words this means that the nominal DBB length equals the length measured with the laser interferometer minus the DBB readout plus a contribution for different DBB ball diameters added with a contribution of non-parallel probing plates minus the alignment error minus the thermal DBB expansion added with errors of the integrated DBB scale. The nominal DBB length and its uncertainty according to document [EA-4] is listed in Table B.2: Summarizing,

quantity	estimate	standard uncertainty	sensitivity coefficient	uncertainty contribution
$L_{laser}$	252.7686 mm	0.5 $\mu\text{m}$	1	0.5 $\mu\text{m}$
$u_{DBB}$	2.1132 mm	0.1 $\mu\text{m}$	-1	-0.1 $\mu\text{m}$
$\Delta D$	0 $\mu\text{m}$	0.1 $\mu\text{m}$	1	0.1 $\mu\text{m}$
$\delta\ell_{probing}$	0 $\mu\text{m}$	0.1 $\mu\text{m}$	1	0.1 $\mu\text{m}$
$\delta\ell_{align}$	0 $\mu\text{m}$	0.1 $\mu\text{m}$	-1	-0.1 $\mu\text{m}$
$\alpha$	$11 \cdot 10^{-6} \text{ K}^{-1}$	$1 \cdot 10^{-6} \text{ K}^{-1}$	0	0 $\mu\text{m}$
$T$	20 $^\circ\text{C}$	0.2 K	$-2.75 \cdot 10^{-6} \text{ mK}^{-1}$	-0.55 $\mu\text{m}$
$\alpha \cdot \Delta T$	0	$2.2 \cdot 10^{-6}$	$-250 \cdot 10^{-3} \text{ m}$	-0.05 $\mu\text{m}$
$\delta u_{scale}$	0 mm	0.1 $\mu\text{m}$	1	0.1 $\mu\text{m}$
$L_0$	250.6554 mm			0.8 $\mu\text{m}$

Table B.2: Uncertainty budget calibration nominal DBB length.

the uncertainty in DBB length is estimated by summing the effect of various error sources independently and is approximated to 0.8  $\mu\text{m}$ , see calibration table B.2. When performing DBB measurements on a multi-axis machine, the

length measurement uncertainty is increased due to sphericity errors of the DBB balls (not present in this calibration), but this contribution is limited to  $0.1 \mu\text{m}$  only and can be neglected.

## Preparation measurement setup

Here the description of the preparation of the presented measurement setup is presented.

### 1. Alignment laser beam with optical bench.

First the laser beam has to be aligned with the travelling guide of the optical bench by an iteration procedure. This means that the laser head position and orientation is adjusted while the laser beam is aimed at a target (e.g. an improvised cross), attached on the travelling guide. The laser head should be rotated when the target is at the end of the optical bench and translated for a proximate target. This procedure is repeated until the target stays in line with the laser beam, typically within  $0.1 \text{ mm}$ .

### 2. Setup laser beams.

Secondly, the laser beam is split into two beams by placing a beam-splitter (the interferometer) in the aligned laser beam path: one beam goes straight (i.e. the vertical component of the incident circular polarized electro-magnetic wave as emitted by the laser head) and the other one leaves the beam splitter (i.e. the horizontal component) on one side perpendicular to the other beam. This deflected beam is oriented parallel to the straight beam by means of a turning mirror. The interferometer and turning mirror should be placed in such a way, that both laser beams can be reflected by the retro-reflectors present at one end of the optical bench, opposing to the laser head. The advantageous property of the retro-reflectors, also called corner cubes, above plane mirrors is their insensitivity for small rotational alignment errors: the reflected beam remains parallel to the incident one. Both retro-reflectors are clamped in an adjustable mount, changing its position perpendicular to the laser beam. One mount is fixed to the optical bench and the other one is connected to a probing plate present on the travelling guide. This probing plate can be accurately translated relative to the travelling guide by means of an adjustment screw.

### 3. Obtain maximum signal strength by adjustments.

Thirdly these retro-reflectors in combination with the beam-splitter and turning mirror have to be adjusted in such a way until the maximum laser beam strength signal possible is obtained. This laser beam strength is displayed and must be rather constant while moving the travelling guide, confirming alignment of the parallel beams. One of these beams is the 'measurement beam' and the other one is the 'optical dead path'. Based on interferometry, the difference in the optical beam length paths can be measured very accurately by counting interference fringes electronically (1 fringe represents a relative guide travel of  $\frac{1}{2}$  wavelength) enhanced with sophisticated interpolation techniques. After this procedure, the length measurement mode of the laser interferometer can be selected and reset. The air sensor is located near the laser beams for correcting the wave length

affected by environmental influences (temperature, air pressure and humidity as described by the Edlèn equation).

4. Prepare DBB mounting on optical bench.

The DBB has to be mounted on the optical bench in two ways. First the DBB is clamped (more or less) perpendicular to the laser beams (see upper-half Figure B.1). Then one DBB ball is put between two parallel probing plates: one plate is connected to the optical bench, the other one is fixed on the travelling guide. Check if the probing plates are parallel by moving the DBB ball in plane with the plates while watching the laser display. If the laser readout varies more than, say 1  $\mu\text{m}$  use the adjustment screws available. If found satisfactory, the roundness errors of both DBB precision balls can be verified easily by rotating a ball while watching the laser display. Checking the ball diameters reduces the measurement error introduced otherwise. Typical DBB ball roundness errors measured are 0.1  $\mu\text{m}$ .

Secondly, the DBB has to be put inline with the (straight) laser beam (see lower-half Figure B.1). Hereby the DBB is clamped on the travelling guide, equipped with a multiple degree of freedom table necessary for alignment. The effect of non-parallelity of the probing plates can be alleviated by adjusting the travelling guide adjustment table in such a way, that the DBB ball is always measured on the same location on the probing plate. Also a temperature sensor must be attached to the DBB to correct for thermal expansion during calibration measurements. The use of gloves is preferable when handling the DBB to minimize thermal disturbances.



## Appendix C

# Alternative error component functions

In this research project the following parametric functions have been considered for describing the unknown error components of a multi-axis machine:

1. Ordinary polynomials;
2. Piecewise polynomials (splines);
3. Orthogonal polynomials;
4. Fourier functions.

The choice between these functions depends mainly on the way an error component changes with axis position and on the accuracy required. In many cases, this change can be described satisfactorily with ordinary polynomials. In some cases however, the application of ordinary polynomials might not be suitable to describe an error component with sufficient accuracy.

When a machine contains one or more axes with a very long range for example (i.e. showing less simple error component behaviour with axis position), the use of piecewise polynomials can be preferable above using ordinary polynomials. These piecewise polynomials have in principle the same properties as ordinary polynomials; only the axis range is divided into several  $(m + 1)$  segments by placing  $(m)$  knots and an ordinary polynomial (of degree  $n$ ) is applied for each interval [Soo 93] [Spa 95]. This can be denoted, using error component  $xtx$  as an example as:

$$xtx(x, \beta) = \sum_{l=0}^n \beta_{xtx,0,l} \cdot x^l + \sum_{k=1}^m \sum_{l=0}^n \beta_{xtx,k,l} (x - t_k)_+^l$$

where:

$$(x - t_k)_+ = \begin{cases} (x - t_k) & \text{if } x - t_k > 0 \\ 0 & \text{if } x - t_k \leq 0. \end{cases}$$

The presence of a term  $\beta_{k,l}(x - t_k)_+^l$  allows a discontinuity at knot  $t_k$  in the  $l$ th derivative of  $xtx(x, \beta)$ . Usually it is sufficient to ensure that each model is continuous with respect to the function value and its first derivative. A disadvantage of the use of piecewise polynomials is that the estimation problem for determining the parameters  $\beta$  easily becomes ill-conditioned due to its high flexibility, especially when many knots are used. When fixed knot positions are used, the parameters  $\beta$  of the polynomials can be estimated by linear regression. If the knot positions and/or the degree of the polynomials used for the segments are considered variable, they enter the regression problem in a non-linear fashion and all the problems arising in non-linear regression are present [Soo 93].

Another kind of functions suitable for describing error components are orthogonal polynomials. Although the capabilities of these functions to describe measurement data is exactly similar to that of ordinary polynomials, these functions possess some advantageous properties. A set of (real-valued) functions, say  $g_m(x)$  and  $g_n(x)$ , is orthogonal if it satisfies the following condition [Kre 88]:

$$(g_m, g_n) = \int_a^b p(x)g_m(x)g_n(x)dx = 0$$

on the interval  $a \leq x \leq b$  with respect to the weighting function  $p(x)$ . Assume that the two functions  $g_m(x)$  and  $g_n(x)$  are used for describing an error component of the X-axis (i.e. a linear and a quadratic term for instance), then the estimated coefficients of these two functions are independent and therefore uncorrelated. However this property is only valid if the data to be fitted is continuous; for finite data this property of orthogonality is violated and can even be lost as found when applying orthogonal Legendre polynomials for describing error component functions [Hol 98]. For this reason the application of orthogonal functions has been rejected.

Fourier functions can also be used for approximating an error component [Gol 76] [Mas 89]. This implies that any function can be approximated by a limited sum of harmonic functions:

$$f(x) \simeq a_0 + \sum_{j=1}^m (a_j \cos(jx) + b_j \sin(jx)).$$

These kind of functions are especially suitable for describing data containing periodic components. In theory, any function can be approximated just by increasing the number of harmonics considered, taking certain conditions and constrains into account (continuity, derivatives, signal power, signal leak, etc.). However the error components of a translational axis are generally not periodic with axis position. This means that relatively many (higher order) harmonic components have to be used for obtaining a reasonable description of an error component. Since the error component variations are of low frequency with respect to the axis range, Fourier functions are not used in this thesis.

An exception should be made for the error components describing the positioning errors of a measurement system, containing a linear encoder: these errors often show periodic components with relatively short wavelength [Soo 93]. The

amplitude of this periodic error however is usually negligible to the change of magnitude of the error component itself and is therefore of minor importance. In addition, the errors of a rotary axis are by their nature periodic. For this class of errors, Fourier functions might be of great value but this is not investigated in this thesis.

Summarizing, several parametric functions can be applied for describing the error components of a multi-axis machine with each their own characteristics. In this thesis ordinary polynomials have been used for describing the error components of a milling machine.





## Appendix D

# Geometrical error model in matrix notation

The error model derived in Chapter 3, Section 3.1 is linear in the parameters  $\beta$  of the error components (see Equation 3.10):

$$\hat{\xi}_i(\mathbf{u}, \mathbf{t}, \beta) = \mathbf{R}_i^T(\mathbf{u}) \cdot \begin{bmatrix} \mathbf{e}_i(\mathbf{u}, \beta) + \varepsilon_i(\mathbf{u}, \beta) \times \mathbf{p}_i(\mathbf{u}, \mathbf{t}) \\ \varepsilon_i(\mathbf{u}, \beta) \end{bmatrix}.$$

Since these parameters  $\beta$  will be determined later on from measurement data (using linear regression, see Section 4.1) this equation will be rewritten in matrix notation, resulting in an explicit formulation of the machine's error vector as a function of the unknown parameters  $\beta$ . To do so, first the vector cross product present in Equation D has to be converted.

A cross-product of two vectors results in a vector perpendicular to the spanned plane (according to the right hand rule) and its length equals the spanned area. Reversing the cross-product therefore results in a minus sign:

$$\varepsilon_i(\mathbf{u}, \beta) \times \mathbf{p}_i(\mathbf{u}, \mathbf{t}) = -\mathbf{p}_i(\mathbf{u}, \mathbf{t}) \times \varepsilon_i(\mathbf{u}, \beta).$$

Since a vector cross product results in an equal dimensional vector, such a cross-product can also be computed by an inner product between a matrix and a vector. By introducing a matrix  $\mathbf{P}_i(\mathbf{u}, \mathbf{t})$  defined as:

$$\mathbf{P}_i(\mathbf{u}, \mathbf{t}) = \begin{pmatrix} 0 & -p_{iz}(\mathbf{u}, \mathbf{t}) & p_{iy}(\mathbf{u}, \mathbf{t}) \\ p_{iz}(\mathbf{u}, \mathbf{t}) & 0 & -p_{ix}(\mathbf{u}, \mathbf{t}) \\ -p_{iy}(\mathbf{u}, \mathbf{t}) & p_{ix}(\mathbf{u}, \mathbf{t}) & 0 \end{pmatrix}$$

and a matrix  $\mathbf{S}_i(\mathbf{u}, \mathbf{t})$ :

$$\mathbf{S}_i(\mathbf{u}, \mathbf{t}) = \mathbf{R}_i^T(\mathbf{u}) \cdot \mathbf{P}_i(\mathbf{u}, \mathbf{t})$$

the machine's positioning error  $\hat{\xi}_i^T$  can be rewritten as:

$$\begin{aligned}\hat{\xi}_i^T(\mathbf{u}, \mathbf{t}, \beta) &= \mathbf{R}_i^T(\mathbf{u}) \cdot \{\mathbf{e}_i(\mathbf{u}, \beta) + \varepsilon_i(\mathbf{u}, \beta) \times \mathbf{p}_i(\mathbf{u}, \mathbf{t})\}, \\ \hat{\xi}_i^T(\mathbf{u}, \mathbf{t}, \beta) &= \mathbf{R}_i^T(\mathbf{u}) \cdot \{\mathbf{e}_i(\mathbf{u}, \beta) - \mathbf{p}_i(\mathbf{u}, \mathbf{t}) \times \varepsilon_i(\mathbf{u}, \beta)\}, \\ \hat{\xi}_i^T(\mathbf{u}, \mathbf{t}, \beta) &= \mathbf{R}_i^T(\mathbf{u}) \cdot \mathbf{e}_i(\mathbf{u}, \beta) + \mathbf{R}_i^T(\mathbf{u}) \cdot \mathbf{P}_i(\mathbf{u}, \mathbf{t}) \cdot \varepsilon_i(\mathbf{u}, \beta), \\ \hat{\xi}_i^T(\mathbf{u}, \mathbf{t}, \beta) &= \mathbf{R}_i^T(\mathbf{u}) \cdot \mathbf{e}_i(\mathbf{u}, \beta) + \mathbf{S}_i(\mathbf{u}, \mathbf{t}) \cdot \varepsilon_i(\mathbf{u}, \beta)\end{aligned}$$

for axis  $i$ . Adding the contribution of all  $n$  axes subsequently results in:

$$\begin{aligned}\hat{\xi}(\mathbf{u}, \mathbf{t}, \beta) &= \sum_{i=1}^n \hat{\xi}_i(\mathbf{u}, \mathbf{t}, \beta), \\ \hat{\xi}(\mathbf{u}, \mathbf{t}, \beta) &= \sum_{i=1}^n \left[ \begin{array}{c} \mathbf{R}_i^T(\mathbf{u}) \cdot \mathbf{e}_i(\mathbf{u}, \beta) + \mathbf{S}_i(\mathbf{u}, \mathbf{t}) \cdot \varepsilon_i(\mathbf{u}, \beta) \\ \mathbf{R}_i^T(\mathbf{u}) \cdot \varepsilon_i(\mathbf{u}, \beta) \end{array} \right], \\ \hat{\xi}(\mathbf{u}, \mathbf{t}, \beta) &= \left[ \begin{array}{ccccc} \mathbf{R}_1^T(\mathbf{u}) & \mathbf{S}_1(\mathbf{u}, \mathbf{t}) & \dots & \mathbf{R}_n^T(\mathbf{u}) & \mathbf{S}_n(\mathbf{u}, \mathbf{t}) \\ \mathbf{0} & \mathbf{R}_1^T(\mathbf{u}) & \dots & \mathbf{0} & \mathbf{R}_n^T(\mathbf{u}) \end{array} \right] \begin{bmatrix} \mathbf{e}_1(\mathbf{u}, \beta) \\ \varepsilon_1(\mathbf{u}, \beta) \\ \vdots \\ \mathbf{e}_n(\mathbf{u}, \beta) \\ \varepsilon_n(\mathbf{u}, \beta) \end{bmatrix}.\end{aligned}$$

By storing the matrices  $\mathbf{R}_i^T(\mathbf{u})$  and  $\mathbf{S}_i(\mathbf{u}, \mathbf{t})$  in a matrix  $\mathbf{F}(\mathbf{u}, \mathbf{t})$  and the error components in a vector  $\mathbf{c}(\mathbf{u}, \beta)$ , the geometrical error model can be denoted as:

$$\hat{\xi}(\mathbf{u}, \mathbf{t}, \beta) = \mathbf{F}(\mathbf{u}, \mathbf{t}) \cdot \mathbf{c}(\mathbf{u}, \beta).$$

In Subsection 3.1.2, the error components  $\mathbf{c}(\mathbf{u})$  have been modelled with higher order polynomials (with exception of the squareness errors) containing parameters  $\beta$ , see Equations 3.2-3.4. By storing the error component functions in a matrix  $\mathbf{Q}(\mathbf{u})$ , the following yields<sup>1</sup>:

$$\begin{aligned}\mathbf{c}(\mathbf{u}, \beta) &= \begin{bmatrix} xtx(\mathbf{u}, \beta) \\ xty(\mathbf{u}, \beta) \\ \vdots \\ zrz(\mathbf{u}, \beta) \end{bmatrix}, \\ \mathbf{c}(\mathbf{u}, \beta) &= \begin{bmatrix} x - x_0 & (x - x_0)^2 & 0 & 0 & 0 \\ 0 & 0 & (x - x_0)^2 & 0 & 0 \\ 0 & 0 & 0 & \ddots & \vdots \\ 0 & 0 & 0 & \dots & z - z_0 \end{bmatrix} \begin{bmatrix} \beta_{xtx1} \\ \beta_{xtx2} \\ \beta_{xty2} \\ \vdots \\ \beta_{zrz1} \end{bmatrix}, \\ \mathbf{c}(\mathbf{u}, \beta) &= \mathbf{Q}(\mathbf{u}) \cdot \beta.\end{aligned}$$

In this way, the geometrical error model can briefly be denoted in matrix nota-

<sup>1</sup>For a squareness error, imagine a 1 on the corresponding position in matrix  $\mathbf{Q}(\mathbf{u})$

tion, by introducing a matrix  $\mathbf{H}(\mathbf{u}, \mathbf{t})$ , as:

$$\begin{aligned}\hat{\boldsymbol{\xi}}(\mathbf{u}, \mathbf{t}, \boldsymbol{\beta}) &= \mathbf{F}(\mathbf{u}, \mathbf{t}) \cdot \mathbf{Q}(\mathbf{u}) \cdot \boldsymbol{\beta} \\ \mathbf{H}(\mathbf{u}, \mathbf{t}) &= \mathbf{F}(\mathbf{u}, \mathbf{t}) \cdot \mathbf{Q}(\mathbf{u}) \\ \hat{\boldsymbol{\xi}}(\mathbf{u}, \mathbf{t}, \boldsymbol{\beta}) &= \mathbf{H}(\mathbf{u}, \mathbf{t}) \cdot \boldsymbol{\beta}.\end{aligned}$$

For determining the model parameters  $\boldsymbol{\beta}$ , length measurement data will be used.



## Appendix E

# Executing Double Ball Bar measurements

In this Appendix, the execution of DBB length measurements on a machining centre is discussed. In order to make the developed method applicable for a large number of existing machines, including less modern ones, several software modules have been developed in corporation with IBS Precision Engineering b.v. With these software modules DBB measurements can be performed on NC (Numerical Control) machining centres with and without DNC (Direct Numerical Control) mode.

In order to analyse the obtained DBB measurement data, it is essential that the relevant state of the machine corresponds with the correct readout of the DBB. Since the machine's positioning error is a function of the machine's coordinates ( $\mathbf{u}$ ) and the tool vector ( $\mathbf{t}$ ), these variables must be stored and synchronised with the corresponding radius (i.e. length) deviation  $\Delta r_u$  as measured by the DBB in that measuring position  $u$ . A PC is used to monitor the measuring process: the DBB length measuring device can be read by an inserted (Heidenhain IK110) card and the state of the machine (i.e. the axis positions) is monitored by a RS232 connection if DNC is available.

For machines with DNC mode communication of a PC with the machine's controller is possible during measurement. In this case the machine is first commanded to move to a certain position and the controller sends a signal to the PC after arriving there. While the machine is waiting in that point the PC reads the length of the DBB after a certain waiting time to let machine vibrations attenuate sufficiently (typically fractions of a second). Subsequently the machine's coordinates and the corresponding DBB readout are read and stored in a file and the PC sends a signal to the machine's controller to execute the next program line, containing the next measuring point in NC code. This sequence is repeated until all measuring points have been measured.

In Figure E.1 a screen print is displayed of the developed Labview program, used for executing DBB measurements.

For many less modern NC machining centres, however, DNC mode commu-

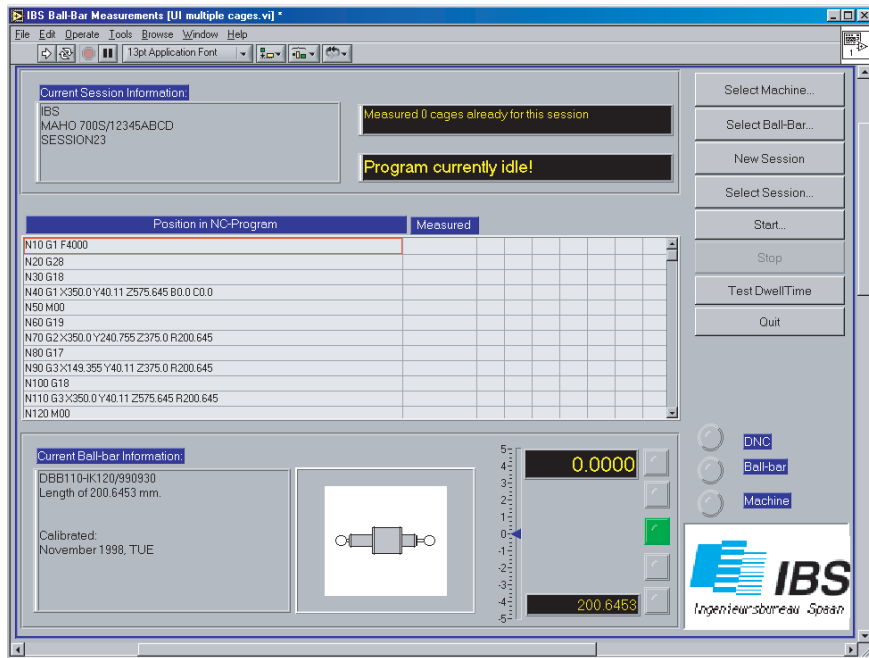


Figure E.1: Screen print of developed DBB measuring program.

nication is not available. In this case communication of a PC with the machine's controller cannot be realised during a measurement sequence. In practise this implies that once a selected NC program file has been activated for execution, it cannot be intervened without stopping the program. In this case, the synchronised storage of the machine's coordinates and the DBB readout is less straightforward.

Firstly, a modified NC program is selected and activated for execution on the machine. Secondly, a developed software program on the PC is started which monitors the entire measuring process. Since the arrival of the machine in a certain measuring point cannot be indicated to the PC anymore (to read the DBB), the problem of synchronisation is circumvented by adding so-called trigger motions in the NC program to be executed. This means that the machine is programmed in such a way that the DBB extends and retracts quickly several mm for each measuring point. When such a trigger movement occurs, this is detected by the PC monitoring the DBB continuously since the DBB passes a reference mark resulting in a detectable signal. By inserting waiting times (2 s) between measuring points in the NC program of the machine (i.e. dwell time) the DBB is read some time after passing the DBB's reference mark but before the machine moves to the next measuring position. In this way, the synchronised storage of the machine's coordinates (as read from the NC program to be executed) and the readout of the DBB can be guaranteed.

---

## NC-code generator

In order to execute a DBB measurement on a NC machining centre a software module has been developed to generate the appropriate NC code programs automatically suitable for any axis configuration. Given the radius (or DBB length) and the DBB measurement centre point position in machine's coordinates, the spatial coordinates of the measuring points can be calculated, depending on the step angles between these measuring points. By inserting the orientation of the machine's axes in relation to the orientation of the desired DBB measurement in this software module, the appropriate NC code can be generated.

In order to prevent DBB wire wind-up, the direction of motion of all successive circles (forming together a semi-spherical grid of measuring points) performed at different height levels is reversed each time i.e. clockwise versus counter clockwise. Also, if a reversal measurement cycle is desired, the same measuring point will always be approached in the opposite direction: if a point was approached in clockwise direction for the first time, the same point will subsequently be approached in counter-clockwise direction in the reversal measurement cycle. This strategy is also applied for machine's without DNC mode: for the first DBB measurement cycle the DBB is triggered outwards (in positive direction of normal vector  $\mathbf{n}_u$  see Figure 3.5) and for the reversal measurement cycle this length instrument is triggered inwards (negative direction of normal vector  $\mathbf{n}_u$ ). In this way, presence of (virtual-) play and backlash of the machine or other irregularities (like dirt, hydraulic pump pulses etc.) during measurement can be detected. This reversal measurement is implemented as an option in the developed software module.

In some situations, however, for instance a stand positioned near the boundary of the machine's workspace, the DBB cannot move along an entire circle but only along a part (or parts, not necessarily connected) of it. By implementing the machine's axes ranges in the software module these problems can be predicted and taken into account. In such a situation, an algorithm searches for alternative paths (perpendicular on the actual plane of movement) to move to a measuring point with a 'problematic' accessibility. In this way, the amount of measuring points that can possibly be reached, is also measured.

## Practical considerations

In this research project the systematic part of the relative positioning and orientation error of a multi-axis machine is studied mainly. This implies that DBB measurements results must be reproducible or at least repeatable to a large extent. In this subsection measures are discussed to obtain highly reproducible DBB measurement results.

Before starting with a DBB measurement, the precision balls of the measuring device and the two magnetic sockets must be cleaned properly. For this reason the use of gloves is preferable but also to minimise warming up of the DBB by body heat while handling the instrument.



Besides cleaning also the initialisation procedure before measuring lengths at certain discrete positions in the machine's workspace requires special attention. First of all, the stand position on the workpiece table will not likely coincide with the programmed centre point of the DBB measurement to be executed since the stand is positioned by eye only according procedure. A stand positioning error of a mm is common. The measuring range of the telescoping DBB ball is limited to 10 mm so a check of this stand position is needed to prevent serious damage of the DBB. Therefore three arc shaped movements in the three orthogonal XY, XZ and YZ planes are executed first. If the stand position error (or DBB readout value) exceeds a value near the DBB measuring range, the software module interrupts the measurement procedure: the stand position must be improved or the centre position when generating the NC codes must be adapted. During experiments it has also been observed that the three initial movements seem to have an improving effect regarding the repeatability of a DBB measurement, probably due to setting of the contact surfaces present.

Before a DBB can be used as an absolute length measuring instrument, it must be initialised first. This means that the telescopic DBB ball must be retracted and/or extended in order to pass a reference mark incorporated in the DBB's encoder. This reference mark is located near the centre of the DBB's measuring range and is usually passed by (a gloved) hand. However, when mounting the initialised DBB on the machine by clicking the DBB balls into the two magnetic sockets, some problems might occur. Due to extreme acceleration values (resulting from increasing non-negligible magnetic forces while surfaces are approaching) the DBB readout value can be shifted entirely and is no longer correct. Although this problem is not understood completely it can be circumvented simply by performing the initialising movement of the telescoping DBB ball by the machine.

The axes of machining centres normally require frequent lubrication. For the milling machine (a Maho 700S) used for instance a lubrication pulse (typically several s) is executed every eight minutes when the machine moves continuously, and for a non-moving machine once in the three hours. This lubrication pulse is necessary to guarantee a certain lifetime of the machine but also affects the machine's positioning behaviour significantly (typically 10  $\mu\text{m}$ ). Such a pulse is generated by a separated hydraulic pump system distributing (viscous) oil to the machine's axes by a flexible tube network. Obviously such a lubrication pulse should not occur during DBB measurements although this is hard to avoid completely. One way to eliminate this problem is to alter some machine constants (MC's) controlling the lubrication rates but this way is not preferable since irreversible machine damage might result. Another way is to perform each DBB measurement cycle several times: since the measuring time of a DBB measurement cycle is a few minutes only the affected measuring points during lubrication can be detected (and rejected) simply. Mainly for this reason, each DBB measurement cycle is performed including a reversal measurement.

## Appendix F

# The singular value decomposition

In this Appendix a brief survey of the singular value decomposition is presented, extracted from G. Strang's "Linear Algebra and its Applications" [Str 88].

The singular value decomposition (SVD) is one of the well known matrix factorisations, which is strongly associated with the eigenvalue-eigenvector factorisation<sup>1</sup> of a symmetric matrix:

$$\mathbf{A} = \mathbf{Q}\mathbf{\Lambda}\mathbf{Q}^T.$$

The eigenvalues are present in the diagonal matrix  $\mathbf{\Lambda}$  and the eigenvectors are present in matrix  $\mathbf{Q}$ . This matrix  $\mathbf{Q}$  is orthogonal:

$$\mathbf{Q}^T\mathbf{Q} = \mathbf{I}$$

because the eigenvectors of a symmetric matrix can be chosen orthonormal.

This eigenvalue-eigenvector matrix factorisation however, can only be done for symmetric matrices, but it is impossible for rectangular matrices. This problem however is therefore circumvented by considering  $\mathbf{A}\mathbf{A}^T$  and  $\mathbf{A}^T\mathbf{A}$ , which are always symmetric and square. By allowing the  $\mathbf{Q}$  on the left and the  $\mathbf{Q}^T$  on the right to be any two orthogonal matrices, not necessarily transposes of each other, this matrix factorisation becomes possible again. Any  $m$  by  $n$  matrix<sup>2</sup>  $\mathbf{A}$  can be factorised as:

$$\mathbf{A} = \mathbf{Q}_1\mathbf{\Sigma}\mathbf{Q}_2^T.$$

The columns of  $\mathbf{Q}_1$  ( $m$  by  $m$ ) are the eigenvectors of matrix  $\mathbf{A}\mathbf{A}^T$  and the columns of  $\mathbf{Q}_2$  ( $n$  by  $n$ ) are the eigenvectors of matrix  $\mathbf{A}^T\mathbf{A}$ . The  $r$  (rank of

---

<sup>1</sup>An eigenvector  $\mathbf{x}$  of a matrix  $\mathbf{A}$  is a vector for which yields:  $\mathbf{A}\mathbf{x} = \lambda\mathbf{x}$ . So for an eigenvector multiplication with its matrix is similar to multiplication with its eigenvalue, which is a scalar. The eigenvalues and the eigenvectors are computed by solving:  $\det(\mathbf{A} - \lambda\mathbf{I}) = 0$ .

<sup>2</sup>For the DBB measurements,  $m$  equals the number of measuring points and  $n$  stands for the number of parameters  $\beta$  that have to be estimated.

matrix  $\mathbf{A}$ ) singular values on the diagonal of  $\Sigma$  ( $m$  by  $n$ ) are the square roots of the nonzero eigenvalues of both  $\mathbf{A}\mathbf{A}^T$  and  $\mathbf{A}^T\mathbf{A}$ .

In order to make this clear, the connection between  $\mathbf{A}\mathbf{A}^T$  and  $\mathbf{A}^T\mathbf{A}$  must hold if the formula  $\mathbf{Q}_1\Sigma\mathbf{Q}_2^T$  is correct:

$$\begin{aligned}\mathbf{A}\mathbf{A}^T &= (\mathbf{Q}_1\Sigma\mathbf{Q}_2^T)(\mathbf{Q}_2\Sigma^T\mathbf{Q}_1^T), \\ &= \mathbf{Q}_1\Sigma\Sigma^T\mathbf{Q}_1^T,\end{aligned}$$

and similarly

$$\mathbf{A}^T\mathbf{A} = \mathbf{Q}_2\Sigma^T\Sigma\mathbf{Q}_2^T.$$

From the first,  $\mathbf{Q}_1$  must contain the eigenvectors of  $\mathbf{A}\mathbf{A}^T$ . The eigenvalue matrix in the middle is  $\Sigma\Sigma^T$ , which is  $m$  by  $m$  with  $\sigma_1^2, \dots, \sigma_r^2$  on the diagonal. From the second,  $\mathbf{Q}_2$  must be the eigenvector matrix for  $\mathbf{A}^T\mathbf{A}$ . The diagonal matrix  $\Sigma^T\Sigma$  has the same  $\sigma_1^2, \dots, \sigma_r^2$ , but it is  $n$  by  $n$ .

For this matrix factorisation, a large singular value  $\sigma$  indicates that the information, present in the corresponding eigenvectors of  $\mathbf{Q}_1$  and  $\mathbf{Q}_2$ , is apparently of major importance. The contribution of the eigenvectors, belonging to a small singular value on the other hand is much less. This can be made clear by simply denoting the SVD matrices as a sum of multiplications of columns and rows:

$$\begin{aligned}\mathbf{A} &= \mathbf{Q}_1\Sigma\mathbf{Q}_2^T \\ &= \mathbf{u}_1\sigma_1\mathbf{v}_1^T + \mathbf{u}_2\sigma_2\mathbf{v}_2^T + \dots + \mathbf{u}_r\sigma_r\mathbf{v}_r^T.\end{aligned}$$

Here, the  $\mathbf{u}$ 's stand for the columns of  $\mathbf{Q}_1$  and the  $\mathbf{v}$ 's are the columns of  $\mathbf{Q}_2$ <sup>3</sup>.

For the DBB measurements, the matrix from which all the machine's parameters  $\beta$  have to be estimated is denoted as:

$$\begin{aligned}\mathbf{y}^* &= \mathbf{X}^* \cdot \beta, \\ \beta &= (\mathbf{X}^{*T}\mathbf{X}^*)^{-1}\mathbf{X}^{*T}\mathbf{y}^*.\end{aligned}$$

Since all the machine's parameters  $\beta$  have to be estimated, matrix  $\mathbf{X}^*$  must have a full rank. Whether this is the case, is determined by the measurement setup. If this setup is weak, this matrix does not have a full rank and  $(\mathbf{X}^{*T}\mathbf{X}^*)^{-1}$  does not exist. Therefore, matrix  $\mathbf{X}^*$  must have a full rank, which should be regarded as a minimum constraint.

But even if this matrix has a full rank, there might still be a discrepancy between the singular values. In order to estimate *all* the parameters  $\beta$  in a more or less reliable way, the ratio between the smallest and largest singular value should be chosen as big as possible. This ratio, which can be regarded as a measure for the quality of matrix  $\mathbf{X}^*$ , is dependent on the distribution of the measuring points in a semi-sphere as discussed in Section 3.2. Numerous numerical simulations revealed that the condition number is always larger when applying the so-called birdcage measuring point distribution compared to the use of a homogeneous measuring point distribution [Flo 97].

<sup>3</sup> $\mathbf{v}_1^T$  is the first row of matrix  $\mathbf{Q}_2^T$ .

## Appendix G

# Design Double Ball Bar adapter

In order to perform DBB measurements on a machine with a rotating spindle, an adapter is required for connecting a DBB ball to the milling head in a safe and reliable way. The purpose of this adapter is to maintain the DBB ball position with respect to the spindle while the machine performs a duty cycle and heats up. During such measurements, the thermal expansion of the adapter introduces a measurement error that has to be minimized. This error has been minimized by optimising the design of the adapter for any duty cycle [Bus 01]. This adapter is discussed in this Appendix.

In Figure G.1 a photograph of the developed adapter is depicted. It consists of the following parts:

- Clamping ring;
- six tubes;
- Lower ring;
- Flange;
- Magnetic socket.

These adapter parts are made of steel with exception of the aluminium flange. A magnetic socket is screwed into the flange of the adapter, necessary to attach a DBB ball to the adapter.

Due to the rotation-symmetrical design of the adapter, thermal deformations of various adapter parts do not affect the DBB ball position in the horizontal plane as depicted in Figure G.1. The vertical DBB ball position with respect to the upper clamping ring is affected by the thermal expansion of various adapter parts. Most of these expansions result in an increase in distance between the clamping ring and the magnetic socket, to be screwed into the flange. This distance, however, is decreased as well by two effects. On one hand the thermal

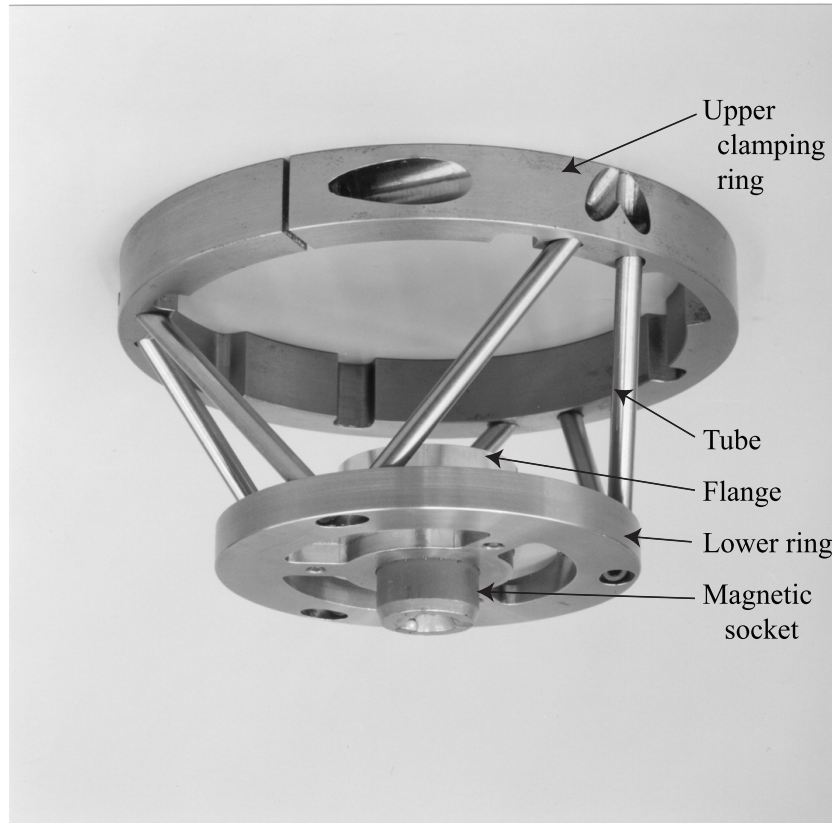


Figure G.1: DBB adapter.

expansion of the aluminium flange results in a lift of the DBB ball socket. On the other hand the upper clamping ring, connected to the milling head, expands more in diameter than the lower adapter ring since the latter increases less in temperature during measurements. Due to this differential expansion, the orientation of the six tubes changes, resulting in a lifting DBB ball socket. By choosing an aluminium flange ( $\alpha_{al} > \alpha_{steel}$ ), the various thermal expansions of adapter parts only have a minimal effect ( $\Delta\ell_{adapter} < 2 \mu\text{m}$ ) on the distance between the clamping ring and the DBB ball socket for any duty cycle [Bus 01].

In order to verify the capabilities of the designed adapter to maintain the DBB ball socket position relative to the milling head, validation measurements have been performed. The measurement setup is depicted in Figure G.2. With this measurement setup, the vertical position of the lower adapter ring with respect to the upper clamping ring is measured with a laser interferometer. Since rotations of the milling head with respect to the workpiece table do affect this displacement measurement, this rotation has to be measured as well. The relative rotations of the milling head have been measured with an autocollimator

and is used to correct the measured relative displacement.

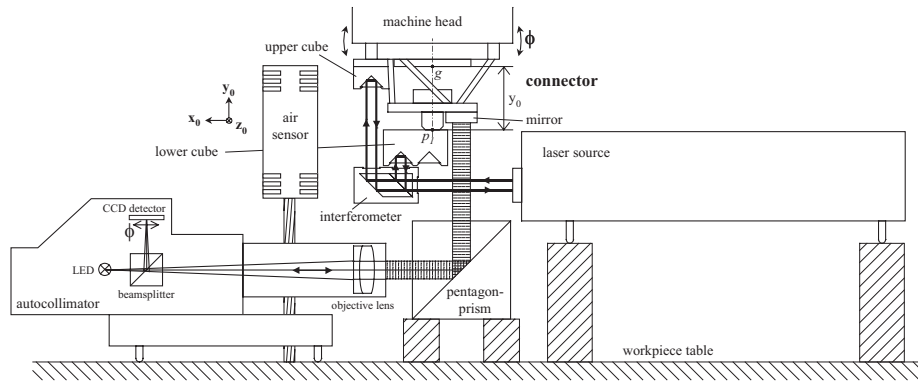


Figure G.2: Validation measurement setup of DBB adapter with laser interferometer and autocollimator.

The measurement results obtained are displayed in Figure G.3. The lines indicated with stars represent the uncorrected adapter displacement measured by the laser interferometer during a DIN8602 duty cycle. Correcting this displacement for relative rotations of the milling head results in the line marked with '\*'. This measurement shows that the thermal expansion of the adapter is less than  $\pm 2 \mu\text{m}$ . Measurements with other duty cycles reveal similar results [Bus 01]. Furthermore, the measured adapter expansion is in good agreement with calculated values, using temperature data of various adapter parts as indicated by the black line, marked with '+'. Summarizing, the introduced measurement

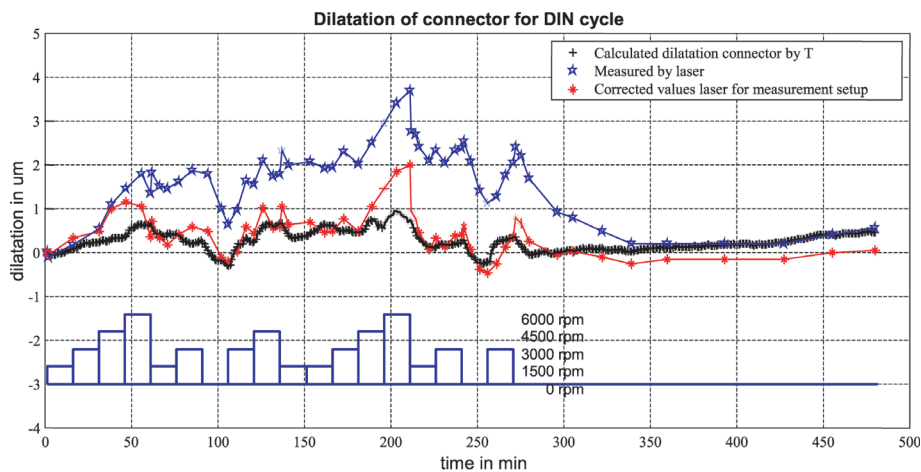


Figure G.3: Measured adapter expansion during a Din8602 duty cycle.

error by the thermal expansion of the adapter is negligible to the error to be measured. Consequently, the developed adapter is suitable for determining the thermally induced drift of a milling machine. Besides the adapter's thermal behaviour, also its finite stiffness and dynamical behaviour has been considered during its design [Bus 01].

# Curriculum vitae

Guido Florussen was born on March 29th, 1973 in Afferden (Gld), the Netherlands. After obtaining his Atheneum degree at Pax Christi College in Druten 1991, he commenced his study of Mechanical Engineering at Eindhoven University of Technology. Three months of this study was conducted at the University of North Carolina, Charlotte, U.S.A. in 1995, dealing with atomic force microscopy. This initial visit resulted also in a student exchange program between both universities, which is still running.

He received his Master's degree on May 23rd, 1997 by analysing the accuracy of multi-axis machine's based on length measurements. This research project was continued in his doctoral studies performed at the section Precision Engineering of Eindhoven University of Technology, which resulted in this thesis. This research project was financially supported by Stimulus (European Community) and the Dutch Technology Foundation (STW).

Besides working for the section Precision Engineering of Eindhoven University of Technology, he also worked for IBS Precision Engineering b.v. as a free-lancer. The research presented in the field of accuracy analysis of multi-axis machines has been conducted in cooperation with this company.





# Acknowledgements

The research described in this thesis has been performed at the Precision Engineering group, Eindhoven University of Technology. This project was financially supported by Stimulus (EU) and STW and I would like to thank these organisations.

First of all, I would like to thank my first promotor, prof.dr.ir. P.H.J. Schellekens for giving me the opportunity to work in his group as a (PhD) student. I greatly benefited from this experience and I cherish good memories to this period. Especially his confidence in me was of great support to me throughout these years.

Furthermore, a special word of thanks goes to dr.ir. H.A.M. Spaan and his company IBS Precision Engineering b.v. The research project described has been realised in corporation with this company, mainly for the development of software, needed for performing DBB measurements on a machine tool.

I would like to express my thanks to all the members of the promotion committee for their support and for reviewing this thesis: prof.dr.ir. M. Steinbuch (second promotor), prof.dr.ir. J. van Eijk, prof.dr.ir. H.E.H. Meijer and my copromotor dr.ir. F.L.M. Delbressine. A special word of thanks goes to prof.dr.ir. M. Steinbuch, prof.dr.ir. J.J. Kok, dr.ir. M.J.G van de Molengraft and dr. H. Haitjema for valuable discussions about parameter estimation techniques. Furthermore I would like to thank dr.ir. F.L.M. Delbressine in particular for the pleasant corporation throughout the last five years.

About 20 students contributed to the research project as described in this thesis and a special word of thanks goes to all of them, especially to ir. K.F. Bustraan for his large contribution concerning thermally induced errors. Furthermore I would like to thank all my former and present colleagues, staff members and students of the Precision Engineering group for the pleasant working climate.

Furthermore, I would like to thank Jan Sturre and Bob Hofstee of the company Heidenhain for their support.

Last but not least I would like to thank my family, my girl-friend Ana and my friends for their unconditional support.